DEVELOPMENT OF A PROTECTION MECHANISM FOR FIBER OPTIC SENSORS IN MONITORING GFRP REINFORCED CONCRETE BEAMS

Behnam Torkan

A Thesis

in

The Department

of

Building Civil and Environmental Engineering

Presented in Partial Fulfillment of the Requirements

For the Degree of Master of Applied Science (Civil Engineering) at

Concordia University

Montreal, Quebec, Canada

March, 2010

Your file Votre référence
ISBN: 978-0-494-67123-8
Our file Notre référence
ISBN: 978-0-494-67123-8

CONCORDIA UNIVERSITY

School of Graduate Studies

This is to certify that the thesis prepared

By: **Behnam Torkan**

Entitled: Development of a protection mechanism for fiber optic sensors in monitoring reinforced concrete structures

and submitted in partial fulfillment of the requirements for the degree of

Master of Applied Science (Civil Engineering)

Complies with the regulations of the University and meets the accepted standards with respect to originality and quality.

Signed by the final examining committee:

_____ Chair

_____ Examiner

_____ Examiner

_____ Supervisor

Approved by _____

Chair of Department of Graduate Program Director

_____20_____ _____

Dean of Faculty

ABSTRACT

DEVELOPMENT OF A PROTECTION MECHANISM FOR FIBER OPTIC SENSORS IN MONITORING GFRP REINFORCED CONCRETE BEAMS

BEHNAM TORKAN

Structural Health Monitoring (SHM) is a procedure of evaluating the in-service performance of structures, assessing the changes in the structural performance profile over a period of time, and aiding in decision making process for optimized maintenance and management of the structure during its life cycle. For strain measurement of civil infrastructure, Fiber Optic Sensors (FOS) are found to be useful for their durability and accuracy. They are known to be significantly more advantageous over conventional electrical strain gauges. However, special care and protection are needed for the installation of FOSs in reinforced concrete structures because of their delicate nature. To mitigate the difficulty in installing and embedding FOS in reinforced concrete structures, it has been proposed previously and developed in the present study that it is pre-installed in a supplemental bar which can be attached to the main reinforcement in a reinforced concrete structure in order to capture the strain in the structural elements. However a number of parameters such as the length, relative diameter of the supplemental bar as compared to the main bar, and the attachment mechanism between the main and supplemental bars can affect the performance of such systems. The purpose of the study is to characterize such bars, for their ability to transfer the strain of the main reinforcements appropriately for the use of engineering analysis. An experimental study

involving tension tests of reinforcing FRP bars with FOS embedded supplemental bars attached to them is conducted to identify the appropriate size, length and attachment method of the supplementary bars in terms of the strain experienced by the supplementary bars as compared to the real strain values of the corresponding main bars. A number of specimens with different combinations of the governing parameters as mentioned earlier are utilized in the test. Some of the specimens were confined in concrete cylinders to study the effect of such confinement in the performance of the proposed system. Adequate number of specimens were built and tested to assure the reliability of the tests, and the preliminary results indicate that the proposed system is viable, cost effective and practical. The results showed that in all cases, supplementary bars with two development length had closest strain capture of the main bar while the proposed attachment method could assure proper strain transfer. Moreover the study revealed that the less the diameter of the supplementary bar is chosen, the better results will appear. In the next step of the study a set of FRP reinforced concrete beams were constructed with the proposed FRP protected FOS systems, and the beams were tested in flexure to study the performance of the proposed protection mechanism for FOS in full scale reinforced concrete components.

ACKNOWLEDGEMENTS

I would like to sincerely thank my thesis supervisors Dr. Ashutosh Bagchi and Dr. Khaled Galal. They provided me with the unique opportunity to work in the research area of structural health monitoring through their expert guidance, support and encouragement at all levels. They generously provided valuable resources, their time and effort to complete my thesis.

The support of the Quebec funding agency on natural sciences and technology (FQRNT) is hereby gratefully acknowledged.

I am also grateful to Concordia University, for providing me with all the facilities during my research.

I also like to thank my wife my mother and sisters for their moral support, inspiration and encouragement to complete my research work.

Finally I would like to appreciate the encouragement and help I received from my colleagues and friends during my research work at Concordia University.

TABLE OF CONTENTS

LIST OF FIGURES

LIST OF TABLES

LIST OF ABREVIATIONS

FOS	Fiber Optic Sensor
RC	Reinforced Concrete
FPI	Fabry Perot Interferometer
FBG	Fiber Bragg Grating
ESG	Electrical Strain Gauge
FRP	Fiber Reinforced Polymer
GFRP	Glass Fiber Reinforced Polymer
CFRP	Carbon Fiber Reinforced Polymer
SHM	Structural Health Monitoring
CHBDC	Canadian Highway Bridge Design Code
CSA	Canadian Standards Association
ESPS	Embedded Sensor Protection System
L_d	Development Length of Reinforcing Bar

LIST OF SYMBOLS

A	Effective tension area of the bars (mm^2)
A_{FRP}	Total area of the GFRP reinforcements (mm^2)
b	Width of the cross-section (mm)
c	Depth of the compression zone in the cross-section of the beams (mm)
d	Effective depth of reinforcing rebars (mm)
d_b	Diameter of the reinforcing bars (mm)
d_c	Concrete cover for the reinforcing bars (mm)
E_{FRP}	Young's modulus of GFRP bars (GPa)
f_{FRP}	Stress in the GFRP rods (MPa)
f'_c	Compressive strength of concrete (MPa)
f_r	Modulus of rupture (MPa)
$F_u, f_{u.FRP}$	Ultimate tensile strength of the GFRP rods (MPa)
h	Depth of the beam's cross-section (mm)
I_{cr}	Moment of inertia of fully cracked section (mm^4)
I_{eff}	Effective moment of inertia of the cracked section (mm^4)
I_g	Moment of inertia of the gross section (mm^4)
M_{cr}	Cracking moment of the beams (kN.m)
M_n	Nominal flexural resistance of the beams (kN.m)
M_r	Resisting moment of the beams (kN.m)
M_f	Factored moment of the beams (kN.m)
M_s	Service moment of the beams (kN.m)

α_1	Stress block factor
β_1	Stress block factor
$\varepsilon_{FRP,u}$	Ultimate tensile strain of the GFRP
$\mu\varepsilon$	Microstrain
ρ_{FRP}	GFRP reinforcement ratio

CHAPTER 1

INTRODUCTION AND BACKGROUND

1.1 Background and Statement of the Problem

The global awareness of old and overused infrastructure (CSCE, 2002) motivated many researchers to focus on deploying new technologies to extend the life and enhance the capacity of civil infrastructure. Structural Health Monitoring (SHM) is an important tool to evaluating the in-service performance of structures, assessing the changes in the structural performance profile over a period of time, and aiding in decision making process for optimized maintenance and management of the structure during its service life. SHM is the procedure of in-situ measurement of structural and ambient parameters in order to study the structural adequacy as well as giving advice for maintenance and rehabilitation. A typical SHM system is composed mainly of a sensor system, a data processing system and a health evaluation system. After sensors are installed, data is acquired, transmitted and stored for further diagnostic and formation management.

Fiber Optic Sensors (FOS) are known to be considerably more advantageous over conventional electrical strain gauges for strain measurement of civil infrastructure due to their durability and accuracy. They have small dimensions, light weight and can be embedded in, mounted on or integrated to many fiber-reinforced materials. They can be multiplexed and are capable of real-time remote sensing yet they are not perturbed by electromagnetic interferences *e.g.* around power lines or lightning storms (Zhou et al., 2002). The abovementioned characteristics make them ideal for damage detection and

monitoring of civil engineering structures. If the structure is highly important or if it is likely to be subjected to extreme events such as earthquake or huge wind gusts, continuous monitoring would be necessary where FOS is the best solution.

There are different types of commercially available FOSs that have found wide applications in different industry sectors such as in aerospace, composites, medicine, chemical products, concrete structures, and in the electrical power industry. Two common varieties of local (vs. distributed) FOS are Bragg Grating and Fabry- Pérot FOSs which differ in their operational principles.

Fiber Bragg Grating (FBG) sensors are based on a passive spectral ratio metric approach using a low power, broad band- width light source. A Bragg Grating is created by inducing a permanent periodic modulation on the refractive index in the core of a single mode optical fiber. The length of a Bragg Grating is usually around 10 mm and it is an intrinsic FOS i.e. light in the sensing segment is modified inside the fiber. It can be easily multiplexed to measure strains at many locations. Germanium doped gratings which is photosensitive, reflect the light sent form the readout equipment to the FBG. When the spacing of the grating sensor changes, it affects the properties of the light received from the sensor by the interrogator which detects the change in optical wavelength. Fig. 1.1 shows the wavelength multiplexing schemes, wavelength shifts and principles of FBG sensors. The reflected wavelength is called the bragg wavelength $\lambda_h=2n\Lambda_1$, where n is the refractive index in the core and Λ_1 is the spatial period of the refractive index modulation. They have been successfully employed in several full-scale structures requiring multiple-point sensing distributed over a long range. This technology has been installed in many bridges in Canada and the USA.

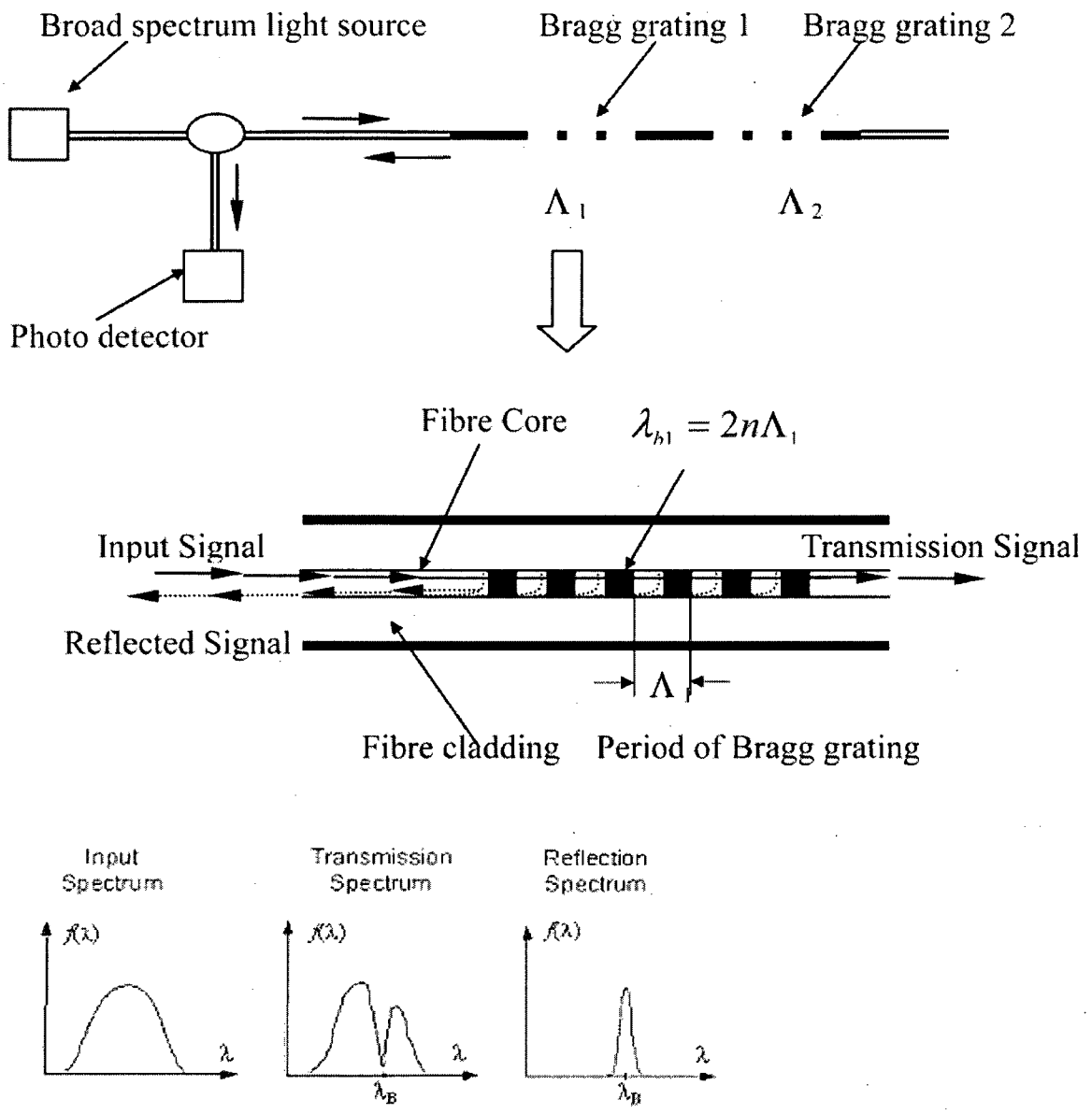

Figure 1.1: Multiplexing schemes, principles and wavelength shift of fiber Bragg grating sensors (Li *et al.*, 2004)

Fabry– Pérot FOSs operate based on white-light cross-correlation principle. They are among interferometric FOSs which offer the best sensitivity hence they are one of the most commonly used local sensors (as compared to long gage sensors).When the length of the cavity in the sensor changes, the sensor measures the average strain between two

fixed points along the gauge with superior accuracy. It is also capable of optional temperature compensation. This sensing technique is based actually on detecting the change in the optical phase which is induced in the light as it spreads out along the optical fiber. Light from a source is equally divided into two fiber-guided paths of which one is a reference. After a mirror beside the cavity in the sensor reflects the light in the other path, the beams are recombined to mix coherently and form a ''fringe pattern'' which is directly related to the optical phase difference experienced between the two optical beams. The readout equipment detects the change in optical wavelength or interference pattern and correlates it to the appropriate strain value.

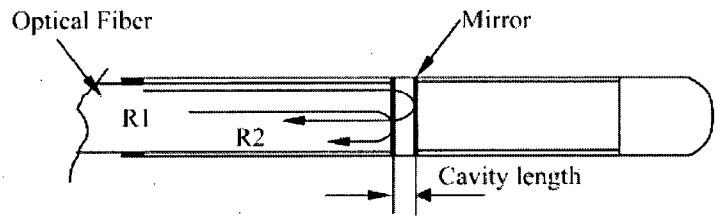

Figure 1.2. Fabry-Pérot FOS (Li *et al.*, 2004)

Fiber optic sensors have been deployed in the SHM of many projects while a number of laboratory and field studies have been conducted on their performances. However, further studies are needed to reach a better understanding about their behavior. Their comparative performance vs. conventional electrical strain gauges under various loading and environmental conditions needs to be studied. Moreover, because of their delicate nature, proper coating and packaging mechanisms are needed to make fiber optic sensors rugged for civil engineering construction, especially in reinforced concrete structures which offer detrimental environment to those sensors due to the construction practice and the high alkalinity of concrete. The performance of such packaging

mechanisms needs to be studied to address the issues arising during the installation and in the monitoring stage.

Fiber-Reinforced Polymer (FRP) composites have been increasingly used as internal reinforcements in concrete as a substitute for steel reinforcement for more than a decade. FRP bars have been studied and used extensively to reinforce concrete structures as an effective means to replace steel reinforcement in various concrete structures such as parking garages and bridge decks. FRPs have high strength-to-weight ratio and non-corrosive characteristics which have introduced them as durable composite materials to civil engineers. Their considerable fatigue properties and electromagnetic transparency make them a real benefit to the service life of the structure. Moreover, their usage in concrete structures has been codified in the most recent Canadian Highway Bridge Design Code (CHBDC) (CSA S6, 2006) and Canadian Reinforced Concrete Structures Code (CSA-S806-02, 2006). Although higher costs is generally considered as their disadvantages, the decreasing cost of FRP as well as lower transportation and handling costs of lighter materials compensates for the cost. The lower fire resistance of FRP is considered to be a problem and thicker concrete cover is recommended in that case.

Using FRP bars as a means for protecting FOS in FRP reinforced bars has been proposed previously (Bagchi *et al.* 2009). However a detailed investigation of such system needs to be performed. Protection method should provide enough security for the sensor and at the same time interfere least in transferring the data to the reading equipment.

1.2 Objectives of the Study

The need for a robust method of protecting FOSs in order to achieve better and more convenient installation and measurements motivates the present study. The scope of the research, briefly, is to fulfill the following objectives:

- Study the performance of Bragg Grating and Fabry- Pérot FOS and the proposed protection mechanisms under static loading.
- Develop a set of guidelines for using the rugged FOS to complement the existing ones, such as the ISIS guidelines on FOS installation and Civionics (ISIS, 2001and 2004).

The proposed research will study, the deployment mechanism of FOS in GFRP reinforced RC beams and the comparative performance of Bragg Grating and Fabry-Pérot FOS attached to the reinforcing bars in those beams, and the performance of FOS mounted on a supplemental FRP bar attached to the main reinforcing bar in a concrete beam. Glass FRPs are focused upon in this study as both concrete reinforcement and protective packaging for fiber optic sensors. Their physical properties are tested in experimental studies to reach the proper packaging system.

1.3 Significance of the Research

Fiber optic sensors for civil infrastructure are indispensable, provided that they survive the installation and the construction processes. Because of their brittleness and susceptibility to alkaline attack, considerable efforts are necessary for installation of bare fiber sensors if they are to be embedded in concrete. As the author participated in the

installation of FBGs in a SHM project in the John Molson School of Business at Concordia University, he is aware of the practical difficulties in installation and protection of sensors in achieving a successful sensing system. In order to mitigate the difficulties in installation and embedding FOSs in RC structures, it has been proposed (Bagchi *et al.*, 2009) that it be pre-installed in a supplemental bar which can be attached to the main reinforcement in a reinforced concrete structure in order to capture the strain in the structural comments. Supplemental bars or patches that can be attached to main reinforcing bars include:

- FRP patch with embedded FOS
- FRP bar with FOS embedded in epoxy filled grooves
- FOS integrated to an FRP bar
- FOS mounted on the surface of an FRP bar

However, a number of parameters can affect the performance of such systems. Although these mechanisms perform well in isolation there are concerns about their performance when they are installed in reinforced concrete structures (Benmokrane *et al.*, 2006). An experimental study has been conducted involving tension tests on reinforcing GFRP bars with FOS- embedded supplemental bars attached to them. The purpose is to identify the appropriate size, length and attachment method of the supplementary bars in terms of the strain experienced by these bars as compared to that of the corresponding main bars. A number of specimens with different combinations of the governing parameters mentioned earlier are utilized in the test. Some of the specimens are confined in concrete cylinders to study the effect of such confinement in the performance of the proposed system. In the next step of the study a set of FRP reinforced concrete beams

have been constructed and tested in flexure to study the performance of the proposed FOS protection mechanism in full scale RC components.

1.4 Organization of the Thesis

This thesis comprises six chapters starting with chapter one, devoted to an introduction to the topic of the research, what this research has aimed to accomplish, and the main factors that necessitate this research. Chapter two reports a brief survey of literature concentrating on applications of FOS in SHM projects and specifically on protection methods used. Chapter three presents the test setup for the preliminary study on supplemental bars as well as the main tests on RC beams. Chapters four and five report the results of the tests on tensile samples and beams respectively. The final chapter summarizes this study and includes discussion on the results of the comparison study and the beam tests. It also presents the conclusions derived based on the study carried out in the course of this research, and recommends the areas for future studies.

CHAPTER 2

LITERATURE REVIEW

2.1 General

This chapter presents a review of the SHM technology and describes some of the laboratory experiments carried out on different types of FOS that is usually used in civil infrastructure. The review includes the works that have been performed in deploying FOS in reinforced concrete structures as well as protection methods that have been invented or developed to make them rugged. As FRPs have been widely used in strengthening and reinforcing concrete structures both in labs and fields, the use of these new materials in available literature is surveyed, specifically those monitored by means of FOS. Literature review indicates a significant advancement in implementation of FOS in SHM in terms of protection methods and techniques to facilitate their installation, however still there are many issues to be addressed.

2.2 SHM and Fiber Optic Sensors

Modern infrastructure should have ''intelligence'' built in to take advantage of the benefits of the advancing technologies available for structural health monitoring. That will also help better repair plans due to more accurate maintenance that SHM will provide. Smart reinforcement is made by incorporation of FOSs within FRP reinforcements or attaching them together. There are many experimental studies available to assess the viability and effectiveness of this technology in civil structural elements.

Burong Zhang *et al.* (2003) performed laboratory studies on thermal, tensile and flexural performance of structural elements with Fabry- Pérot fiber-optic sensors to assess the behavior and applicability of such sensors for strain monitoring of engineering materials and structures. They were compared to electrical strain gauges and fiber Bragg gratings. Tensile tests were conducted on different types of material samples, including GFRP sand-coated, steel rebars, and CFRP grid. The Fabry- Pérot sensors were installed on the surface of the tensile specimens to investigate the monitoring behavior of the sensors. A one-way reinforced-concrete slab was constructed and tested in order to investigate the service performance of FOSs in the conditional monitoring of structural elements. Thermal behavior and static and cyclic loading were monitored by the preinstalled FOS on the reinforcement. Results show that those sensors perform linearly in monitoring tensile and compressive strains of infrastructure elements, and demonstrate good response to thermal variations and static and dynamic loading conditions.

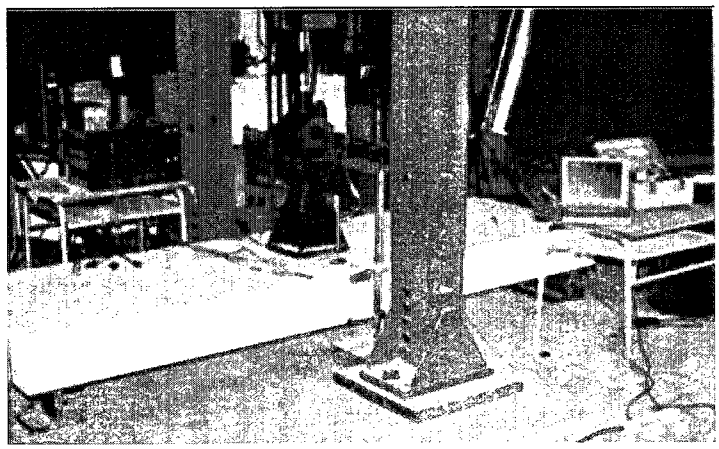

Figure 2.1. Flexural test setup of concrete slab (Burong Zhang *et al.*, 2003)

Durability of FOSs as a key issue has been also under investigation in the researchers study plans such as the one conducted by Gheorghiu *et al.* (2005). They

performed an experimental program on the durability of Fabry-Perot fiber optic sensors bonded onto CFRP plates used to externally strengthen reinforced concrete beams. The objective was to study the long-term behavior of FOS in RC structures in adverse conditions. The specimens were RC beams with an additional external CFRP reinforcement subjected to the combined effects of sequential fatigue and monotonic loading conditions. The fatigue tests on the FOS-instrumented beams were followed by a monotonic test to failure. The results have shown that the FOS employed are precisely measuring strains up to a limited strain value below 4000με (micro strains) and the load amplitude and the number of fatigue cycles had no influence on the FOS readings for strains smaller than 3300με and a number of cycles less than two million. It also revealed that the FOS accurately measured monotonic strains after the fatigue cycling .The post fatigue monotonic tests to failure demonstrated the excellent FOS performance for strains lower than 3200με. The drops observed in the readings given by the FOS at high strain values were probably caused by the degradation of the FOS–CFRP bond surface. When the system was tested under monotonic condition only, the strain limit value was higher than when specimens were first cyclically loaded for a number of cycles. However, even in these cases, the sudden changes in FOS readings happened at strains approaching the maximum value of the FOS operating range. Overall, these test results confirmed that the FOS were capable of measuring strains precisely for a variety of loading conditions, load ranges, and number of fatigue cycles.

Durability and feasibility of embedded Fabry–Pe´rot fiber optic sensors in detecting the cracks progression was assessed by Maalej *et al.* (2004) by inducing corrosion of the rebars of RC beams to create cracks. They made various concrete mixtures to build four

series of concrete beams with different level of corrosion and subjected all specimens to the same accelerated corrosion environment. The embedded Fabry–Pe´rot sensor placed between two reinforcing bars was deployed to measure the transverse tensile strains associated with the longitudinal crack along the reinforcing bars resulting from the radial expansion of the corroding rebars. The strain data obtained by the FOS showed great correlation with the reductions in the load-carrying and deflection capacities as well as the amount of steel loss resulting from accelerated corrosion. FPI sensors exhibited excellent durability throughout the study with no notable decrease in functionality.

2.3 Applications of FRP in Concrete Structures and FOS Monitoring

Although the role of FRP in auto industry and mechanical engineering as well as aerospace had been proven to be important, FRP was exploited as a new composite material to be utilized in civil engineering structures since mid-80's. They have been investigated in various applications of reinforcing new structural components and in rehabilitation and retrofitting existing structures of insufficient strength. Having superior advantages over steel, such as corrosion resistance and higher durability, motivated several research works conducted in the field of concrete structures. Beddington Trail Bridge in Calgary, Alberta, was one of the first bridges in Canada to be outfitted with FRP tendons and integrated optical sensors for remote monitoring. Fiber optic Bragg grating strain and temperature sensors were used to monitor structural behavior both during construction and under serviceability conditions. Crowchild Bridge in Calgary, Alberta and Hall's Harbour Wharf in Nova Scotia both having steel free concrete decks are being monitored for long-term behavior using Fiber Optic technology. SHM projects

on Manitoba's Taylor Bridge in Headingley, and the Joffre Bridge, spanning the Saint Francois River, were other significant contributions to the increasing usage of the FOS sensing technology (Mufti, 2002).

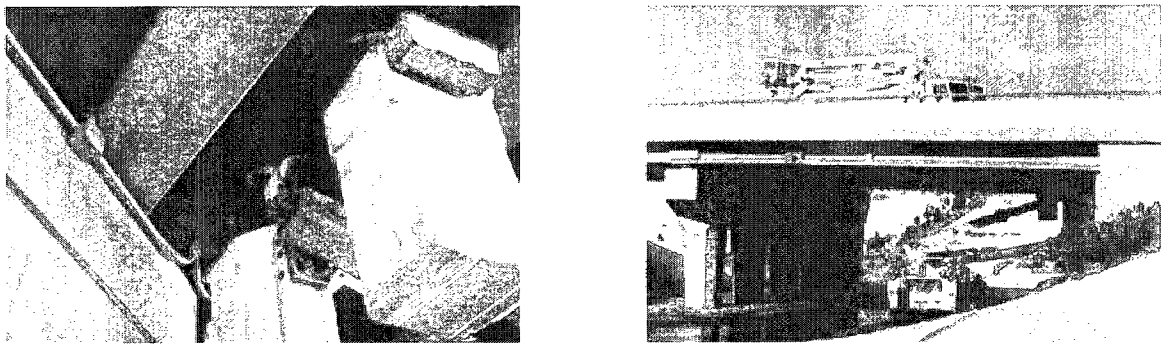

Figure2.2. On-site monitoring (left) and testing (right) of Beddington Trail Bridge (Mufti, 2002)

The Morristown Bridge located over the Ryder Brook on in Vermont, USA and the Magog Bridge over the Magog River on Highway 55 North, in the province of Québec underwent SHM projects using Fiber Optic Sensors to measure strains in the concrete, reinforcing bars and steel girders (Benmokrane *et al.* (2005)).

2.4 Protection Methods

In order to protect FOS in concrete structures it should be kept safe during the casting period from abrasion of the aggregate and the silica fiber should be protected within the alkaline environment of concrete. Over the past decade, considerable studies have been developed to invent or develop protection methods for FOS and to assess their reliability and practicality.

Bagchi *et al.* (2009) proposed a FRP protection system to be used as supplementary bar attached to the main FRP reinforcement. An experimental study was conducted on the performance of Bragg Grating FOS embedded in the epoxy filled grooves of FRP bars

attached at the mid-span of simply supported reinforced concrete beams and for the sake of comparison, electrical strain gauges at the same longitudinal location were attached to the supplemental FRP bar and the main rebar. The strain recorded by the electrical stain gauges and the rugged FOS shows a good agreement. The proposed protection system is further developed in the current study.

Protection methods could involve various materials and techniques. Leng *et al.* (2005) designed models and implemented, tested various fiber optic sensor protection systems for development in concrete structures. Three types of embedded sensor protection system (ESPS) based on metal, CFRP composite and ESPS concrete materials were designed with different application fields. Various types of steel flanges in the form of disc, cone and inverted cone were chosen on dumb-bell like steel protection. They also proposed a rebar based ESPS that could be used to mount the fiber optic sensor into the drilled cavity in the rebar in concrete structures using adhesive. The assembly can be welded to the primary rebar. Although robust, the metal based protection is time consuming to manufacture and subjected to corrosion. Hence, the option of using carbon fiber reinforced composites (CFRP) was considered due to its ease of manufacture and corrosion resistance. Unidirectional CFRP-based ESPS in the forms of rolled-up, dumb-bell, and also complex shapes such as rebar has been developed. CFRP wrapped concrete cylinder with FOSs was another type of protection method in that study. Protected extrinsic FPI and FBG sensors have been used to monitor the structural health status of plain and composite wrapped concrete cylinders and the obtained results indicate that the protection system for the sensors performs well in concrete environment.

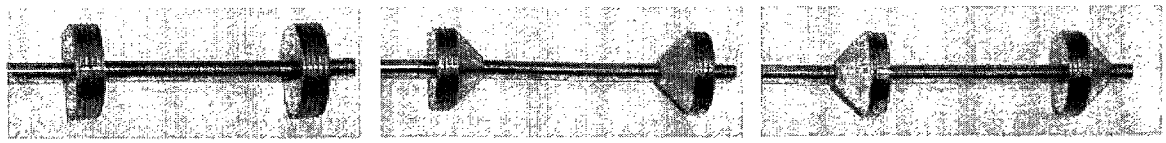

Figure 2.3. Disc, cone and inverted cone of steel flanges for ESPS (Leng *et al.*, 2005)

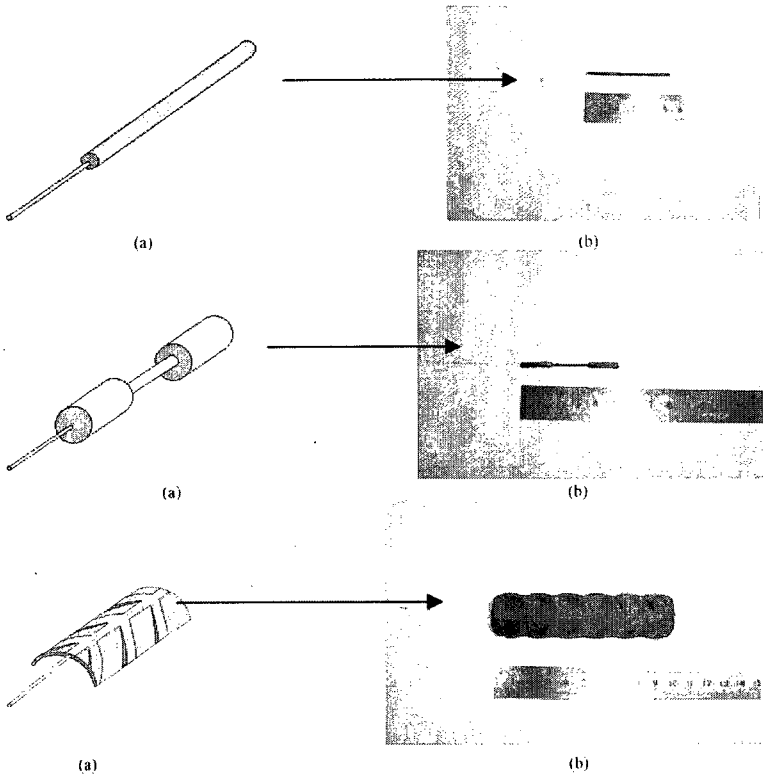

Figure 2.4. Rolled- up, dumb- bell, rebar- shape CFRP based ESPS (a) schematic illustration and (b) photograph (Leng *et al.* (2005))

Integration of FRP and FOS technology founded an interesting SHM project on a road bridge performed by Kister *et al.* (2006) using optical fiber Bragg grating sensors. The bridge which is entirely made of glass and carbon FRP is named the West Mill Bridge in Oxfordshire, UK. Bonding methodology was developed and appropriate protection systems consisting of flat thin glass fiber composite strips for the sensors were implemented to make the use of Bragg grating sensors possible and let them survive the construction and installation of the bridge. In order to assess bonding integrity of the

adhesive, pullout test on optical fibers bonded on bridge tests coupons was carried out. Durability test of the sensor protection were performed by immersing protected optical sensors in water. The study showed that environmental conditions do not influence the protection failure mechanism and that the protection system isolated effectively the sensors from the moisture ingress. The proposed protection also provided enough resistance to chemicals, flexibility and robustness for the optical sensors. Figure2.5 presents a diagram of the sensor protection system. The overall thickness of the sensor protection system was 1.8 mm and the maximum length of the composite strips or covers was 1 m. Three years after installation of sensors, a second controlled load test demonstrated that sensors survival was achieved the recorded strains were similar to those obtained during the first load test that was performed after the construction of the bridge.

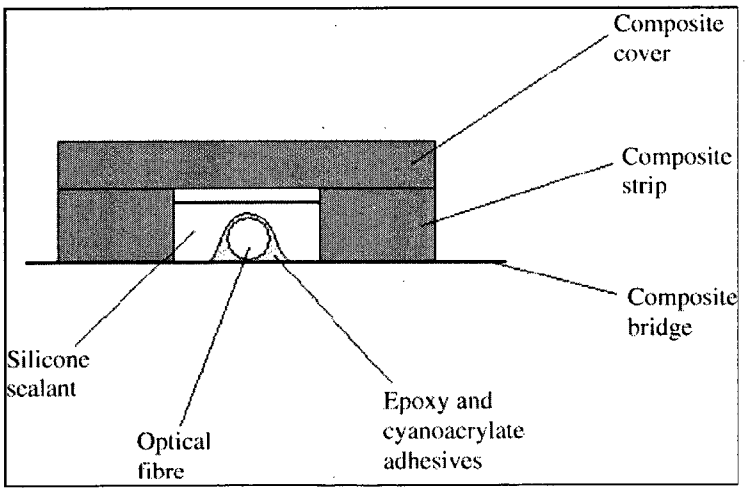

Figure2.5. Schematic illustration of the sensor protection system on the West Mill Bridge (G. Kister *et al.*, 2006)

CHAPTER 3

METHODOLOGY AND EXPERIMENTAL PROGRAM

3.1 Introduction

The experimental study conducted in this research project comprises of two parts:

First part consists of the pilot tests that were meant to examine the characteristics of the protective supplemental bar and help make the best choice in terms of physical properties of those bars to best transfer the strain with the least interference in the true captured strain value of the main bar. It also consists of deriving the gauge factor of those sensors in comparison with electrical strain gages.

Second part of the program contains the main tests that include testing two medium-scale GFRP-reinforced concrete beams to evaluate the performance of the proposed protection system. All the tension specimens and beams were constructed and tested in the structural lab of Concordia University.

3.2 Auxiliary pilot Tests

3.2.1 Free in Air Tensile tests

The idea of using a supplementary bar as a protective tool for FOS has intrigued SHM engineers. However, two main questions arise here. The first is how to choose the physical properties of those supplementary bars and the second is how to attach them together. To study them experimentally, it was proposed to carry out a set of tests on

different combinations of the two bars as well as their type of attachment. Main bars of 19 or 13 mm diameter GFRP and supplementary bars of 10 or 6 mm diameter were chosen to give a measure of the effect of cross section areas. The length of each supplementary bar was chosen as a multiplier of its development length (L_d) *i.e.* one, one and a half and two times L_d. The ($2L_d$) case was only tested on 6 mm diameter bars due to the practical limitations of the testing machine. Development length is the minimum length of straight reinforcing bar which is required to anchor it in concrete. Hence stress can be developed in a free rebar of length of at least $2L_d$ in concrete without slippage. Since the bars are going to be under tension in concrete, L_d was the best measure to choose the length on that basis.

In order to study the attachment method, the "perfectly connected at two sides" bars were compared with "simply attached bars in concrete." The former case was created using CFRP sheets, which bound the two bars at the ends of the supplementary bar by means of a special two-component epoxy.

An electrical strain gage was installed on each bar and the specimen was pulled from its two ends in the tensile testing machine to compare the readings of the two ESGs. In first category cases, a third strain gage was also installed on the main bar, on its "single bar" area to get the strain of the single main bar subjected to the load.

3.2.2 Requirements

In order to carry out the tension test on the FRP bars, Canadian Standards Association (CSA S806-02, 2002) specifies the requirements to provide sufficient anchorage for testing FRP specimens under various types of tensile loading tests. Because of the non- homogeneous, non-isotropic nature of FRP bars, it is impossible to pull the FRP bars in tension tests by putting the bare FRP bar in the steel jaws as is

usually the case for steel rebars. The reason for that is because FRP bars are weak in compression and need proper anchorage while being tested in tension to avoid getting smashed. To facilitate the gripping of the specimens, the requirements of an anchor for FRP reinforcement specimen are stated as follows:

The inner diameter of the steel anchor cylinder should be 10 to 14 mm greater than the nominal diameter of the FRP bar. The length of the steel tube at each side shall be at least equal to $F_u \times A/350$ not less than 250 mm, where F_u stands for ultimate tensile stress resistance of the bar and A is the bar cross section area. The cylinder wall thickness shall be at least 5mm and the free length of specimen shall be $40d_b$, with d_b representing the bar's diameter. There are also other specifications and provisions for the surface preparation and anchor casting procedure in terms of casting position, preparation, mixing, handling and filling resin.

3.2.3 Specimen types

Different combinations of GFRP bars in diameter and length are chosen in this study. Since this test is conducted using a testing machine and not in the real beam condition, it is referred to as "free-in-air" as opposed to the beam tests. Two different types of specimens were designed and built to compare the effect of the difference between the physical properties of the main and supplementary bars.

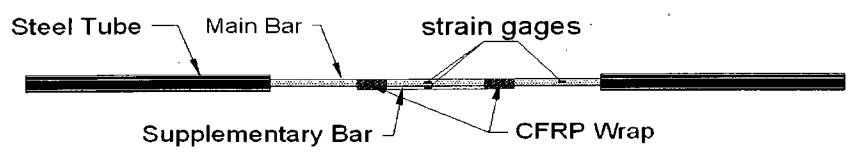

Figure 3.1. Typical tensile specimen for the pilot test

Table 3.1. Pilot test specimen types and characteristics

specimen type	main bar size mm	supplementary bar size mm	steel tube length at each side mm	bar length between anchors	CFRP attachment sheet length
1	13	6 or 10	420	>520 mm	350-400 mm
2	19	6 or 10	600	800 mm	400-450 mm

Table 3.2. Matrix of tensile specimens for the pilot study

Supple. Bar length	Main bar size	Suppl. bar size	wrapped	confined	C-W
L_d	13	6	2	2	1
		10	2	2	-
	19	6	2	2	-
		10	2	2	-
$1.5L_d$	13	6	2	2	1
		10	2	2	1
	19	6	2	2	1
		10	2	2	1
$2L_d$	13	6	2	2	1
	19	6	2	2	1

In each type, GFRP bars of size 13 or 19 millimeters were used as main bars and GFRP bars of size 10 or 6 millimeters were used as supplementary bars. Specimens with various combinations of main and supplementary bars were built and tested as tabulated in table 3.2. Specimens were built in three categories to compare the effect of the type of

attachment in transferring the strain. The first type was designed to attach the two bars by means of CFRP sheets at two ends of the supplementary bars so that the bars connect rigidly. In the second specimen category, the two bars were attached simply by plastic ties, but confined in a concrete cylinder that kept the two bars together in order to simulate the tension side of a concrete beam. As concrete has small tensile strength, it just acted as an attachment agent. The third case is the combination of the two cases, i.e. wrapped by CFRP sheets and confined in concrete. Two specimens were built and tested of each of the first two categories. The third case was tested on some of the same bar combinations mentioned in table 3.2.

3.2.4 Materials and Manufacturing

The GFRP rebars depicted in Figure3.2 that were used in this study are known as V-RODTM and manufactured by Pultrall Inc. located in Québec (Pultrall, 2007). Epoxy used to fill the steel pipes for the anchorage of tension members was Sikadur35 (Sika Canada Inc.). The CFRP sheets used to attach the two bars were "Tyfo® SCH-11UP" Composite, The outer diameters of the steel pipes used were 1 5/18 and 1 3/18 inches (32.45 and 29.6 mm) for 19 and 13 millimeter bars, respectively. Normal concrete with no additives was made for tensile confined specimens with 28 day compressive resistance of 25MPa.

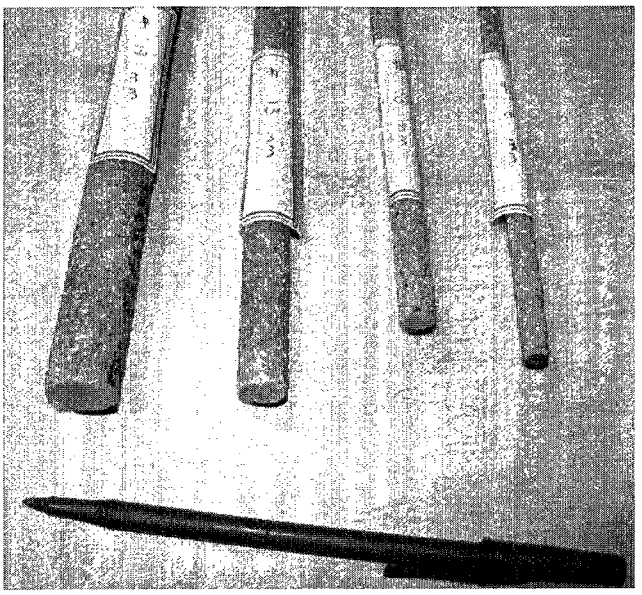

Figure 3.2. Different GFRP bars utilized in this study

To abide by the code requirements, steel pipes for each bar were chosen of proper dimensions and filled with Sikadur35 epoxy after the bar was properly placed, centered in the pipe. In order to center the main bar properly, two Plexiglas pieces were built and placed at two ends of each pipe and the gaps were sealed by silicon. The epoxy casting was done in a vertical position. About twenty hours after casting the epoxy in one anchor tube, the specimen was turned upside down and the other side underwent the same procedure as it is required by the code.

After the epoxy dried, it was time to attach the supplementary bar to the main bar. This bar is placed in the middle of the free length of the main bar as shown in the figure 3.1. In categories where the two bars had to get fixed (1^{st} and 3^{rd} type), the supplementary FRP bar got attached to the main bar by means of the narrow epoxy coated CFRP sheets. In order for that to be implemented, the two bars were attached and fixed in their place using plastic ties. CFRP sheets of 40 mm width, with lengths of 350-450 mm, were then

coated with the two component epoxy and used to wrap the two-bar assembly at each side of the supplementary bar. In order to capture the strain of each bar, one electrical strain gage was installed on the midpoint of each bar. In the first category, a third strain gage was installed on the main bar within the single bar region. The strain gages were Quarter Bridge, 120 Ω resistant. The 2nd and 3rd category specimens were covered by concrete after they underwent strain gage installation.

3.2.5 Strain gauge bonding

The first stage in strain gauge bonding is surface preparation. The basic purpose of surface preparation is to develop a chemically clean surface with an appropriate roughness for the requirements of gauge installation, a surface alkalinity corresponding to a pH of 7 or so and apparent gauge layout marks for orienting and locating the strain gauge. There are five basic operations for surface preparation in the order that follows:

1. Surface grinding and degreasing by solvent, which can be GC-6 Isopropyl Alcohol or acetone
2. Preparing the flat surface by dry and wet abrading
3. Application of strain gauge layout lines
4. Conditioning using the phosphoric acid conditioner (solvent A)
5. Neutralizing by the alkali solvent B

The surface is abraded to remove any loosely bonded adherents or rust etc. and to develop a surface texture suitable for bonding. For coarse surfaces like FRP bars it is necessary to start with a grinder or file. Finish abrading is done with silicon-carbide paper of the appropriate grits like 220, 320 and 400 that are suitable grit sizes for our case to be

used subsequently. A relatively smooth surface (in the order of 2.5μm) is suitable. The abrading should be done while keeping the surface wet with conditioner A, which is a mildly acidic solution (phosphoric acid) that accelerates the cleaning process. After the location of the strain gage on the test surface is lined, the surface should be "washed" by Conditioner A. It should be applied repeatedly, and the surface scrubbed with cotton tipped applicators. This procedure should run until a clean tip is no longer discolored. When clean, the surface should be dried by wiping through the cleaned area with a single slow stroke of a gauze sponge and then, with another fresh sponge in the opposite direction. It is important to note that the sponge should never be wiped back and forth, to avoid recontamination from the un-cleaned boundary. The final step in surface preparation is neutralizing. This should be done by applying M-Prep Neutralizer 5A to the cleaned surface, and scrubbing the surface with a clean cotton-tipped applicator. When neutralized, the surface should be dried by wiping through the cleaned area with a single slow stroke of a clean gauze sponge. The strain gauge should be placed while bonding side down, on a clean surface. A 100-mm piece of gauge installation tape is placed over the gauge in the center of the tape. The assembly then is lifted at a shallow angle to specimen surface and positioned over the layout lines on the specimen. The loose end of the tape then is tucked under and pressed to the specimen surface so that the gauge lies flat, with the bonding surface exposed. The M-Bond 200 catalyst (marked as C in Figure3.3) can now be applied to the bonding surface of the gauge and terminal in a very little amount and in a thin, uniform coat and allowed to dry at least one minute under normal ambient conditions before proceeding. The tucked-under tape end of the assembly is lifted, and adhesive is applied at the surface. While holding the tape slightly taut, with

a single wiping stroke over the gage/tape assembly using a piece of gauze, the gauge is brought back down over the alignment marks on the specimen. A firm pressure with fingers is needed when wiping over the gauge. A very thin, uniform layer of adhesive (marked as D in Figure 3.3) is desired for optimum bond performance. Immediately after wiping out the adhesive, firm thumb pressure must be applied to the gauge area for at least one minute. After the tape is removed, an acrylic coating liquid (marked as E in Figure 3.3) will be applied to protect the strain gauge. In case the strain gauge is going to be buried in concrete, it should be covered by a bitumen-like protecting material from being touched by the aggregate casting. There are of course special safety precautions and considerations in terms of working safely with the grinding devices and also dealing with toxic materials where all procedures and safety measures should be approved by the safety standards (Vishay manual, document#11127).

Figure 3.3 Components used to install strain gauges

3.2.6 Confined specimens

The 2nd and 3rd specimen categories were designed to get covered by a concrete cylinder around the supplementary bar area. To implement that, sets of special formwork were designed and built to cover all the supplementary bar area by a concrete cylinder of 10 cm diameter with the main bar centered in the cylinder.

3.2.7 Testing Procedure

When epoxy cures 28 days after casting, the specimen is ready to be tested under the tensile load using the TINIUS OLSEN tension machine which is depicted in Figure 3.4.tension test machine. For the confined cases, testing is carried out 28 days after casting of concrete. Specimen gets fixed between the jaws of the machine and the strain gauges get calibrated at zero load. Then the loading starts monotonically until failure and the strains of the strain gauges on both bars are recorded continuously once per second.

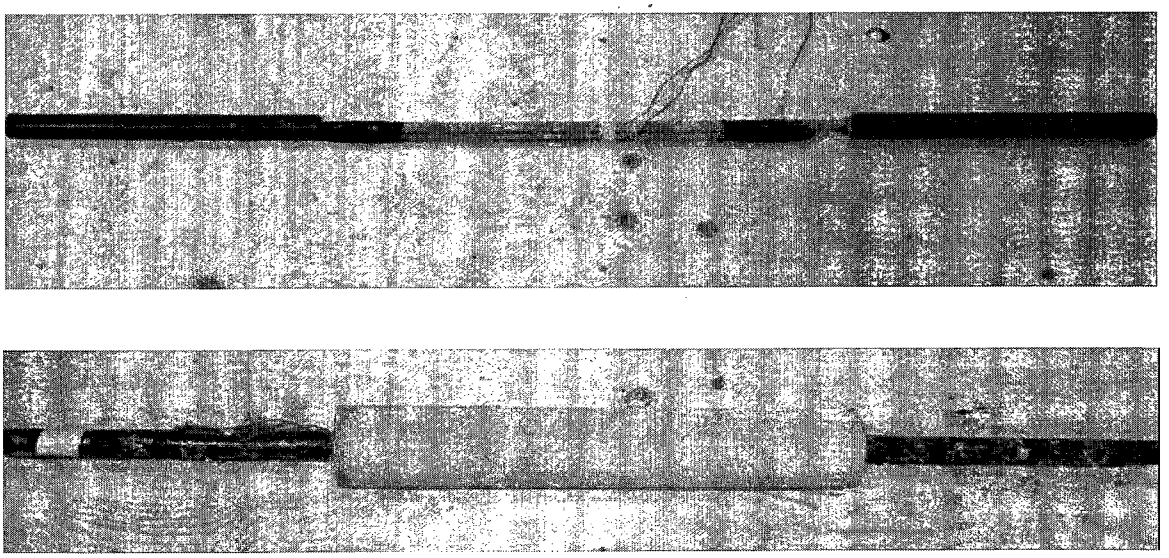

Figure 3.4 Wrapped (above) and confined (below) specimens

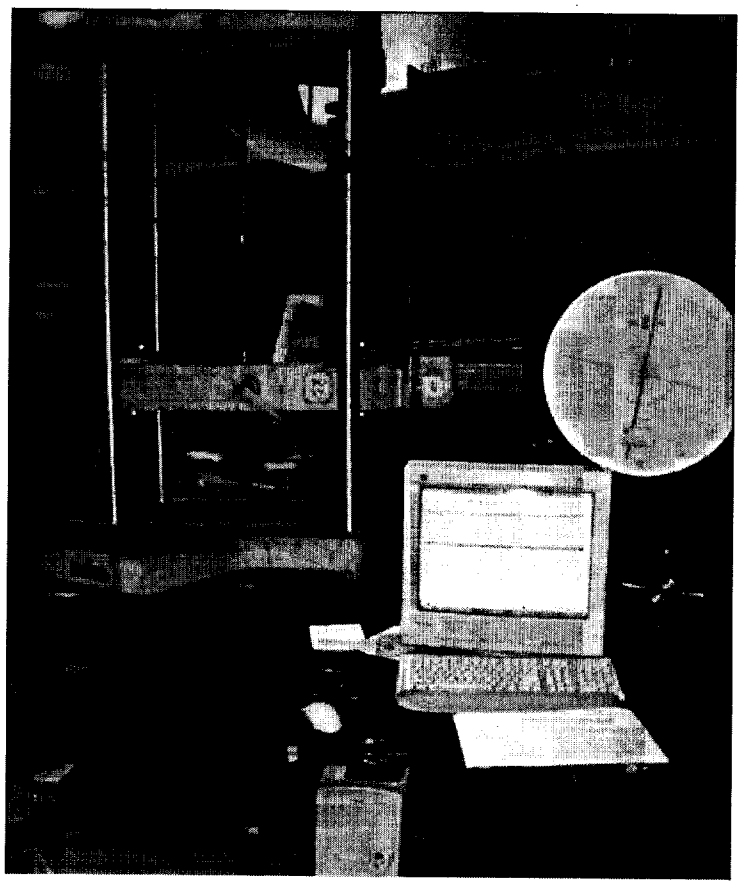

(a)

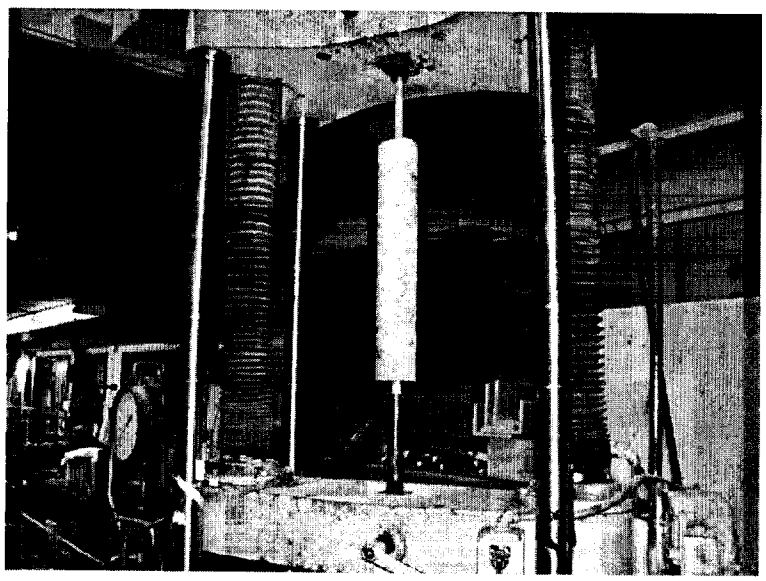

(b)

Figure 3.5 Testing machine and the data acquisition system, testing on (a) wrapped and (b) confined specimens

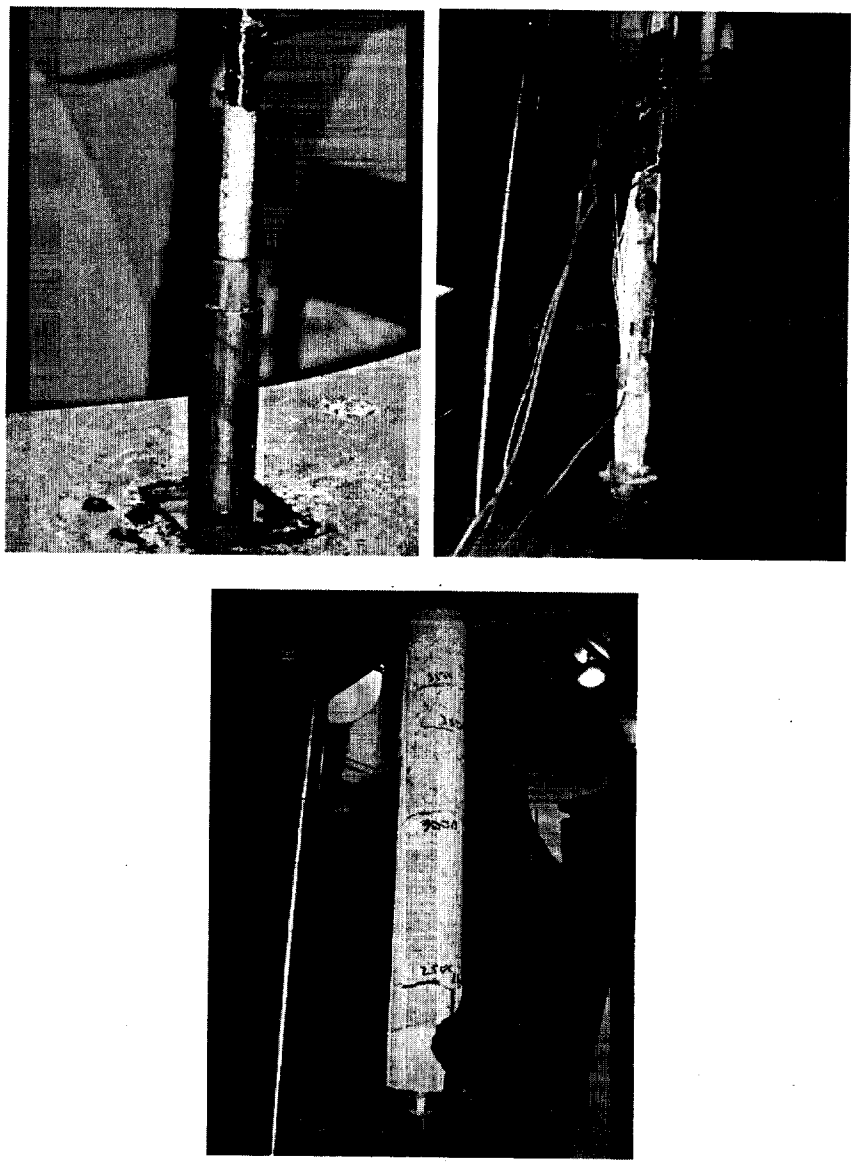

Figure 3.6. Specimens after failure

The specimens underwent tension tests to get a measurement of the percentage of strain that the supplementary bar captures from the main bar. These tests also show how reliable the attachment method could be, in terms of transferring the force to the supplementary bar. The force is exerted until the failure of the specimen. Failure might happen in different modes. The test session is over if the attachment of the two FRP bars fails, if the FRP bar ruptures, or if the epoxy anchorage is pulled out of its steel pipe. To

avoid early slippage of epoxy out of its cage, holes were drilled into the steel pipe walls to increase the pipe-epoxy mechanical connection. Besides, in the confined cases, if the concrete cover spalls or if the cracks open so widely that the strain transfer gets dramatically affected, it is considered as a failure point. Some cases ended in malfunction or disconnection of the strain gage because of the cracks or slipping of the concrete cover.

3.2.8 Comparison Tests

In order to compare the readings of the two types of fiber optic sensors that were going to be installed in the concrete beam, a set of tension tests were performed. As differrent types of sensors were planned to be tested in one set of beams, sensor tests were needed to determine the gauge factor of each type. Gauge factor is a value which expresses a sensor's sensitivity to strain. In other words, it was necessary to find out what strain each sensor reads at any given load. Tension tests were carried out on a tension specimen with three differrent types of sensors externally bonded on its surface. The tension member was similar to a19 mm diameter GFRP bars that were manufactured for the tension tests. Manufacturing of the specimen was similar to that of a tension specimen with a 19 mm GFRP bar with epoxy anchorage in steel pipes at two ends. Two electrical strain gauges, one Fabry- Perot, and one Fiber Bragg Grating FOS were externally bonded onto its surface. Electrical strain gauges were installed on opposite sides of the bar to check bending of the bar and to assure uniform stress distribution. The choice of a thick bar made it possible to have a more uniform distribution of the load throughout the specimen length and also allowed a higher range of loading to be exerted on the bar.

The specimen was then tested in tension to compare readings of different sensors under monotonic or step loading. First, load was applied in steps with known increments until a maximum load amount was reached, and then decreassed with the same increments. In the next part, loading was applied increasingly monotonically to a maximum and then unloaded monotonically down to zero. This test was repeated several times to achieve sufficiently confident results to rely upon for the final beams' testing step. As it can be seen in the figure 3.5, three data acquisition systems were set up and the software of each case was installed on a computer to receive data. Step loading with different increments of 250, 500 and 1000 pounds up to maximum of 10000 were applied and strains were recorded. Then, monotonic loading was applied up to the same maximum force.

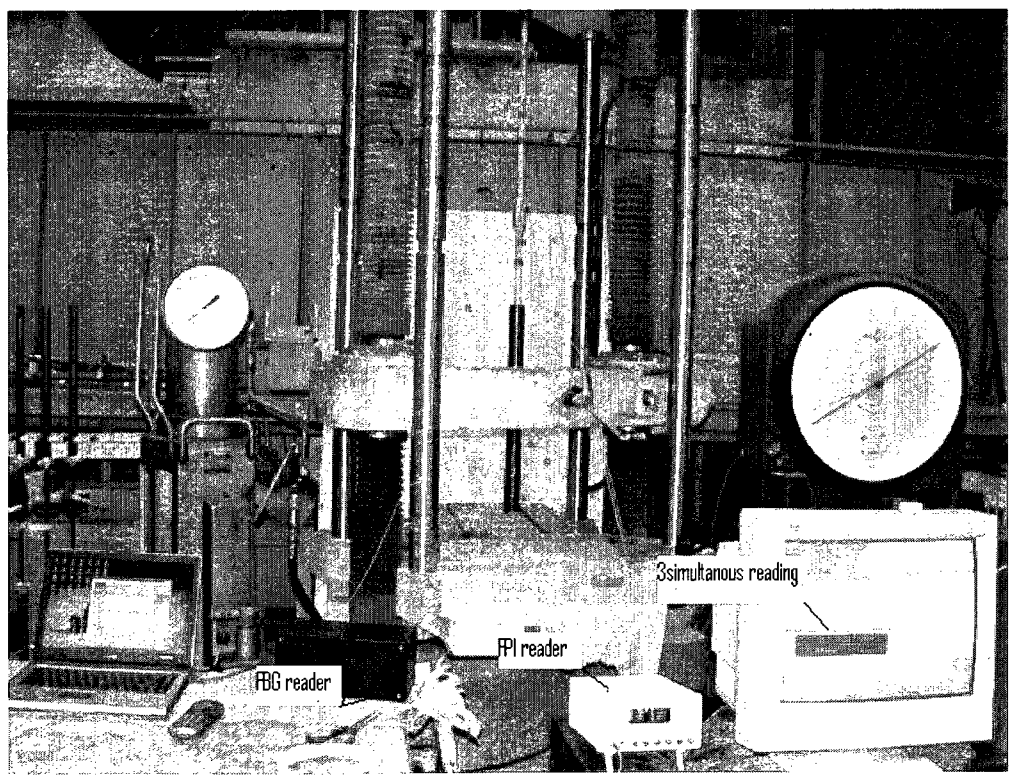

Figure 3.7. Comparison test setup with three DAQ systems for 3 different sensor types

3.3 Tests on GFRP-reinforced concrete beams

The main part of the experimental program in this study consists of testing two medium-scale GFRP-reinforced concrete beams under in-plane bending. The objectives of this test are as follows:

1. Deploy FOSs in monitoring flexural behavior of concrete beams
2. Compare measurements of FPI and FBG vs. conventional ESG
3. Evaluate the proposed protection method for FOS in FRP reinforced concrete beams

3.3.1 Description of the Beams

Each specimen was a GFRP reinforced concrete beam with nominal dimensions of 3 m×0.24 m ×0.32 m cast in plywood formworks. Figures 3.7 and 3.8 contain photos of the construction of the beams and their completed instrumentation in Concordia University's structural laboratory. Both beams were designed "over reinforced" to undergo compression mode of failure. Design parameters and results are explained in appendix B. Four #13 mm glass FRP bars used on the tension side of the beam section and two 6 mm diameter GFRP were used in the compression side. The shear reinforcement of 10 mm diameter GFRP was spread throughout the beam length based on the shear design. Only plastic ties were used to tie the bars in order to have a completely no-steel reinforced beam.

Beams were constructed, cured, hardened and then transferred and laid horizontally by crane on the setup using steel hooks designed for this purpose. Standard cylinder compression tests showed 28 day average resistance of 30 MPA of the concrete.

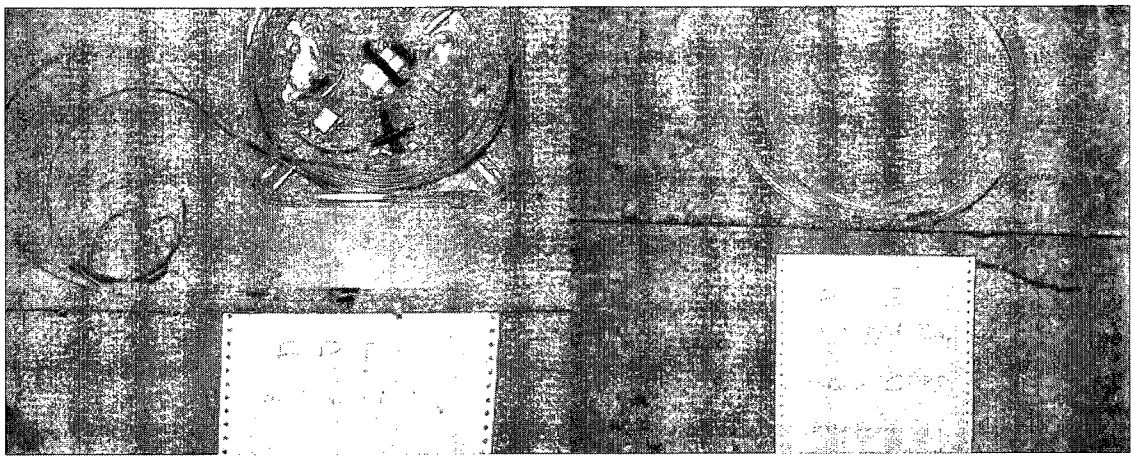

Figure 3.8. GFRP bars instrumentation before being placed in the beams formwork, FPI (left) and FBG (right)

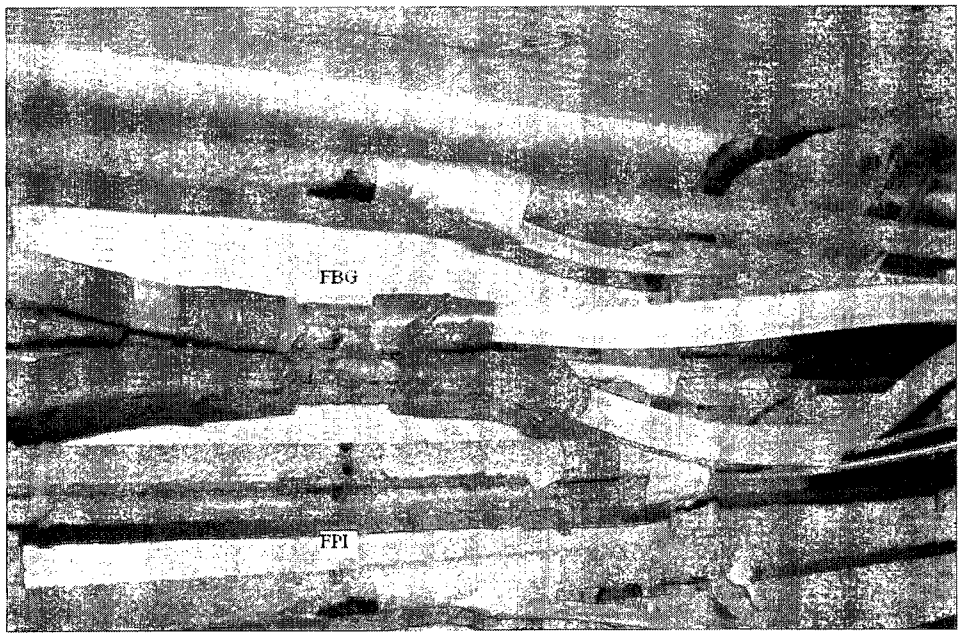

Figure 3.9. Sensors location on the bars before concrete casting

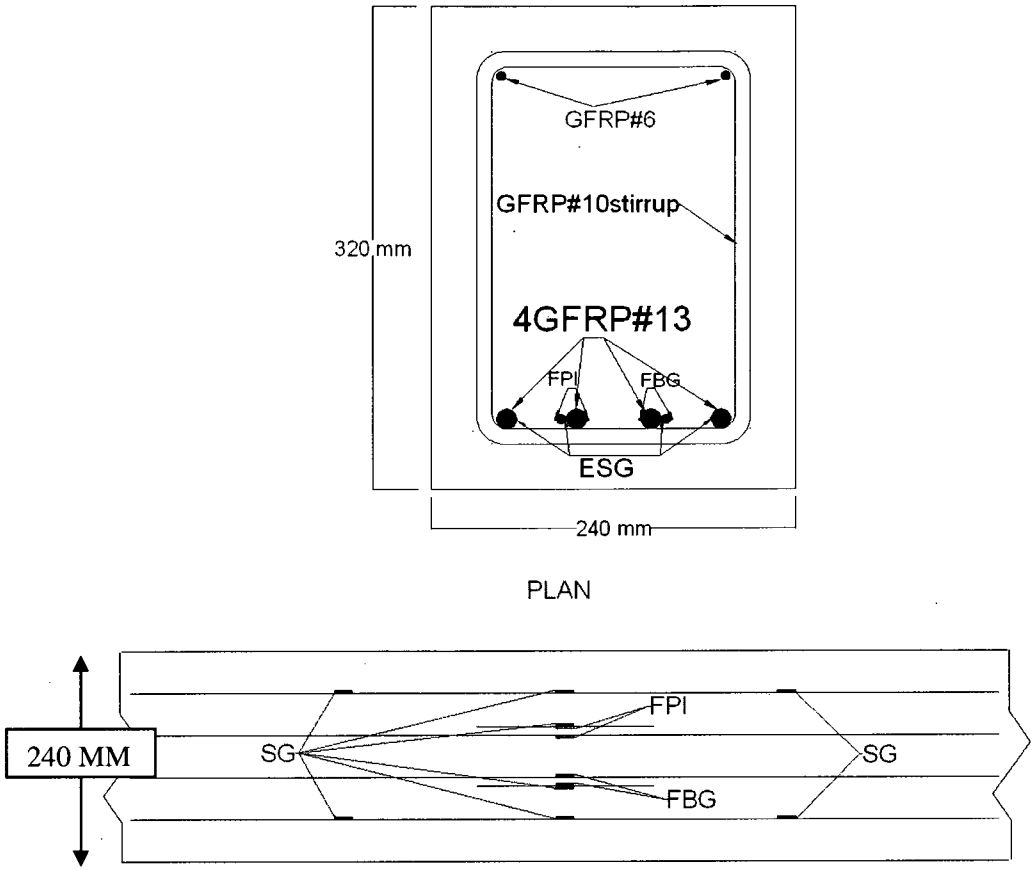

Figure 3.10. Sensors location on the bars, section (above) and plan (below)

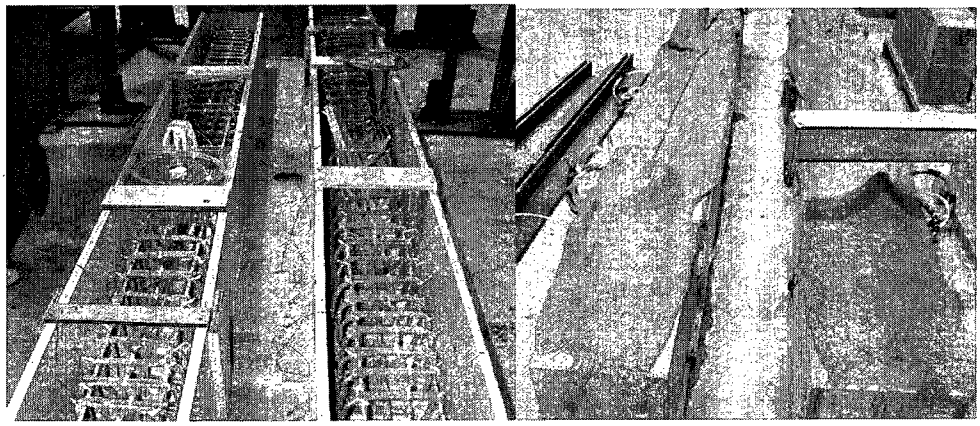

Figure 3.11 Beams before and after concrete casting

3.3.2 Test Setup and Instrumentation

Beams were tested in a four point loading setup, shown in the Figures 3.12 with an effective span of 2.4 m. Two point loads, at third spans, were applied and monotonically

increased by a 25-ton hydraulic actuator, reacting against a rigid steel loading frame, up to the ultimate failure. The maximum stroke of the hydraulic jack that was used was 25.4 cm (10 ") and a load cell of maximum capacity of 250 KN was used to measure the applied force. Load was transferred through the loading apparatus and applied over two 152.4 mm (6") wide channels to avoid crushing the beam due to stress concentration. The beams were tested while positioned horizontally on a hinge at one end and a roller at the other end. Potentiometers were located to measure the displacement at four different points of each tested beam (two at mid-span and two under each loading point), in order to obtain the longitudinal profile of the beam at various load levels.

The strain gauges and Fiber Optic Sensors were installed on the GFRP reinforcement before being placed in concrete as shown in the above figures. Strain gages were installed on the two of the main tension bars in the mid-span and quarter-span to record axial strain. FOS were mounted on the other two longitudinal bars as well as on supplementary bars attached next to them. Moreover, strain gauges were installed in the midpoints of the compression bars and also on two of the stirrups at d/2 distance from the supports. Four FOS namely two FBGs and two FPIs were installed in each beam. One of each type was installed on the main bar and one on the supplementary bar next to it. Two 62cm- long ($2L_d$), 6 mm diameter GFRP bars were used as supplementary bars to locate the FOSs beside two of the same kind on the main bar to compare the readings of the two sensors. The installation process of FOS is similar to the strain gauge installation but uses a different bonding agent which is a special two-component epoxy. Supplementary bars were attached to the main bar using carbon FRP sheets in the first beam as compared to

the second beam with free ended supplementary bars, simply tied by plastic cable ties to the main bar in order to study the difference between the two attachment methods.

3.3.3 Testing Procedure

Since three different types of sensors were installed in the beam, the correspondent data acquisition system of each type of sensor was utilized. Hence, all of them had to be checked for properly acquiring the data prior to the test. "Fisocommander" software for FPI , "Micron Optics "for FBGs and "Strain smart" software for ESGs, potentiometers and load cell measurements, were all installed on the same computer to collect the data. After the data acquisition systems had launched, recording the applied load, deformations, and tensile strains, the in-plane vertical load was applied and increased monotonically until the ultimate failure of the beam occurred. The cracks at each known load were marked on the beam to exhibit the crack pattern during the loading session. After the failure in compression, the failed beams were removed in a secure manner for relocation.

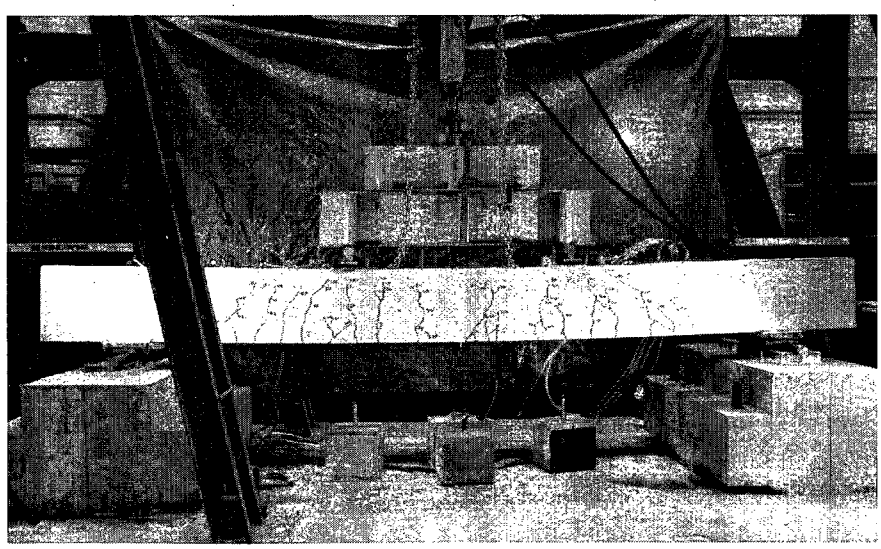

Figure 3.12 Beam set up under testing load close to failure

CHAPTER 4

RESULTS OF THE PILOT STUDY

4.1 General

Chapter 4 is divided into two parts. The first part is about the results and observations of the pilot tests and the second part is allocated to the discussions and comparisons of the qualitative behavior of the conducted tests.

4.2 Results of the tensile pilot Tests

The test results of the free-in-air specimen tests are presented in the following sections starting with the wrapped-only specimens and followed by the concrete-confined ones (with ascending GFRP bar size) and at last the wrapped-confined cases. Samples of results are presented here and the rest are reported in appendix A. The choice of different main bar sizes helps to show the effect of attachment on strain readings as the contribution of the supplementary bar is less in bigger sized main bars due to the lower size ratio of the two bars and vice versa. Photos of some of the specimens at different stages of loading, and also deformed ones prior to and at failure, as well as force-tensile strain curves, are shown. The focus in this part is mainly on the transferred stress from the main to the supplementary bar comparing them with the single main bar strain. As for the force-strain curves the slope of the best trend line of each case is found and the slopes of the continuous readings are compared. The failure mode of specimens falls within 5 different types which have been mentioned for each case. This might happen due to breach of the bar, failure of the CFRP attachment, disintegration of concrete cover,

slippage of the anchorage or disconnection of the strain gages due to failure or slippage of the attachment.

The ratio of the best trend line slope of the supplementary bar sensor reading to that of the main bar is reported as the average captured strain in percent. Moreover, the ratio of readings of the second and third strain gauges has been mentioned as the contribution of interference of the cross section area of the supplementary bar in reading real values. The ratio between the strain gauge's average reading of the single main bar and that of the supplementary bar will represent the correction factor that should be applied to the reading of the sensor on the supplementary bar to get that of the single main bar as if there had been no added cross section area to it.

4.3 CFRP wrapped specimens

As mentioned before, in the test series of wrapped-only specimens, three strain gauges were installed on this type of specimen. The first and second sensors were installed on the main and supplementary bars within the two-bar area and third one on the main bar, in the single-bar area. The main bar of 13 mm or 19 mm diameter and supplementary bar of 6 mm or 10 mm diameter were attached by means of epoxy dipped CFRP sheets. Strain gauges on the main, supplementary and the single part of the main bar are called first, second and third respectively. Hence, the first strain gauge shows the strain of the main bar in the area of connection with the supplementary bar, the second one indicates the captured strain by the supplementary bar and the third strain gage shows the real strain of the single bar due to the applied load. Since the response of the GFRP bar to load is linearly constant, in cases where only 2 strain gages were installed, third sensor results of previous acceptable tests are used as comparative measures to find the

contribution of the attachment. The third strain gauge can be reliably used only on the CFRP wrapped cases to get the effect of the interference of the added cross section area of the supplementary bar on the reading. In the initially tested confined cases it did not work well; henceforth the third strain gage was no more installed on confined specimens afterward.

The test on specimens with supplementary bar sizes of 10 mm was carried out only on the length of one and one and a half development length and not on $2L_d$ case, due to the practical restrictions of the testing machine. Two strain gages were installed on the main and supplementary bars to compare their readings.

Each specimen is labeled by the main bar diameter vs. that of the supplementary bar, followed by the length of the supplementary bar which has been mentioned as a multiplier of its development length. Samples of the sensor readings are shown in the first specimen's explanation as well as the properties of the specimens and the force-strain graphs to compare the slope of the best trend lines as a comparative measure of the abovementioned parameters. The test was conducted on two identical specimens. Properties and samples of the results of the specimens are explained in the following tables.

The strain in the single main bar can be calculated as $\varepsilon_1 = P/(A_1E)$ where P is the applied force, A_1 stands for the cross section area of the main bar and E is the modulus of elasticity of GFRP. Assuming the complete attachment between the two bars, the assembly cross section will experience tensile strain of $\varepsilon_2 = P/(A_1+A_2)E$, A_2 representing the cross section area of the supplementary bar. However it was revealed in the tests that

the two bars show different tensile strains which is due to the effect of the attachment and physical properties of the two bars. As for the force-strain curves, considering P= (AE) ε, the slope of each graph is equal to AE for the single bar (#19 or #13) or the assembly of the two bars. Theoretical values for the slope of the graphs are compared with the experimental values along with the properties of bars tabulated in table 4.1. The slope of the assembly is calculated assuming one rigid attachment between the two bars.

Table 4.1. Properties of the bars and theoretical slopes of the force- strain graphs

	#19	#13	#10	#6
Cross section area (A) mm^2	285	126.7	71.3	31.7
Young's modulus (E) Gpa	47.6	46.3	45.4	46.1
Theoretical Slope when assembled with #6 (10^{-6} N/mm^2)	15.027	7.328	_	_
Theoretical Slope when assembled with #10 (10^{-6} N/mm^2)	16.803	9.104	_	_
Theoretical Slope of the single bar (10^{-6} N/mm^2)	13.566	5.866	_	_

Comparative values are derived based on the experimental results. The contribution of attachment was calculated by dividing the second strain gage reading by the third one and subtracting the result from a hundred percent. The correction factor is the value that

should be multiplied by the reading of the supplementary bar to get the strain of the main bar as if there were no bars attached. This was obtained by dividing the third strain gage value by the second one. Samples of each category's results are mentioned here and the rest are brought in the appendix A.

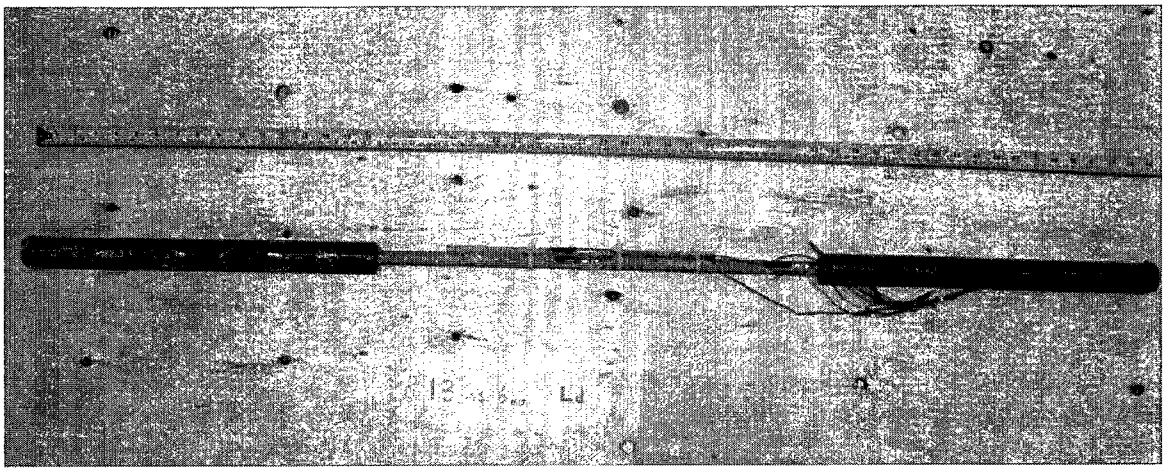

Figure 4.1 #13 vs. #6, L_d First specimen before getting confined in concrete

4.3.1 #13mm main bar vs. #6mm supplementary bar of one development length (310mm) CFRP wrapped

Table 4.2. First Specimen results for13 vs.6, L_d

Failure load	Avg. Captured by supplementary bar	Contribution of attachment	Correction factor	Failure mode
77.85KN	83%	21%	1.54	FRP bar ruptured
		Sg1	Sg2	Sg3
Slope of best trend line		7.11	8.58	5.58
Strain at failure		11037	8487	13850

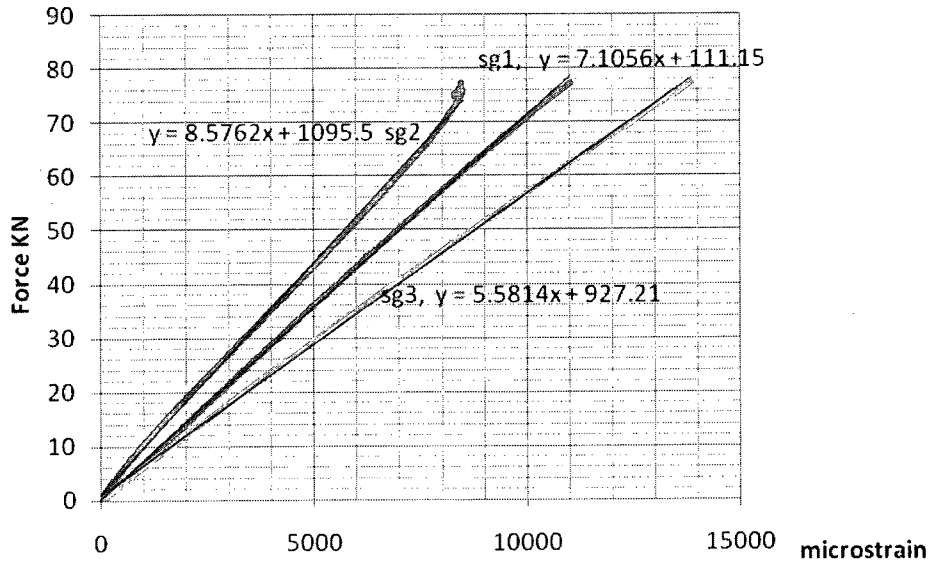

Figure 4.2. Force - strain, 13 vs.6, L_d first specimen

Table 4.3. Sample readings for 13 vs.6, L_d first specimen

Force KN	Sg1	Sg2	Sg3	Sg2/sg1
2.2	339	172	356	0.507
4.4	681	386	738	0.567
11.11	1572	1063	1832	0.676
17.78	2523	1884	3013	0.747
24.44	3386	2659	4104	0.785
31.11	4343	3522	5326	0.811
37.78	5258	4336	6510	0.825
44.44	6192	5162	7719	0.834
51.11	7122	5943	8921	0.834
57.77	8057	6714	10142	0.833
64.44	9000	7455	11358	0.828
71.1	10009	8127	12632	0.812
75.55	10656	8469	13430	0.795
77.85	11037	8487	13850	0.769

4.3.2 #19mm main bar vs. #6mm supplementary bar of two development length (620mm) CFRP wrapped

Table 4.4. First Specimen results for19 vs.6, $2L_d$

Failure load	Avg. captured by supplementary bar	Contribution of attachment	Correction factor	Failure mode
107.9KN	97.64	13%	0.85	Connection failure
		Sg1	Sg2	Sg3
Slope of best trend line		15.378	15.75	n/a
Strain at failure		7012	6311	n/a

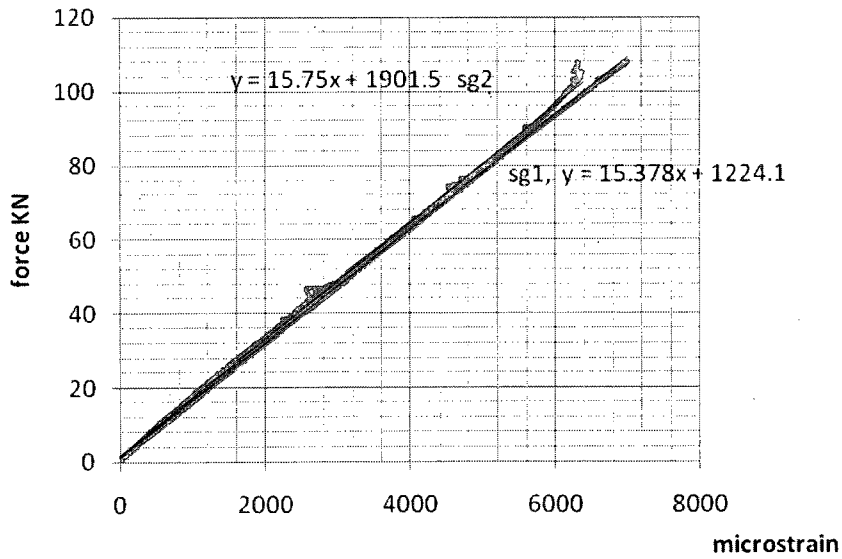

Figure 4.3. Force - strain, 19 vs.6, $2L_d$ first specimen

4.4 Specimens confined in concrete

In order to assess the reliability of concrete cover in the tension area of a beam as the connecting agent between the two bars, this category was designed, built and tested. Strain gauges were installed on the main, supplementary and the single part of the main bar which are called first, second and third respectively. However the third sensor did not respond well compared to the previous category. Hence in this part the focus will be only on the two first strain gauges. The first strain gauge shows the strain of the main bar in the area of connection with the supplementary bar and the second one indicates the captured strain by the supplementary bar.

After the installations of the strain gauges, the two bars were attached by means of plastic ties and then they were covered with a concrete cylinder of 100 mm diameter, main bar centered. Concrete completely covered the supplementary bar to make the friction work on the designated length. Test was conducted on two identical specimens. In order to simplify specimens' labeling each case is labeled by the main bar vs. supplementary bar diameter, and then length of the supplementary bar which is mentioned as a multiplier of development length.

After commencement of the test, subtle change was observed in the readings of the sensors since strain did not transfer until concrete cylinder cracked. This led to force-strain graph to be nonlinear. After concrete cracked the readings changed dramatically as mentioned in the table and the graph. As the test went on to higher stages of loading, since the cracks widened, integrity of attachment decreased and consequently a decrease in the readings of the second sensor was noticed. In order for the graph to be linear to

allow comparison of the readings, the force-strain curve before the crack was removed in order to compare the linear part. Following graphs are samples of the tests and the entire results are brought in the appendix A.

4.4.1 #13mm main bar vs. #6mm supplementary bar of two development length (620mm), confined in concrete

Table 4.5. First confined specimen results for13 vs.6, $2L_d$

Failure load	Avg. captured by supplementary bar	Failure mode
68.72KN	117%	Anchorage failure
	Sg1	Sg2
Slope of best trend line	9.295	7.937
Strain at failure	9256	8941

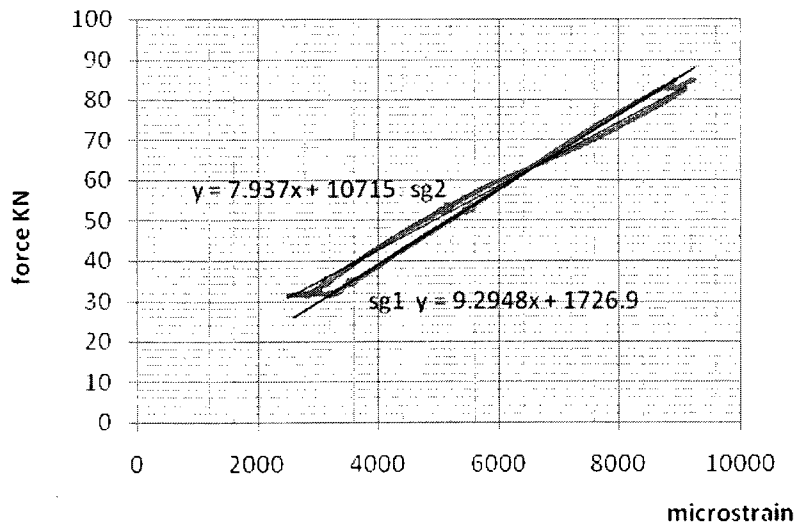

Figure4.4. Force - strain, 13 vs.6, $2L_d$ first confined specimen

4.4.2 #19mm main bar vs. #6mm supplementary bar of two development length (620mm), confined in concrete

Table 4.6. First confined specimen results for19 vs.6, $2L_d$

Failure load	Avg. captured by supplementary bar	Failure mode
74.7KN	90.9%	Anchorage failure
	Sg1	Sg2
Slope of best trend line	14.9	16.4
Strain at failure	3621	3284

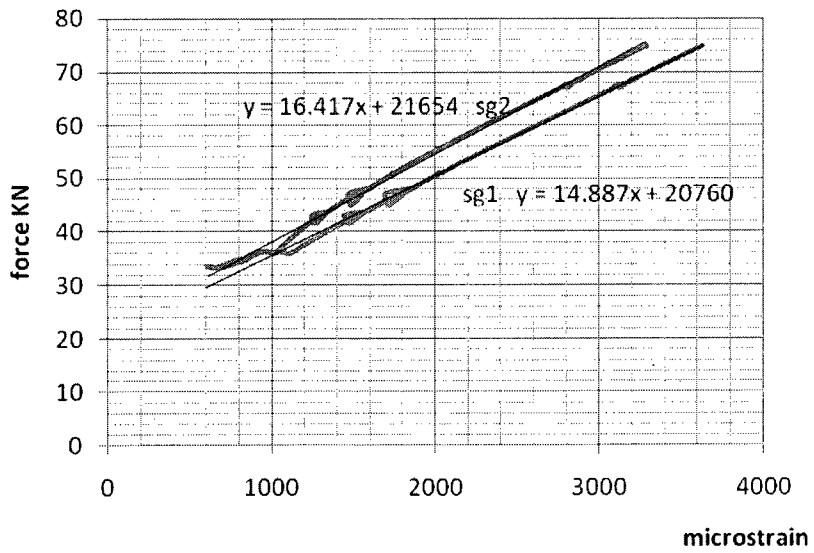

Figure4.5. Force - strain, 19 vs.6, $2L_d$ first confined specimen

4.5 Wrapped-confined specimens

In order to study the effect of the CFRP wrapped attachment in concrete, third category of specimens were built and tested. In other words the effect of combined two cases was tested to evaluate the efficiency of wrapped attachment in concrete in transfering strain values from the main to the supplementary bar. After installation of the gages, the two bars were attached by CFRP sheets and then they were covered with a concrete cylinder of 100 mm diameter, main bar centered. Concrete covered the supplementary bar completely to make the friction work on the designed length simirar to the previous case. In this case the specimens are labeled by the main bar vs. supplementary bar diameter followed by length of the supplementary bar mentioned as a multiplier of development length. "C-W" stands for confined, wrapped specimens. Sample of results of the tension tests as well as force- strain graphs are presented in the following and the rest are reported in appendix A.

4.5.1 #13mm main bar vs. #6mm supplementary bar of one development length (310mm), CFRP wrapped and confined in concrete

Table 4.7. C-W specimen results for13 vs.6, L_d

Failure load	Avg. captured by supplementary bar	Failure mode
57.46KN	83.3%	Sensor went off scale
	Sg1	Sg2
Slope of best trend line	7.62	9.15
Strain at failure	7450	6246

Table 4.8. C-W specimen readings sample for13 vs.6, L_d

Force KN	Sg1	Sg2	Sg2/sg1
11.16	53	62	1.17
14.44	73	81	1.11
17.73	98	101	1.031
24.44	3080	2431	0.79
31.2	4038	3110	0.77
37.77	4877	3824	0.78
44.4	5745	4609	0.8
51.1	6626	5423	0.82
57.46	7450	6246	0.84

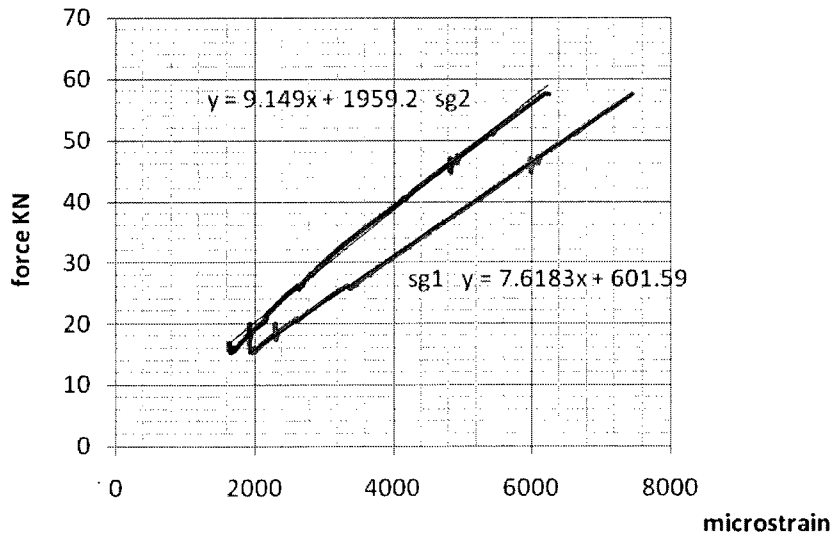

Figure 4.6. Force - strain, 13 vs. 6, L_d C-W specimen

4.5.2 #19mm diameter Main bar vs. of #10mm supplementary bar, one and a half development length (630mm) long, CFRP wrapped and confined in concrete

Table 4.9. C-W specimen results for19 vs. 10, $1.5L_d$

Failure load	Avg. captured by supplementary bar	Failure mode
108KN	98%	Sensor went off scale
	Sg1	Sg2
Slope of best trend line	14.1	13.8
Strain at failure	6340	6013

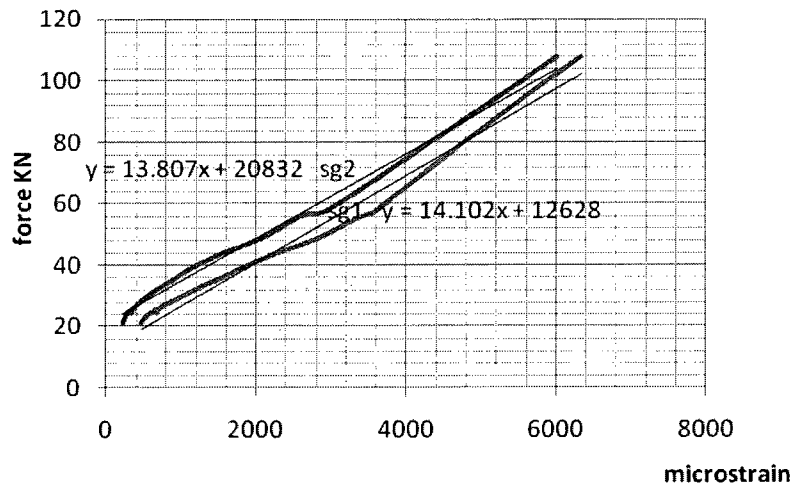

Figure 4.7. Force - strain, 19 vs.10, 1.5 L_d C-W

4.6 summary

Table 4.10 summarizes the results of the pilot tests. The first column in that table shows the specimen type and its components. First number shows the main bar diameter versus that of the supplementary bar. After that the length of the supplementary bar comes as a coefficient of the development length. "W" here stands for "Wrapped, as "C" for "confined and "C-W" for "Confined- Wrapped". Second column, shows the average captured strain by supplementary bar which was obtained by dividing the average strain measured by the sensor on the supplementary bar by that of the main bar. Third column shows the contribution of the attachment cross section in the assembly strain reading and was calculated by dividing the second strain gage reading by the third one and subtracting the result by a hundred percent. The forth column shows the correction factor that should be multiplied by the reading of the supplementary bar to get the strain of the main bar as if there were no bars attached. This last value was obtained by dividing the first strain gage value by the third one. In tables 4.11 and 4.12 same labeling principle has been used with "C" representing the confined and "C-W" for confined and wrapped specimens. Since only two strain gauges in these categories were installed, the ratio between ESG on the supplementary and main bar is calculated and tabulated herein as "average captured by supplementary bar".

Table 4.10. Summary of the results of the pilot tensile tests on wrapped specimens

Wrapped Specimens	Avg. Captured by supplementary bar	Contribution of attachment	Correction factor
13vs.6, L_d1st W	83%	21%	1.525
13vs.6, L_d2ndW	79.6%	24%	1.653
13vs.6, 1.5L_d1st W	89.4%	25%	1.491
13vs.6,1.5L_d2nd W	95%	16%	1.253
13 vs.6, 2 L_d 1st W	92%	23%	1.411
13 vs.6, 2 L_d2nd W	97%	23%	1.339
13 vs.10, L_d1st W	66%	32%	2.228
13 vs.10, L_d2nd W	71%	32%	2.071
13vs.10,1.5L_d1st W	70%	43%	2.506
13vs.10,1.5L_d2nd W	66%	32%	2.228
19 vs.6, L_d1st W	83.5%	19.7%	1.491
19 vs.6, L_d2nd W	80.4%	10.2%	1.385
19 vs.6, 1.5L_d1stW	89.3%	11.6%	1.266
19 vs.6, 1.5L_d2ndW	83.8%	11.7%	1.351
19 vs.6, 2L_d1stW	97.6%	13%	1.177
19 vs.6, 2L_d2ndW	93.7%	10%	1.185
19 vs.10, L_d1stW	67.1%	13%	1.712
19 vs.10, L_d2ndW	66.5%	17.5%	1.822
19 vs.10, 1.5L_d1stW	81.4%	22.8%	1.592
19 vs.10, 1.5L_d2ndW	78.6%	22%	1.631

Table 4.11. Summary of the results of the pilot tensile test on confined(C) specimens

Confined Specimens	Avg. Captured by supplementary bar	Confined Specimens	Avg. Captured by supplementary bar
13 vs.6, L_d1stC	82.85%	19 vs.6, L_d1stC	82%
13 vs.6, L_d2ndC	74.32%	19 vs.6, L_d2ndC	91.6%
13 vs.6, 1.5L_d1stC	69.8%	19 vs.6, 1.5L_d1stC	85.4%
13 vs.6, 1.5L_d2ndC	87.1%	19 vs.6, 1.5L_d2ndC	45%
13 vs.6, 2L_d1stC	98%	19 vs.6, 2L_d1stC	90.9%
13 vs.6, 2L_d2ndC	98.7%	19 vs.6, 2L_d2ndC	83.2%
13 vs.10, L_d1stC	*26%	19 vs.10, L_d1stC	74.5%
13 vs.10, L_d2ndC	71.6%	19 vs.10, L_d2ndC	65%
13 vs.10, 1.5L_d1stC	70%	19 vs.10, 1.5L_d1stC	86.5%
13 vs.10, 1.5L_d2ndC	96.6%	19 vs.10, 1.5L_d2ndC	81.8%

*Concrete cover did not integrate the bars

Table 4.12. Summary of the results of the confined - wrapped (C-W) specimens

Wrapped-Confined specimens	Avg. strain Captured by supplementary bar	Wrapped-Confined specimens	Avg. strain Captured by supplementary bar
13 vs.6, L_d C-W	83.3%	19 vs.6, L_d CW	N/A
13 vs.6, 1.5L_d C-W	98%	19 vs.6,1.5L_dCW	96.4%
13 vs.6, 2L_d C-W	95%	19 vs.6,2L_d CW	93.4%
13 vs.10, L_d C-W	N/A	19 vs.10,L_d CW	N/A
13 vs.10, 1.5L_d C-W	99.5	19vs.10,1.5L_dCW	98%

4.7 Discussion

Observation of the above tables show that while 10mm supplementary bar captures about seventy percent of the strain of the main bar, in wrapped cases, 6mm bar shows significantly higher values of over 90 percent. The fact that 19mm main bars showed better agreement with the supplementary bar reveals that the less the diameter of the supplementary bar, the less the correction factor.

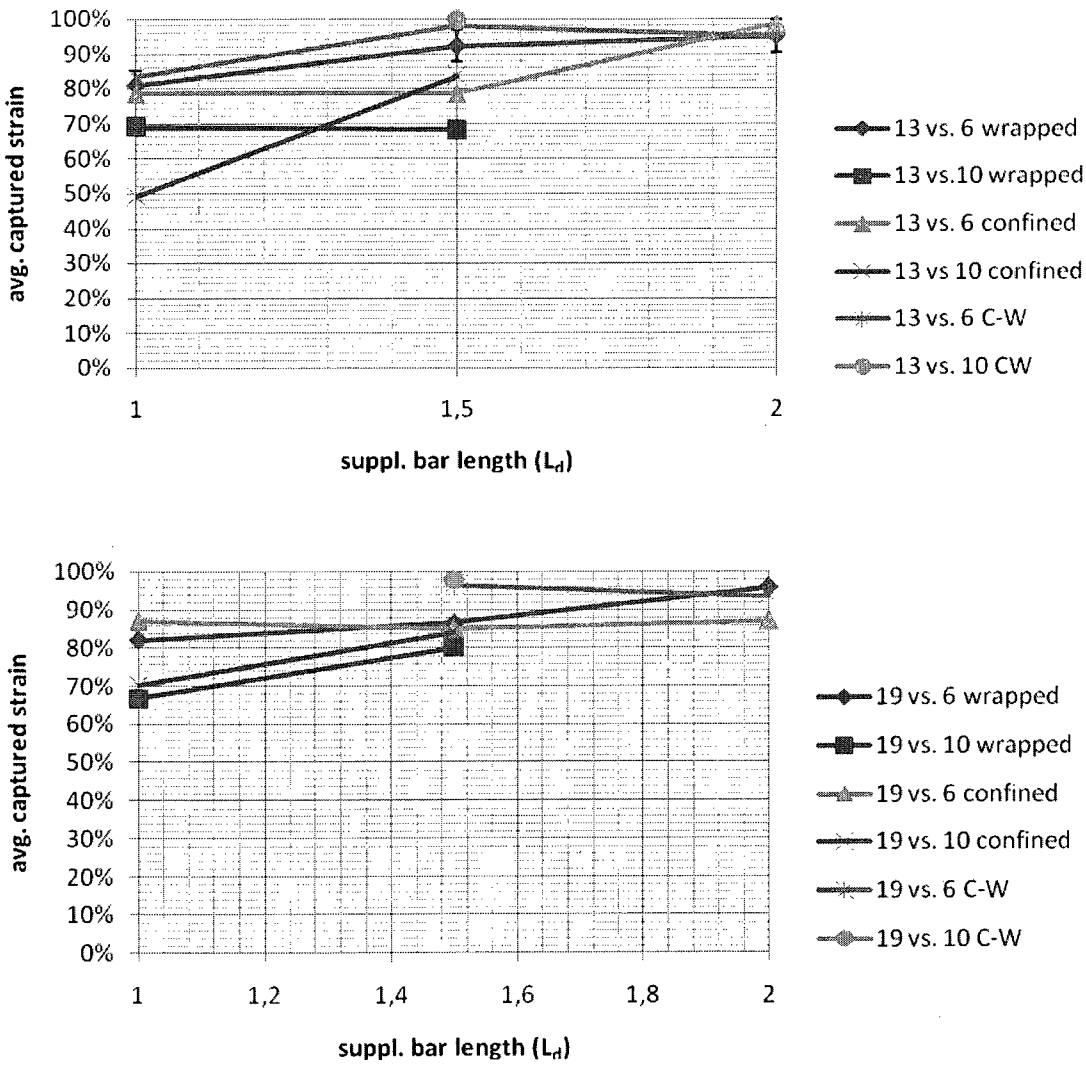

Figure 4.8 Comparison summary curves of average captured strain by #13 mm samples (top) and #19 mm samples (bottom)

4.8 Comparison Test

This test was conducted to get the gage factor for each type of sensors that were planned to be tested in each beam. In fact it was necessary to find out at any given load what strain each sensor reads. A set of tension tests was carried out on a tension specimen with three differrent types of sensors externally bonded on its surface. Two electrical strain gages, a Fabry- Perot, and a Fiber Bragg Grating FOS were externally bonded onto the specimen's surface. Loading was applied in step and monotonic loading. The readings of the two FOS types were compared to that of electrical strain gauges since their readings were close to theoretical values. Data acquisition system of the FBG sensors reads the shift in vawelength which needs the gage factor to convert to strain. The scaling factor for FBG came out to start from 1270 decreasing finally to 900 as the force was increased. The FPI reader reports strain values directly; However they were not consistent with those of the strain gauges as well as with the analytically determined values. The FPI readings needed correction factor starting from 1.8 and decreased to 1.27 at maximum loading.

CHAPTER 5

RESULTS OF THE TESTS ON RC BEAMS

5.1 General

This chapter is divided into two main parts. The results and observations of the beam tests are described separately for each beam in the first part. The second part is allocated to the discussions and comparisons about the qualitative behavior of the different types of sensors installed in the beams.

5.2 Results of the two tested beams

The test results of the two full-scale GFRP reinforced concrete beams are presented in the following sections. Photos of the beams at failure and deformed longitudinal profiles of the beam prior to and at failure associated to each specimen as well as force-deformation and force-tensile strain curves are shown. The strain gauges reading in the mid-section and quarter-beam as well as scaled readings of the FOSs are graphed in here.

The recorded displacement of mid-span and third-spans of the centerline were employed in developing the longitudinal profile of the beams since no notable relative or torsional deformation was observed along the width of the beam during the tests. The mid-span deflection measured continuously by the potentiometers was employed for the purpose of drawing the force deformation curves. As for the force-strain curves, the mid-span strain of the rods was chosen to be the reference of the data. Beams were designed to undergo compression failure under 187.4KN of loading where the cracking moment was calculated to happen at 15.7 KN which were close to the experimental results. The

only difference in design and manufacture of the two beams was that in the first one, supplementary bars were attached to the main bar using CFRP sheets while in the second beam they were attached merely by plastic ties. This could give us a comparison of the performance of the attachment with and without CFRP sheets.

5.3 Sensors

Three different types of sensors were deployed in this test. In order to read the electrical strain gauges, potentiometers and the load cell, "strain smart" software was used which is compatible with the inter-technology reading devices. After defining each sensor, they were calibrated and zeroed before running the test and then they were launched before loading started. Electrical strain gauges were quarter bridges with 120 Ω of resistance. Potentiometers were used to measure the deflection of the beams. Two of them were used in the middle of the beam; one at each side and two more were placed below the two loading points. Variation in strain readings versus force or any other variable can be read or plotted during the test. Readings were recorded with rate of one per second.

Fiber Bragg gratings readings were acquired using the "Micron Optics" software, installed on the computer. The data acquisition system for FBG has four connecting channels that are extendable to 16 using an auxiliary device. Each channel can read a sensor or a series of multiplexed channels. By default, each sensor shows their original wave length at zero load which can be zeroed by the reference setting action. As strain changes, wavelength recorded by the sensors is displayed or graphed in nanometers. This can get converted to strains using the scaling factor derived in the previous stage. Readings can be recorded with the accuracy of 1000Hz, i.e. 1000 readings per second. In

order for the readings to be consistent with other sensors, data was acquired once per second for all the sensors. Data was saved in the form of a text file.

The software associated with the Fabry-Perot sensors is called "Fiso commander 2". The data acquisition device has 8 channels and it reads the data directly in form of strains although scaling was needed afterward. Each sensor had an index number which was inserted in the channel specified to that sensor. Then the sensor was zeroed and strains could be shown graphically or digitally. The FPIs cannot be multiplexed as opposed to the FBGs due to their functioning method.

5.4 Beam#1

Both beams were reinforced with four 13-mm GFRP rebars. First beam failed at 198KN in compression failure. The flexural cracks in the constant moment zone set off after the beam encountered force of 30KN which had been calculated to happen at 35KN. Cracks then propagated until at failure the compression part of the beam cracked smoothly between the two loading points. Fabry- Perot sensors survived until about 3600 mincostrains in the first beam whereas FBGs survived the whole loading range. Working range of FPIs is about 3300-4000 and they stayed within their working range limit. However FBGs survived until the breaking points of the beams of above 8000 micro strains. Both types showed great agreement with the theoretical values and with the electrical strain gages. Sensors on supplementary bars of two development length showed good agreement with those on the main bars. The small discrepancy between the readings of the two FBGs could have happened due to malfunctioning of the attachment or poor installation of the sensor. The FBGs used in this experimental program, had no cover on the pigtail, hence the installation process was extremely tough. During the tests, since the

load cell was not showing reasonable values of force, loading was interrupted at 87kN to check the calibration and then it was reloaded until failure. The strain values before and after the interruption were later synchronized to match the two parts. The maximum mid-span deflection of the beam at failure was 39 mm.

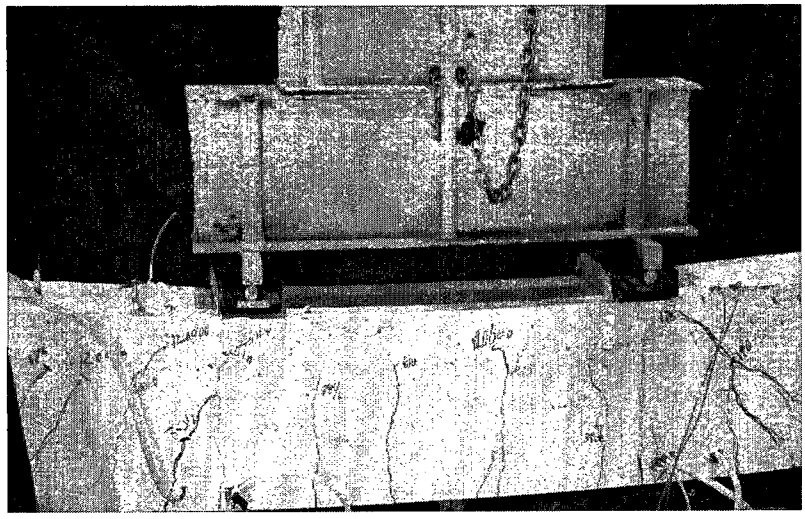

Figure 5.1. Beam#1 at failure

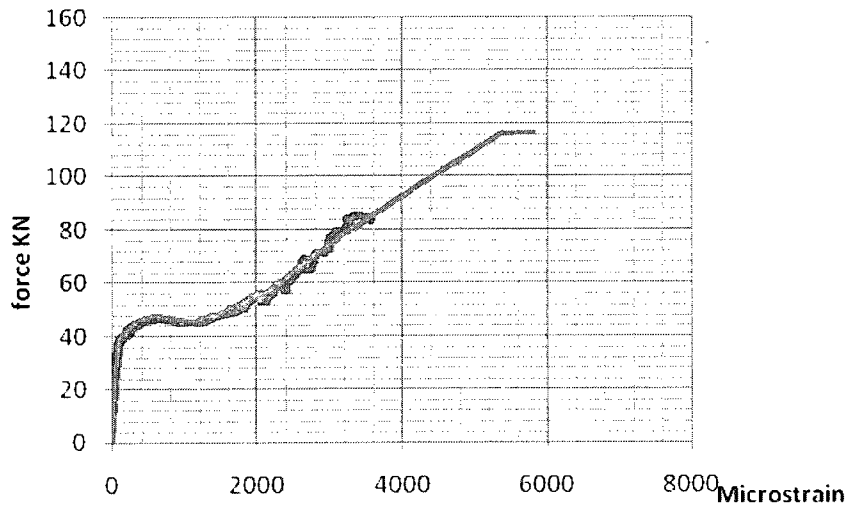

Figure 5.2. Mid-span tensile strain reading of the two FPIs compared with ESG

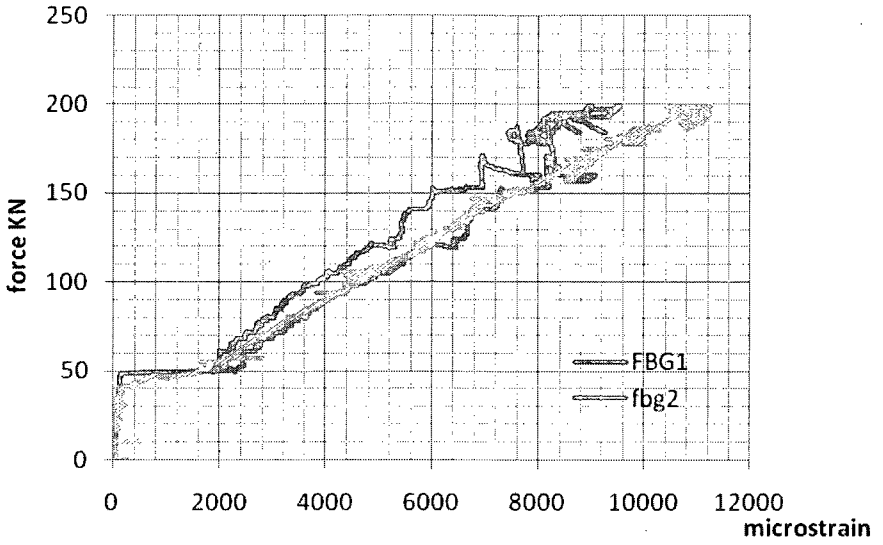

Figure 5.3. Mid-span tensile strain reading of the two FBGs compared to ESG

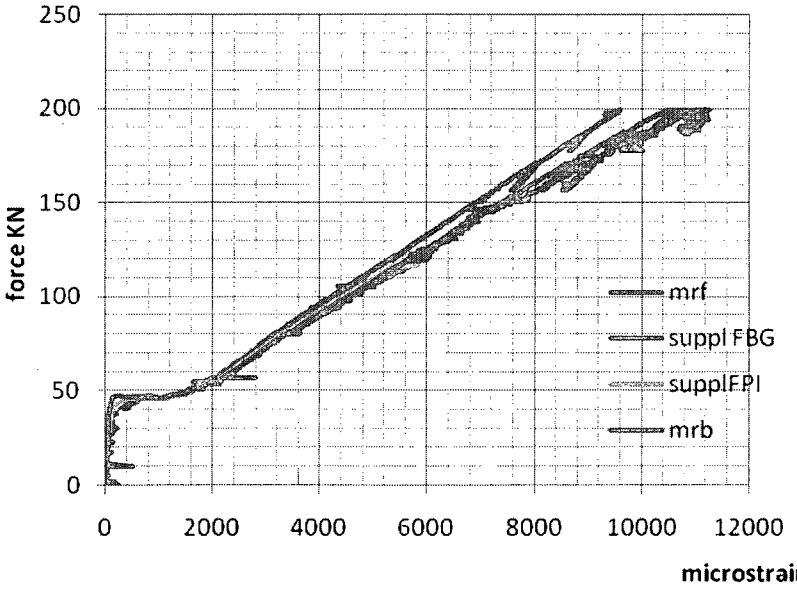

Figure 5.4. Comparison of mid-span tensile strain reading of the ESGs

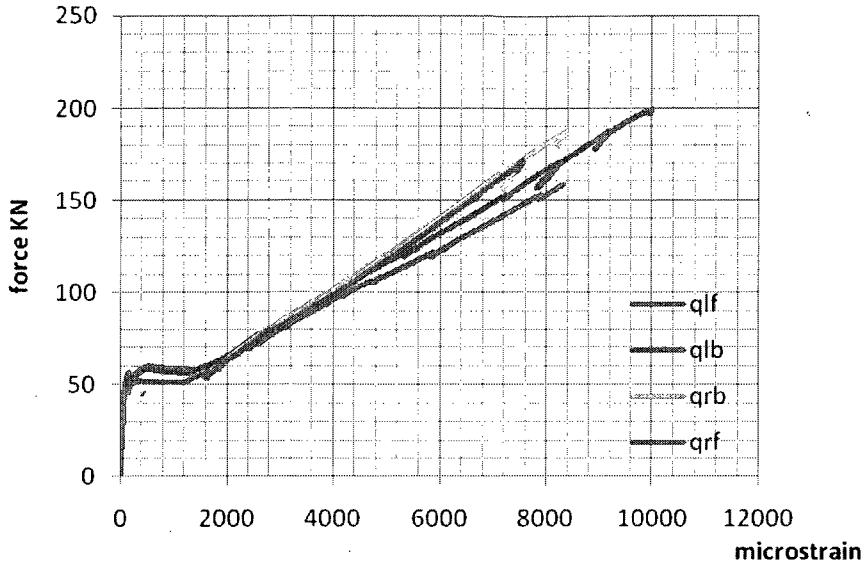

Figure 5.5. Comparison of Quarter-span tensile strain reading of the ESGs

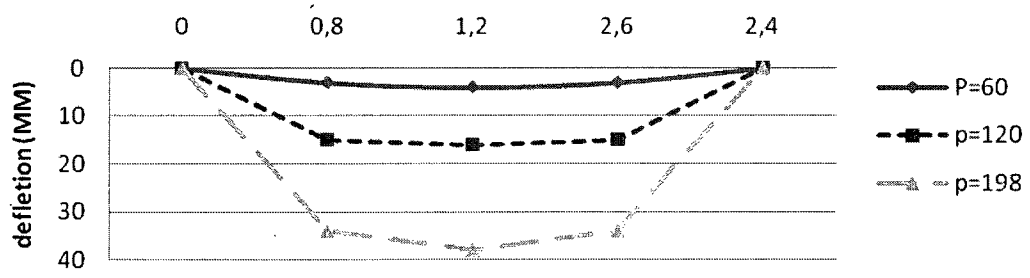

Figure 5.6. Longitudinal profile of the beam#1

5.5 Beam#2

The loading on the second beam was terminated at 150KN where all the sensors except for the FBG had become off scale. The flexural cracks in the constant moment zone set off after the beam encountered force of 48KN as compared to the calculated value of 40KN. Fabry- Perot sensors survived until over 4000 με whereas FBGs survived the whole loading range until the ending points of the test where strain in the mid-span

had exceeded 8000 με. Both types showed great agreement with the theoretical values and with the electrical strain gages. Although all the sensors were responsive after installation, casting concrete and placement of the beam on the supports, unfortunately some of them did not survive until the testing date. The FBG sensor on the supplementary bar did not survive probably due to fiber problem as they had no cover on the pigtail. However the FBG on the main bar and the two FPIs survived and responded very well regarding the theoretical values. The maximum mid-span deflection of the beam at failure was 39 mm.

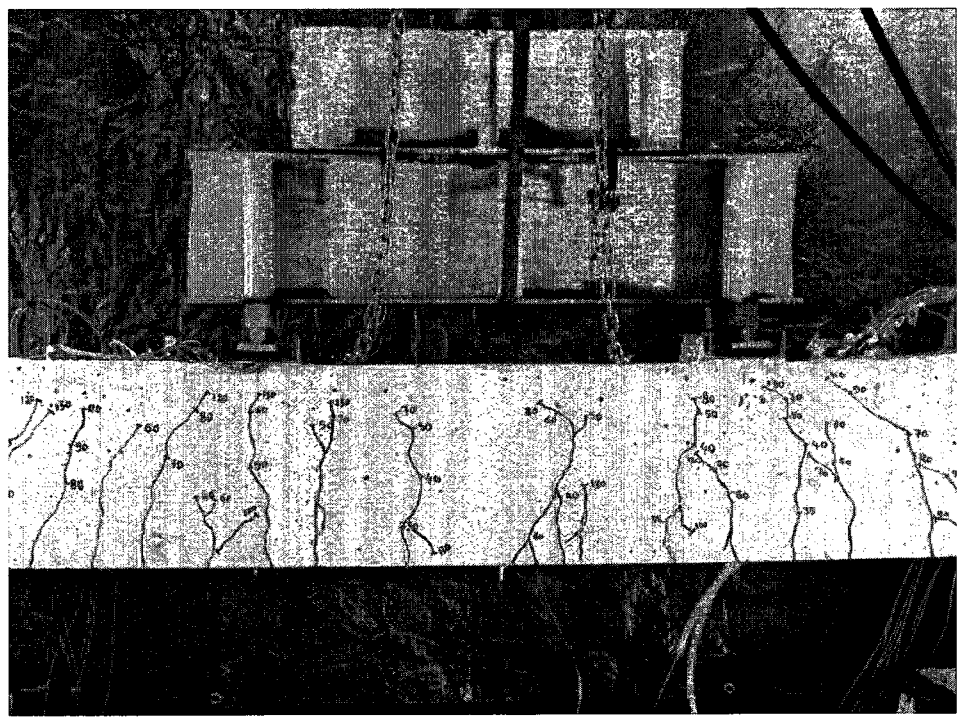

Figure 5.7 Beam#2 at failure

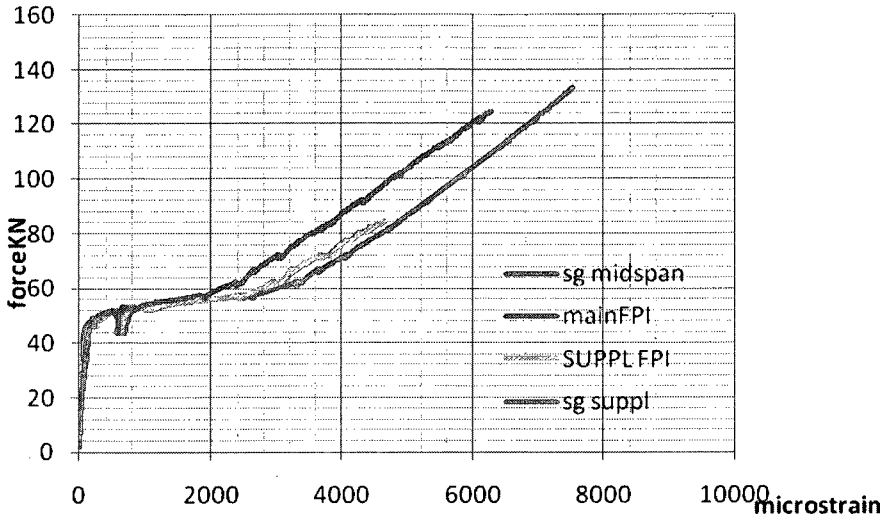

Figure 5.8. Mid-span tensile strain reading of the two FPIs compared to ESG

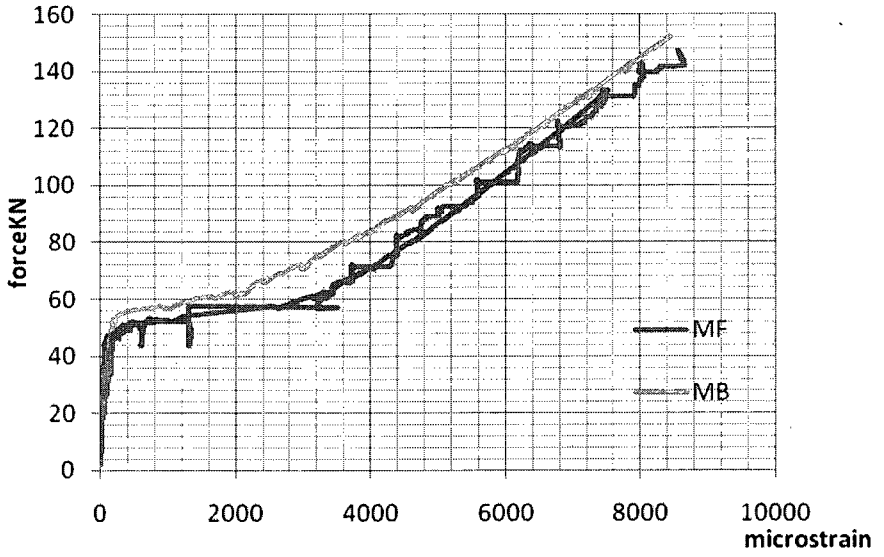

Figure 5.9. Mid-span tensile strain reading of the two ESGs compared to that of the FBG

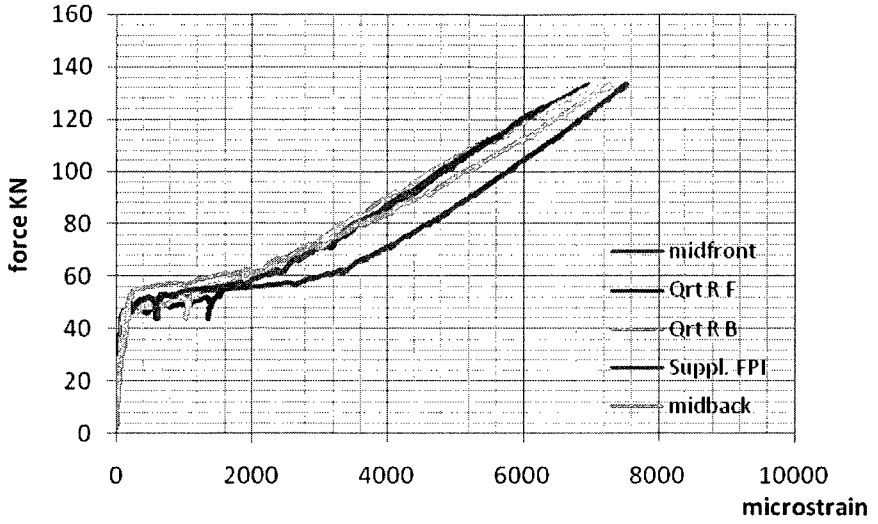

Figure 5.10. Comparison of mid-span and Quarter-span tensile strain reading of the ESGs

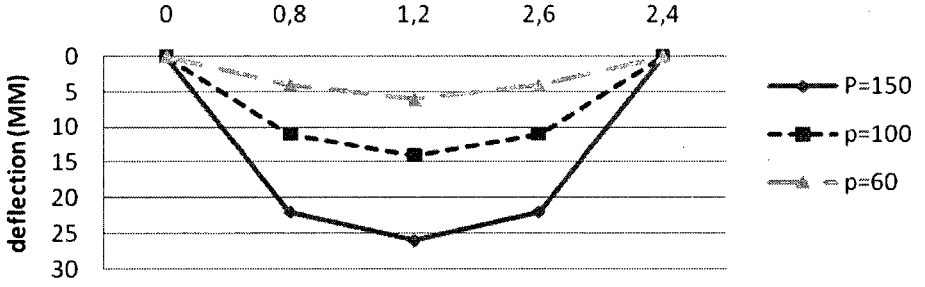

Figure 5.11. Longitudinal profile of the beam#2

Table 3.1 Theoretical values vs. experimental results of the beams

	M_n(kN.M)	ε_u	M_u(exp.)	$\varepsilon_{main\ bar}$	$\varepsilon_{suppl.\ bar}$
Beam#1	75	0.0129	79.2	0.00951	0.00899
Beam#2	75	0.0129	*80.2	*0.01379	*0.0115

*Values obtained by extrapolation

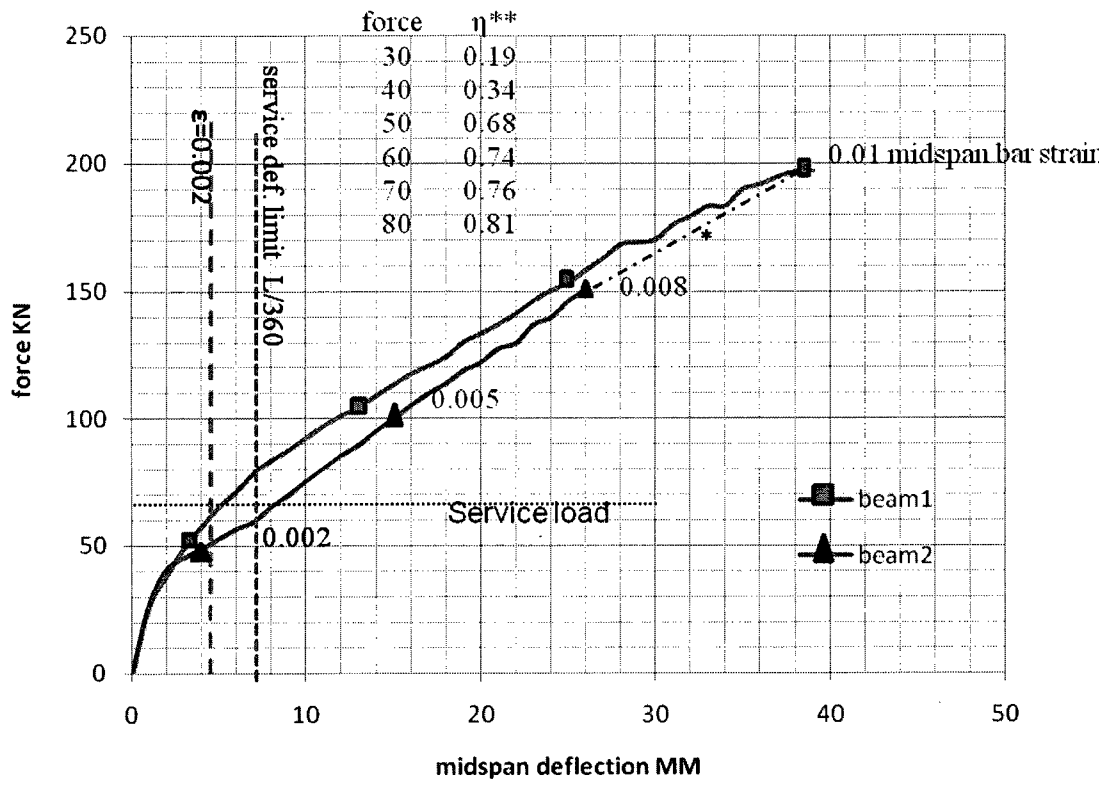

Figure 5.12. Beams deflection curves compared with service load and limitations

*Obtained by extrapolation

**η representing crack penetration has been caculated by deviding the crack hight by the section height and compared to force (KN)

5.6 Discussion

Observation of the result of the two beams shows that in both samples, strain readings of the sensors on supplementary bars were close to those of the main bars with low discrepancies. Comparing that to the results of pilot tests where discrepancies had come out to be averagely 5% and 6% it justifies the test results. Another aspect to highlight is the fact that in real beams or the efficiency of the protection method will be higher since the number of rebars is usually more than one which decreases the

interference in cross section area effect of the supplementary bar and shows strains closer to the reality. In terms of FOSs, both types responded very well within their working limit. The fact that FBGs last longer than FPIs makes them better candidates if strain of more than 3000 is to be measured. However fluctuations in the readings of FBGs might be an issue in deriving accurate local strain points while FPIs show smooth increase in reading when load increases.

CHAPTER 6

SUMMARY, CONCLUSIONS, AND FUTURE WORK

6.1 Summary

Fiber optic sensors are known as one of the best types of sensing devices for their accuracy and durability and have been frequently used in infrastructure in the past decade. However, lack of robustness of the bare fiber has been a major concern for the SHM engineers when it comes to deploying them in concrete structures. This deficiency can be mitigated by means of proper protection that would preserve the sensor and interfere least in the stress transferring from the reinforcement to the sensor. Fiber reinforced polymers are known as one of the most common new structural materials that are widely used as either reinforcing new structure or retrofitting the damaged structure. It had been proposed before and was developed in this study that FRP bar be used as the protection needed for making the FOS rugged. The sensor could be embedded in the grooved bar or mounted on the filed surface of the FRP bar.

The objective of this study was to study on the length and size of the protective GFRP bars as well as their type of attachment to the main bar in terms of optimized stress transfer and least interference in the strain reading.

In order to fulfill the goals of this research, an experimental study was planned and performed. A pilot study was performed on different lengths and sizes of supplementary bars which were attached to the main bar to host the sensor and protect it. The matrix of specimen consisted of two main bar sizes, namely #19 and #13 combined with two

supplemental bar sizes which were #10 or #6. The supplementary bars were chosen of different lengths of one, one and a half or two development length to assess its effect.

Specimens were tested in three categories in terms of attachment between the two bars. First type was planned to combine the two bars by means of CFRP sheets and was meant to show the stress transfer of the bars using such attachment method. Supplemental bars of the second category were attached to the main bars simply by plastic ties but then were covered by a concrete cylinder of 10 centimeters to see how concrete would act as a combining agent in the stress transferring process. The third category of specimens was a combination of the two previous cases, i.e. attached by CFRP sheets and confined in concrete. All the specimens were tested under tensile loading until failure. The stress transfer from the main to the supplemental bar was studied by monitoring the readings of the strain gauges that were installed on each bar. In the first category a third strain gauge was also installed on the main bar in the single- bar area.

The second part of the experimental study comprises testing on two medium- scaled GFRP reinforced RC beams to evaluate the protection method presented in the previous stage. Supplemental bar in the first beam were attached to the main bar by means of CFRP sheets while in the second one there were bound together by plastic ties. Three different types of sensors were installed on the reinforcing bars to capture their strain through the course of the loading. Two type of FOS namely FPI and FBG as well as electrical strain gages were deployed. Prior to that, an experimental comparison test was performed to derive scaling factor of each sensor. Beams were then tested under four point loading until failure and deflections and flexural strains were recorded.

6.2 Conclusions

Based on the results of the main and auxiliary tests, the following can be concluded:

1. The length of the supplemental bars of twice the development length ($2L_d$) showed the closest strain reading to the main bar regardless of the attachment method. However, the third category specimens showed good results even with supplemental bars of one and a half development length. This fact shows that the proposed attachment works well in concrete confinement. It could be concluded that in case due to any restrictions, supplementary bar of twice its development length cannot be used, shorter bar but no less than one and a half L_d could be used provided that they are appropriately attached to the main bar using attachment similar to the one proposed here.

2. It was observed that for all the tested specimens, the diameter of the supplemental bar has inverse effect on the transferred strain value. This would imply that smaller diameter for supplemental bar interferes less in the strain reading of the main bar.

3. The proposed protection method acts very well in hosting the fiber optic sensors and transferring the main bars strain as obviously there was subtle discrepancy between the reading of the sensors on the main and supplemental bars in the beam tests results.

4. Both types of fiber optic sensors used here show good agreement with the electrical strain gauges in strain readings. They work well within their working range limit. FBGs have shown to have survived until the final loading stage on the beams while FPIs did not work beyond their operating range of about 400 microstrains. The multiplexing capability

of FBGs is another useful feature that allows connecting multiple sensors to one channel. However more local oscillations were observed in the reading of FBGs as compared to smooth response of the FPIs.

6.3 Recommendations and future work

It should be noted that the abovementioned conclusions are based on the limited experimental work described herein and further experiments and analytical studies on FRP-protection and attachment methods should be conducted in order to validate and generalize the findings of this experimental program. Different types of loading such as dynamic or fatigue loading can affect the performance of such protections. Hence they have to be tested under those types of loading as well.

Since the compressive performance of GFRP is not notable, the response of the protective bars when subjected to compressive axial loads should be also inspected. More importantly, it is required to carry out further research on them while being installed in other types of structural elements such as walls or columns to study the effect of various internal loading on them.

Lastly, the results of this study can imply similar results for steel protection for FOS to be used beside steel reinforcement in concrete beams since development length is a general concept for all materials being used as reinforcement. Hence similar study on steel bar protection is recommended. Moreover, in order to decrease the length of the supplementary bar, hooked shapes or similar forms of supplementary bars could be also tested. Further investigation should be focused on different aspects of behavior of protected FOSs in order to ensure that their benefits last in long term as well.

REFERENCES

Bagchi, A., Murison, E., Mufti, A.A. and Noman, A.S., 2009, "Evaluation of a Rugged Fiber Optic Sensor System for Monitoring Reinforced Concrete Structures", Experimental Techniques, the Journal of the Society of Experimental Mechanics, In Press. (Published online in May, 2009, http://www3.interscience.wiley.com/cgi-bin/fulltext/122381150/PDFSTART).

Benmokrane, B., Quirion, M., El-Salakawy, E., Debaiky, A. and Lackey T. (2004). "Fabry-Perot Sensors for the Monitoring of FRP Reinforced Bridge Decks." Proc. SPIE, Vol. 5393, 95.

Benmokrane, B., Debaikey, A., El-Ragaby, A., Roy, R., El_gamal S., and El-Salakawy, E., "Laboratory and Field Performance of FOS Sensors in Static and Dynamic Strain Monitoring in Concrete Bridge Decks", SPIE/NDE Conference, San Diego, California, USA, March, 2006.

Canadian Standards Association (CSA). (2006). "S6-06: Canadian Highway Bridge Design Code (CHBDC)." Mississauga, Ontario.

Canadian Standards Association (CSA). (2002 and 2006). "S806-02: Design and Construction of Building Components with Fiber-Reinforced Polymers." Mississauga, Ontario.

CSA-A23.3 (1994). Design of Concrete Structures, Rexdale, Ontario: Canadian Standards Association.

CSCE, Canadian Society of Civil Engineering, Montreal. (2002) "Critical Citation: Canada's Infrastructure at the Crossroads", Quebec.

Choquet, P., Juneau, F. and Bessette, J. (2000). New generation of Fabry-Perot fiber optic sensors for monitoring structures. In: Nollet, M.-J. and Tre´panier, M. (eds), Proceedings of SPIE's 7th Annual International Symposium on Smart Structures and Materials, Newport Beach, California.

Fernando, G. F., Hameed, A., Winter D., Tetlow, J., Leng, J., Barnes, R., Mays, G. and Kister, G. 2003. "Structural Integrity Monitoring of Concrete Structures via Optical Fiber Sensors: Sensor Protection Systems." Journal of Structural Health Monitoring; 2; 123

Gebremichael, Y.M., Lia W., Boyle W.J.O., Meggitt B.T., Grattan K.T.V., McKinley B. , Fernando G.F. , Kister G. ,Winter D. ,Canning L. ,Luke S. "Integration and assessment of fiber Bragg grating sensors in an all-fiber reinforced polymer composite road bridge" Journal of Sensors and Actuators A: PhysicalVolume 118, Issue 1, 31 January 2005, Pages 78-85

Gheorghiu, C, Labossie`re, P. and Proulx, J. (2005). "Fiber Optic Sensors for Strain Measurement of CFRP-strengthened RC Beams" Journal of Structural Health Monitoring; 4; 67

Gheorghiu C., Labossiere, P., Proulx J. (2004) "Fatigue and Post-Fatigue Reliability of Fabry-Perot FOS Installed on CFRP-Strengthened RC-Beams", Second International Workshop on Structural Health Monitoring (SHM 2004), Winnipeg, Canada, September 21-23, pp 215-228.

Grossmann, B.G. and Huang, L-T. (1998). Fiber optic sensor array for multi-dimensional strain measurement. Smart Materials and Structures, 7, 159–165.

http://www.fyfeco.com/products/pdf/tyfo%20sch-11up%20comp.pdf

Hong-Nan L., Dong-Sheng L., Gang-Bing S. Recent applications of fiber optic sensors to health monitoring in civil engineering.

ISIS Canada (The Canadian Network of Centres of Excellence on Intelligent Sensing for Innovative Structures) (2001). "Design manual No. 1: Installation, use and repair of fiber optic sensors." Winnipeg, Manitoba.

ISIS Canada (2001). "Design manual No. 2: Guidelines for structural health monitoring." Winnipeg, Manitoba.

ISIS Canada (2001). "Design manual No. 3: Reinforcing concrete structures with fiber reinforced polymers." Winnipeg, Manitoba.

ISIS Canada (2001). "Design manual No. 6: Civionics Specifications." Winnipeg, Manitoba.

Kister, G., Badcock, R.A., Gebremichael, Y.M., Boyle, W.J.O., Grattan, K.T.V., Fernando, G.F. and Canning, L. 2007. "Monitoring of an all-composite bridge using Bragg grating sensors" Journal of Construction and Building Materials 21

Kister, G., Winter, D., Badcock, R.A., Gebremichael, Y.M., Boyle, W.J.O., Meggitt, B.T., Grattan, K.T.V., Fernando, G.F. (2007). "Structural health monitoring of a composite bridge using Bragg grating sensors. Part 1: Evaluation of adhesives and protection systems for the optical sensors" Journal of Engineering Structures 29 440–448

Maalej, M., Ahmed, S.F.U., Kuang, K.S.C. and Paramasivam, P. (2004). "Fiber Optic Sensing for Monitoring Corrosion-Induced Damage" Structural Health Monitoring; 3; 165

Mufti, A.A. (2002) Structural health monitoring of innovative Canadian civil engineering structures. Structural Health Monitoring, 1(1), 89–103. 15. Rivera E, Mufti A. A, Thomson D J, "Civionics specifications", ISIS Canada Design Manual, 2004.

Roctest Ltd. (2000). Sensoptic Fiber Optic Sensors, Strain Gauge Fabry-Perot, FOS Series (Instructions Manual), Roctest Ltd., St-Lambert, Québec (in French).

Sika Canada Inc. http://www.sika.ca/con-msds-sikadur35himodlv-ca.pdf

Tennyson, R.C., Mufti, A.A., Rizkalla, S., Tadros, G.and Benmokrane, B. (2001). Structural health monitoring of innovative bridges in Canada with fiber optic sensors. Smart Materials and Structures, 10(3), 560–573.

Vishay-Micro-Measurements Strain Gage Installations with M-Bond 200 Adhesive Document No.: 11127

Zhang, B., Benmokrane, B., and Nicole, J.F. (2003). "Laboratory Evaluation of Fiber-Optic Sensors for Strain Monitoring" American Society of Civil Engineers.

Zhou, G. and Sim, L.M. (2002). Damage detection and assessment in fiber-reinforced composite structures with embedded fiber optic sensors – review. Smart Materials and Structures, 11, 925– 936.

APPENDIX A: Pilot Study Results

A.1. #13mm main bar vs. #6mm supplementary bar of one development length (310mm) CFRP wrapped

Table A.1. Second Specimen results for 13 vs.6 L_d

Failure load	Avg. Captured by supplementary bar	Contribution of attachment	Correction factor	Failure mode
47.67KN	79.6%	24%	1.65	Anchorage failure
		Sg1	Sg2	Sg3
Slope of best trend line		7.14	8.98	5.45
Strain at failure		6708	5175	8750

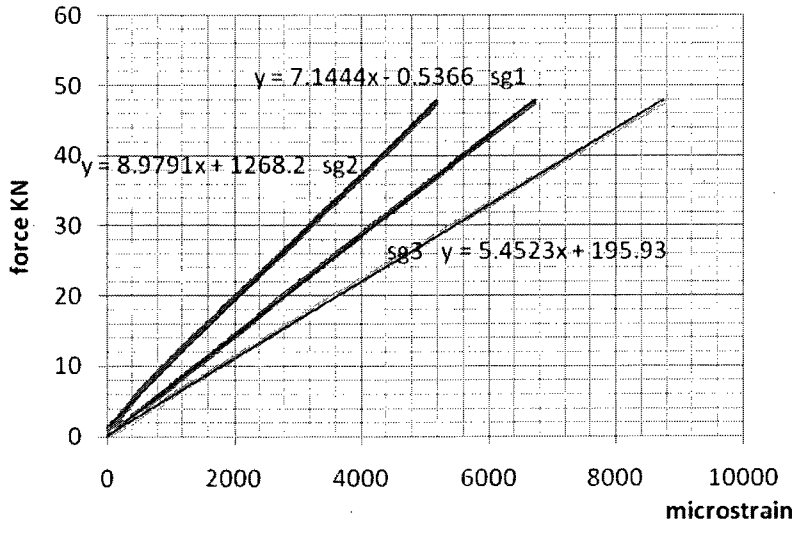

Figure A.1. Force - strain, 13 vs.6, L_d second specimen

A.2. #13mm main bar vs. #6mm supplementary bar of one and a half development length (465mm) CFRP wrapped

Table A.2. First Specimen results for13 vs.6, 1.5 L_d

Failure load	Avg. Captured by supplementary bar	Contribution of attachment	Correction factor	Failure mode
42.9KN	89.4%	%25	1.49	Anchorage failure
		Sg1	Sg2	Sg3
Slope of best trend line		7.29	8.16	5.48
Strain at failure		5796	5141	7764

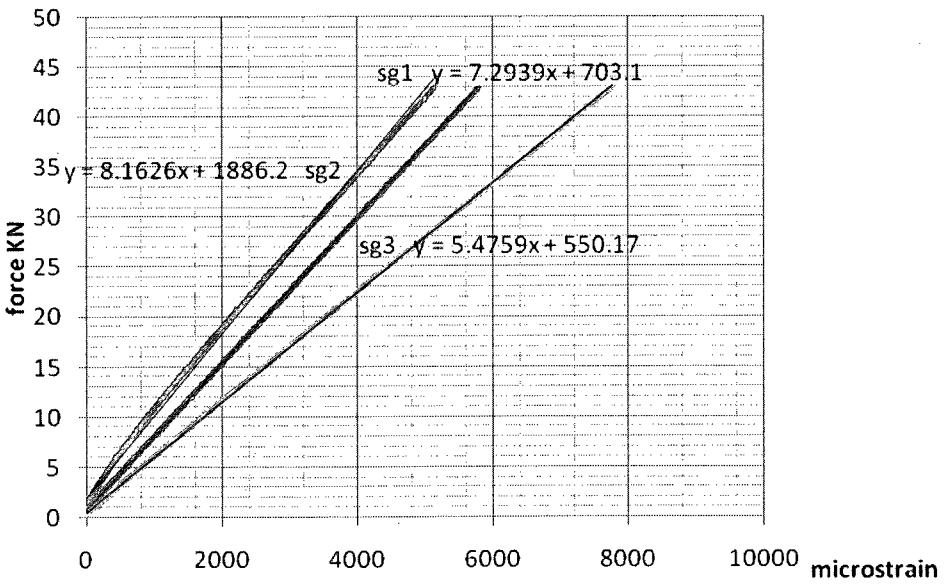

Figure A.2. Force vs. strain, 13 vs.6, 1.5L_d first specimen

Table A.3. Second Specimen results for13 vs.6, 1.5 L_d

Failure load	Avg. Captured by supplementary bar	Contribution of attachment	Correction factor	Failure mode
64.77KN	95%	16%	1.25	Anchorage failure
		Sg1	Sg2	Sg3
Slope of best trend line		7.25	7.61	6.1
Strain at failure		8901	8168	10562

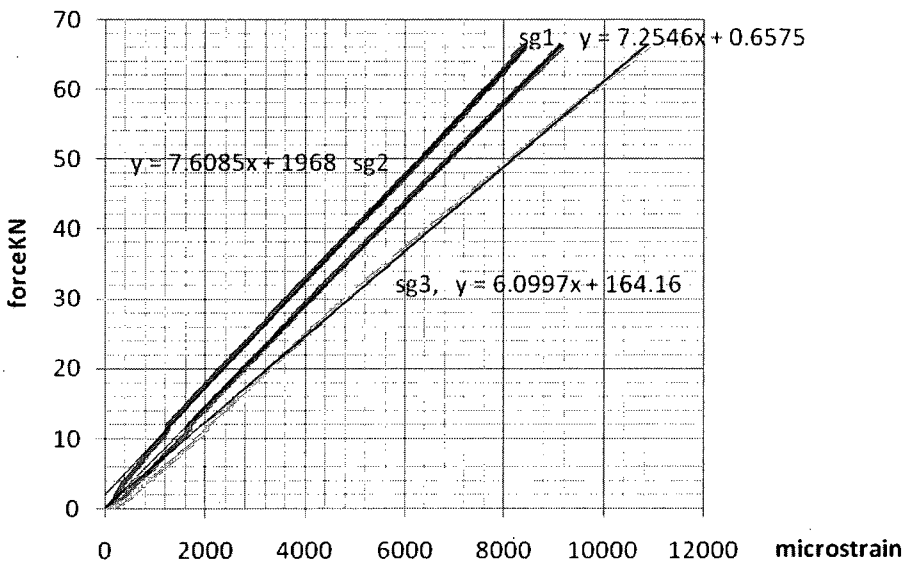

Figure A.3. Force - strain, 13 vs.6, 1.5 L_d second specimen

A.3. #13mm main bar vs. #6mm supplementary bar, two development length (620mm) CFRP wrapped

Table A.4. First Specimen results for13 vs.6, 2 L_d

Failure load	Avg. Captured by supplementary bar	Contribution of attachment	Correction factor	Failure mode
22.78KN	92%	23%	1.41	Anchorage failure
		Sg1	Sg2	Sg3
Slope of best trend line		8.9	9.6	n/a
Strain at failure		2390	2194	n/a

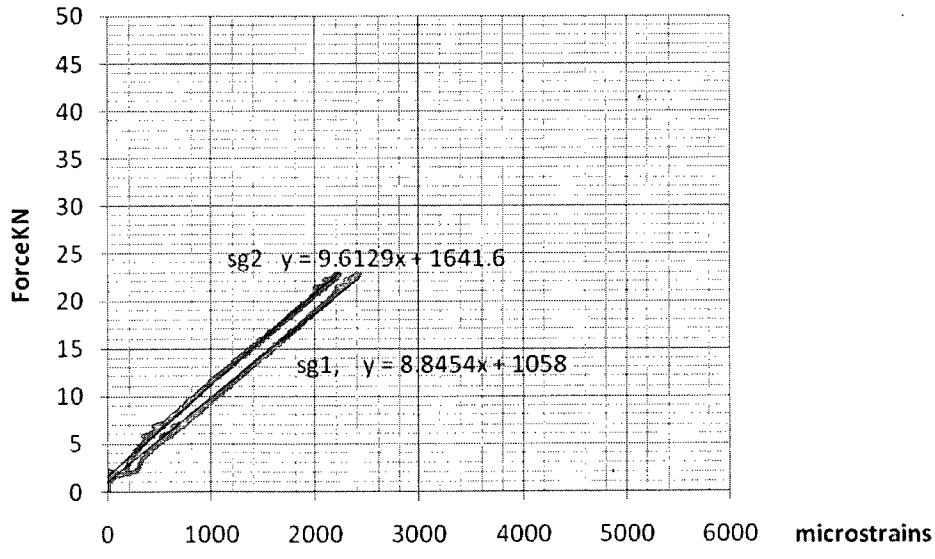

Figure A.4. Force - strain, 13 vs.6, 2 L_d first specimen

Table A.5. Second Specimen results for13 vs.6, $2L_d$

Failure load	Avg. Captured by supplementary bar	Contribution of attachment	Correction factor	Failure mode
23.26KN	97%	23%	1.33	Anchorage failure
		Sg1	Sg2	Sg3
Slope of best trend line		9.279	9.03	n/a
Strain at failure		2342	2372	n/a

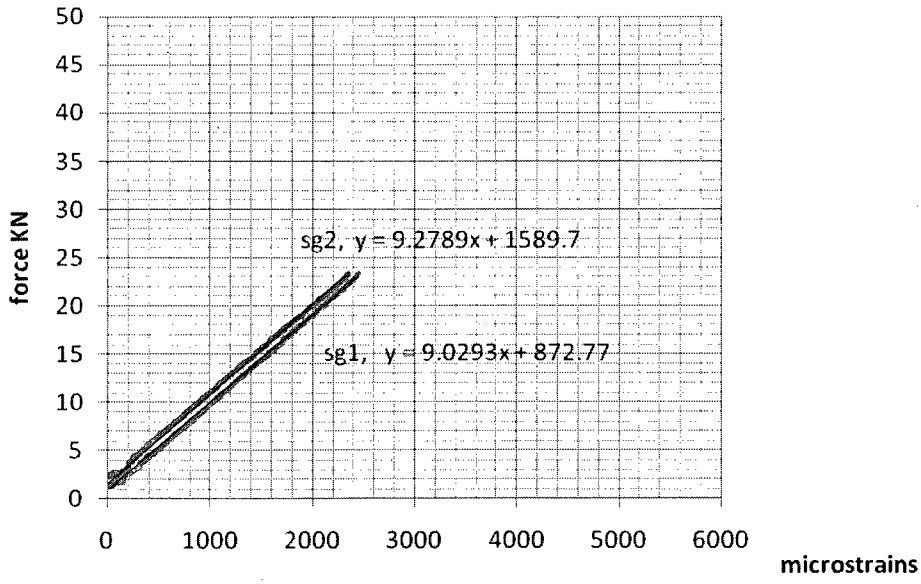

Figure A.5. Force - strain, 13 vs.6, 2 L_d second specimen

A.4. #13mm main bar vs. #10mm supplementary bar of one development length (420mm) CFRP wrapped

Table A.6. First Specimen results for13 vs.10, L_d

Failure load	Avg. Captured by supplementary bar	Contribution of attachment	Correction factor	Failure mode
60KN	66%	12%	2.22	FRP bar ruptured
		Sg1	Sg2	Sg3
Slope of best trend line		6.6438	10	n/a
Strain at failure		9702	5351	n/a

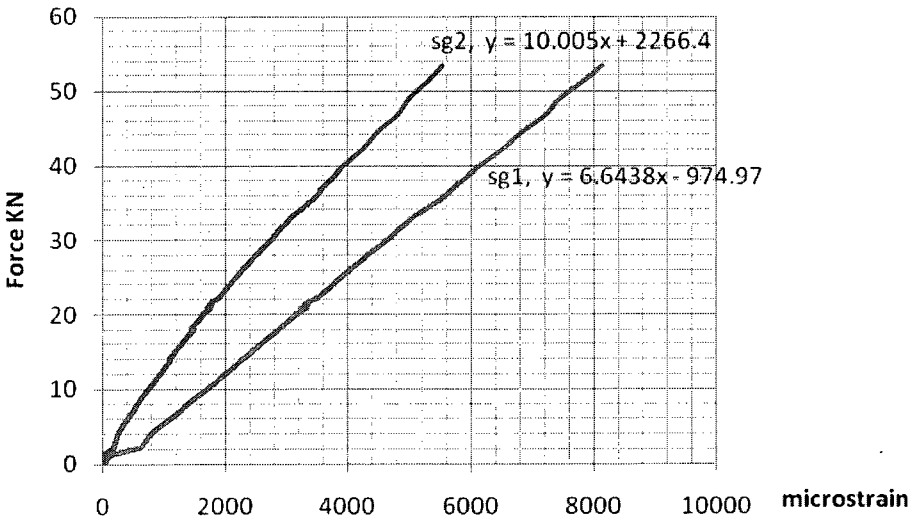

Figure A.6. Figure force vs strain, 13 vs.10, L_d first specimen

Table A.7. Second Specimen results for13 vs.10, L_d

Failure load	Avg. Captured by supplementary bar	Contribution of attachment	Correction factor	Failure mode
56.16KN	71%	32%	2.08	FRP bar ruptured
		Sg1	Sg2	Sg3
Slope of best trend line		8.1	11.3	n/a
Strain at failure		7347	4879	n/a

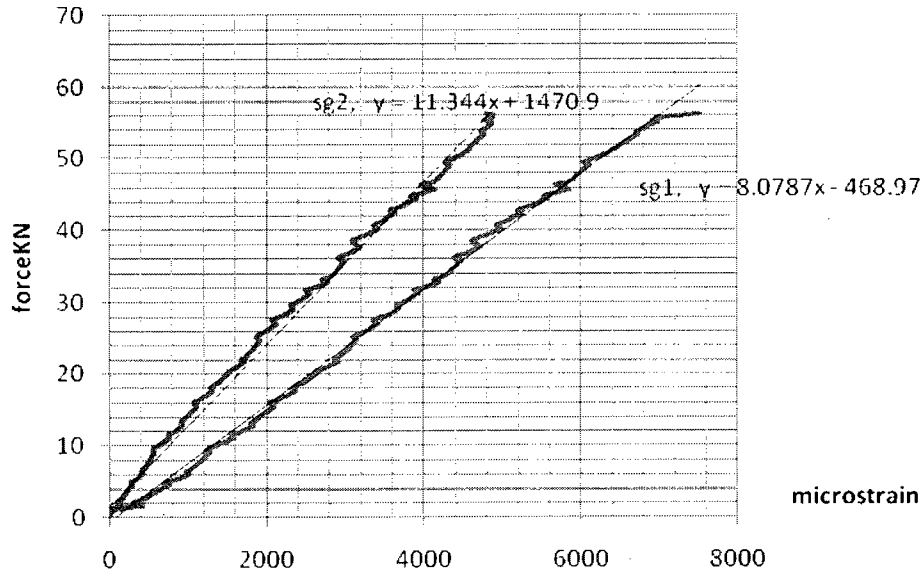

Figure A.7. Force vs strain, 13 vs.10, L_d second specimen

A.5. #13mm main bar vs. #10mm supplementary bar of one and a half development length (630mm) CFRP wrapped

Table A.8. First Specimen results for13 vs.10, 1.5Ld

Failure load	Avg. Captured by supplementary bar	Contribution of attachment	Correction factor	Failure mode
24.4KN	70%	43%	2.5	Anchorage failure
		Sg1	Sg2	Sg3
Slope of best trend line		8.6	12.29	n/a
Strain at failure		3005	1966	n/a

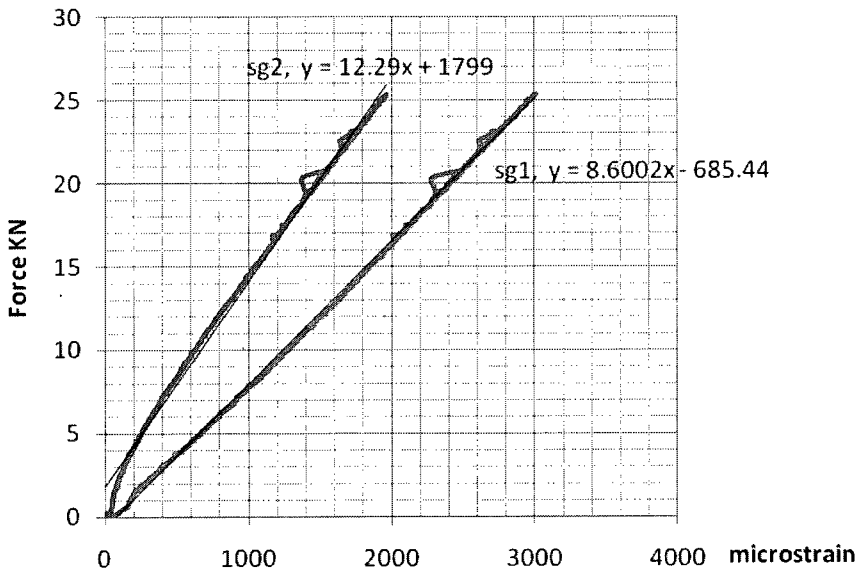

Figure A.8. Force vs. strain, 13 vs.10, 1.5L_d first specimen

Table A.9. Second Specimen results for13 vs.10, 1.5Ld

Failure load	Avg. Captured by supplementary bar	Contribution of attachment	Correction factor	Failure mode
23.3KN	66%	32%	2.22	Anchorage failure
		Sg1	Sg2	Sg3
Slope of best trend line		7.93	14.59	n/a
Strain at failure		2976	1561	n/a

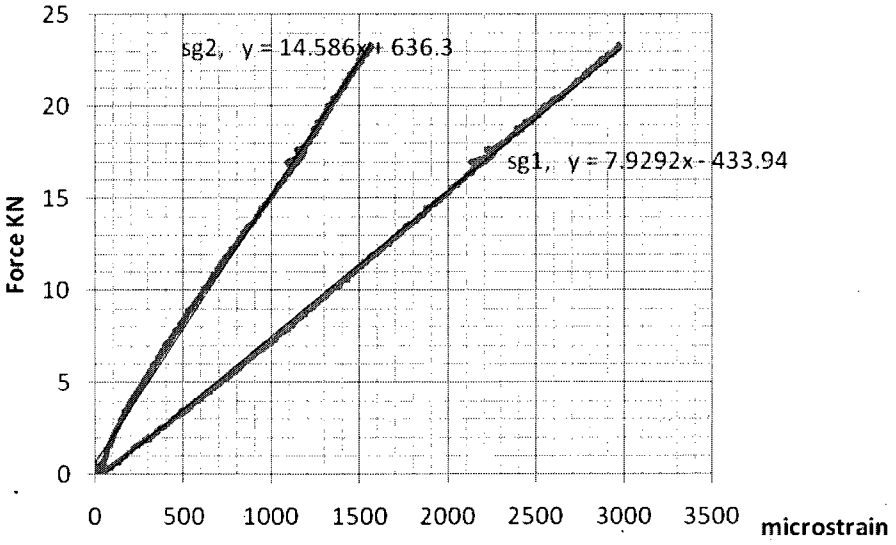

Figure A.9. Force vs. strain, 13 vs.10, 1.5 L_d second specimen

A.6. #19mm main bar vs. #6mm supplementary bar of one development length (310mm) CFRP wrapped

Table A.10. First Specimen results for19 vs.6, L_d

Failure load	Avg. Captured by supplementary bar	Contribution of attachment	Correction factor	Failure mode
77.58KN	83.53%	19.7%	1.41	Anchorage failure
		Sg1	Sg2	Sg3
Slope of best trend line		15.72	18.76	13.13
Strain at failure		4933	4108	5872

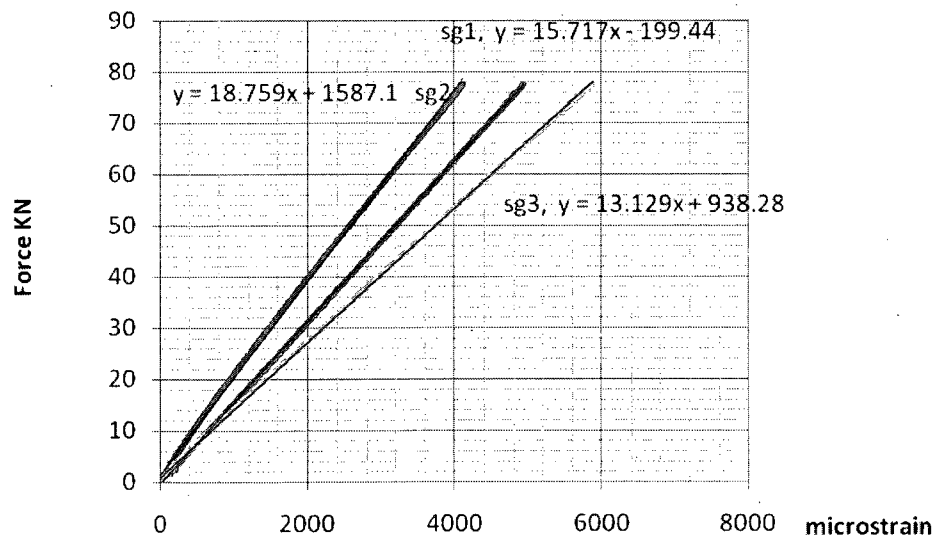

Figure A.10. Force vs. strain, 19 vs.6, L_d first specimen

Table A.11. Second Specimen results for19 vs.6, L_d

Failure load	Avg. Captured by supplementary bar	Contribution of attachment	Correction factor	Failure mode
79.49KN	80.4	10.2%	1.37	Connection failure
		Sg1	Sg2	Sg3
Slope of best trend line		14.822	18.444	13.449
Strain at failure		5397	4271	5858

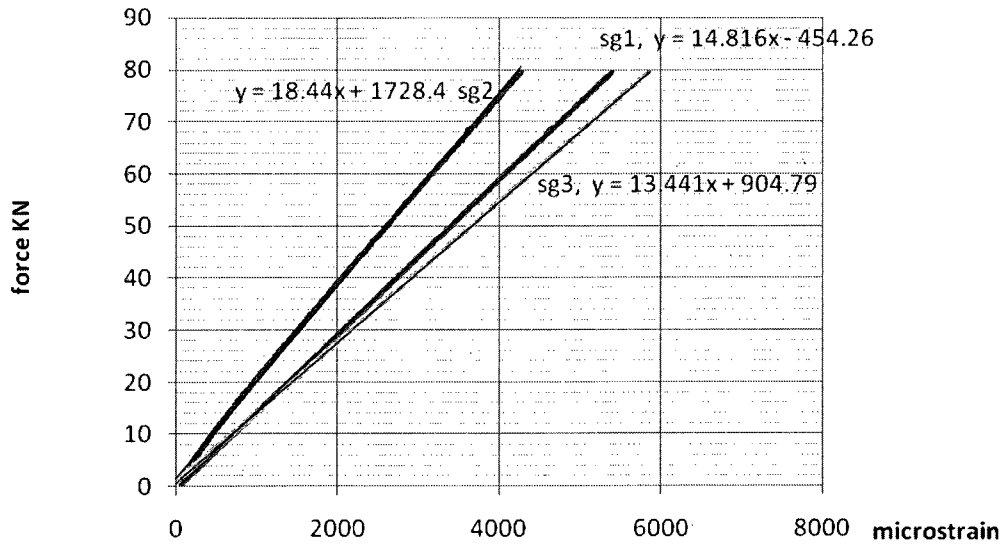

Figure A.11. Force vs. strain, 19 vs. 6, L_d second specimen

A.7. 19mm diameter main bar vs. 6mm diameter supplementary bar of one and a half development length (465mm) CFRP wrapped

Table A.12. First Specimen results for19 vs.6, $1.5L_d$

Failure load	Avg. captured by supplementary bar	Contribution of attachment	Correction factor	Failure mode
100.12KN	89.27	11.55%	0.79	Anchorage failure
		Sg1	Sg2	Sg3
Slope of best trend line		15.1	16.9	13.6
Strain at failure		6650	5698	7393

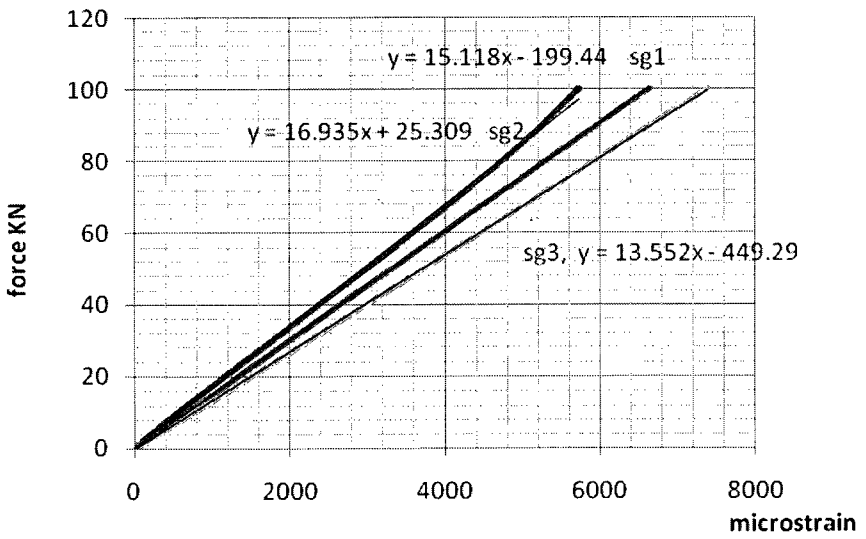

Figure A.12. Force - strain, 19 vs.6, $1.5L_d$ first specimen

Table A.13. Second Specimen readings for19 vs.6, $1.5L_d$

Failure load	Avg. captured by supplementary bar	Contribution of attachment	Correction factor	Failure mode
161.2KN	83.8	11.66%	0.74	Anchorage failure
		Sg1	Sg2	Sg3
Slope of best trend line		15.16	18.09	13.578
Strain at failure		10726	7844	11821

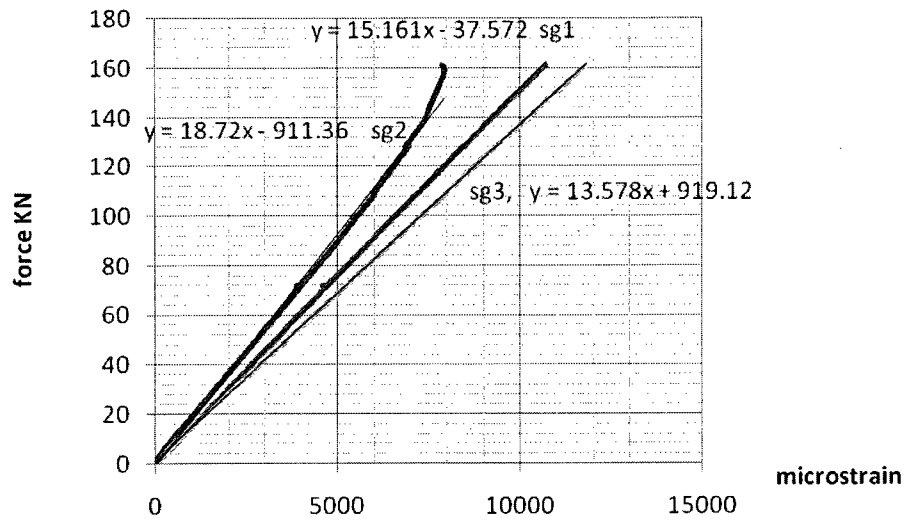

Figure A.13. Force- strain, 19 vs. 6, $1.5L_d$ second specimen

A.8. #19mm main bar vs. #6mm supplementary bar of two development length (620mm) CFRP wrapped

Table A.14. Second Specimen results for19 vs.6, $2L_d$

Failure load	Avg. captured by supplementary bar	Contribution of attachment	Correction factor	Failure mode
97.13KN	93.74%	10%	0.84	Connection failure
		Sg1	Sg2	Sg3
Slope of best trend line		14.94	15.937	n/a
Strain at failure		6546	6081	n/a

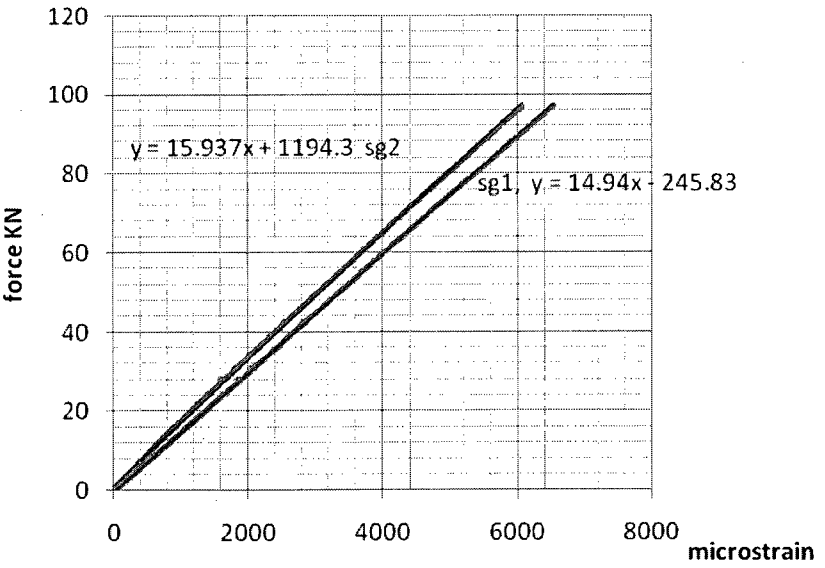

Figure A.14. Force- strain, 19 vs.6, $2L_d$ second specimen

A.9. #19mm main bar vs. #10mm supplementary bar of one development length (420mm) CFRP wrapped

Table A.15. First Specimen readings for19 vs.10, L_d

Failure load	Avg. captured by supplementary bar	Contribution of attachment	Correction factor	Failure mode
101KN	67.12%	13%	0.58	Anchorage failure
		Sg1	Sg2	Sg3
Slope of best trend line		15.933	23.738	13.9
Strain at failure		6347	4088	7315

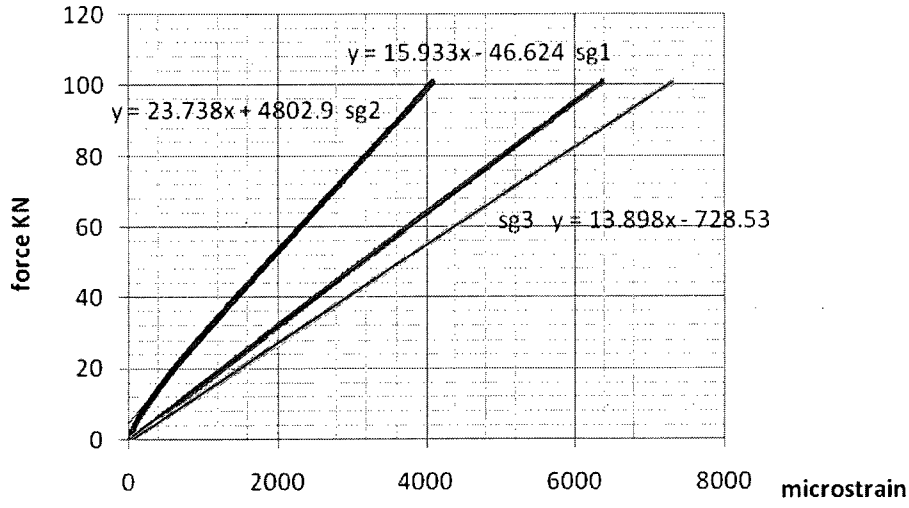

Figure A.15. Force - strain, 19 vs.10, L_d first specimen

Table A.16. Second Specimen readings for19 vs.10, L_d

Failure load	Avg. captured by supplementary bar	Contribution of attachment	Correction factor	Failure mode
59.75KN	66.51%	17.47%	0.55	Anchorage failure
		Sg1	Sg2	Sg3
Slope of best trend line		16.425	24.695	13.555
Strain at failure		3467	2373	4409

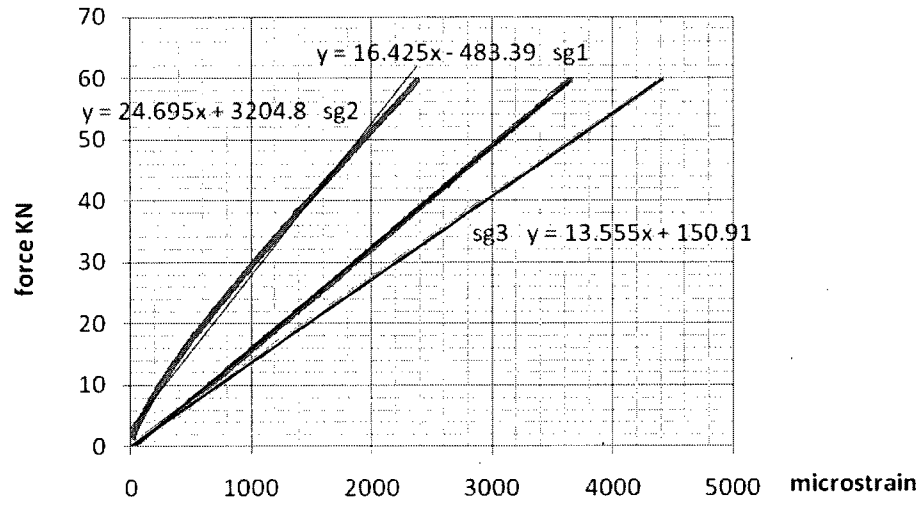

Figure A.16. Force- strain, 19 vs.10, L_d second pecimen

A.10. #19mm Main bar vs. #10mm supplementary bar of one and a half development length (630mm) CFRP wrapped

Table A.17. First Specimen readings for19 vs.10, $1.5L_d$

Failure load	Avg. captured by supplementary bar	Contribution of attachment	Correction factor	Failure mode
91.25KN	81.39%	22.83%	0.63	Anchorage failure
		Sg1	Sg2	Sg3
Slope of best trend line		16.6	20.4	12.8
Strain at failure		5531	3969	6972

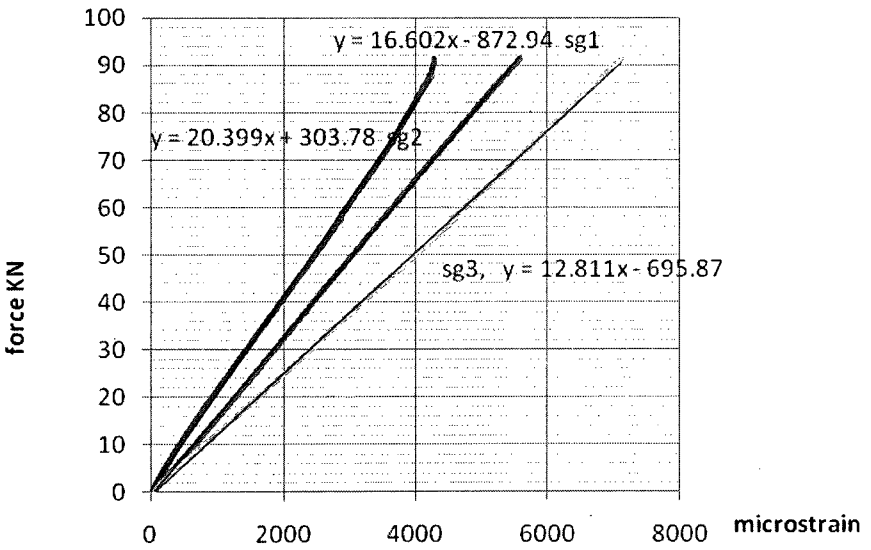

Figure A.17. Force - strain, 19 vs.10, $1.5L_d$ first pecimen

Table A.18. Second Specimen readings for19 vs.10, $1.5L_d$

Failure load	Avg. captured by supplementary bar	Contribution of attachment	Correction factor	Failure mode
78.5KN	78.61%	22%	0.61	Anchorage failure
		Sg1	Sg2	Sg3
Slope of best trend line		16.943	21.552	13.2
Strain at failure		4675	3465	5928

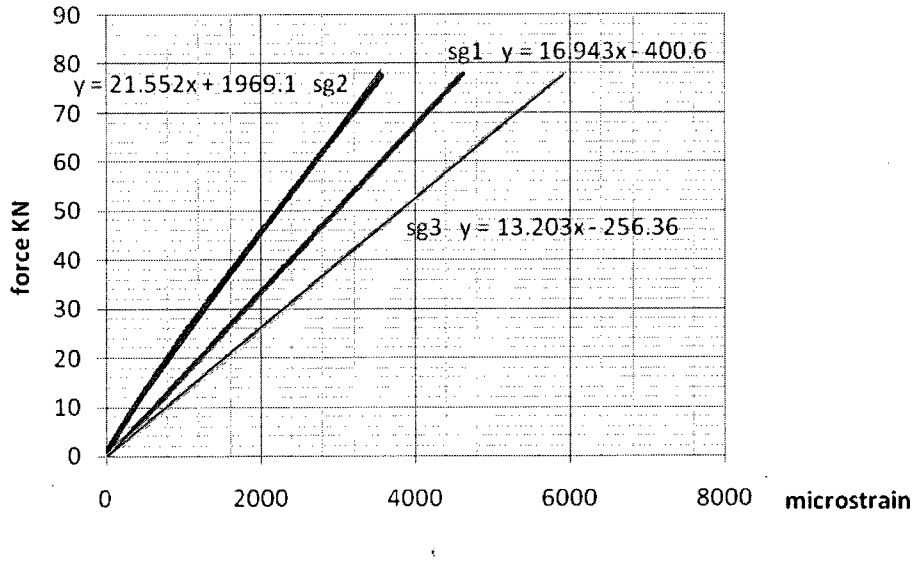

Figure A.18. Force - strain, 19 vs.10, $1.5L_d$ second pecimen

A.11. #13mm main bar of vs. #6mm supplementary bar of one development length (310mm) long, confined in concrete

Table A.19. First confined specimen results for13 vs.6, L_d

Failure load	Avg. captured by supplementary bar		Failure mode
75.32KN	82.85%		FRP bar ruptured
		Sg1	Sg2
Slope of best trend line		7.87	8.85
Strain at failure		9454	3924

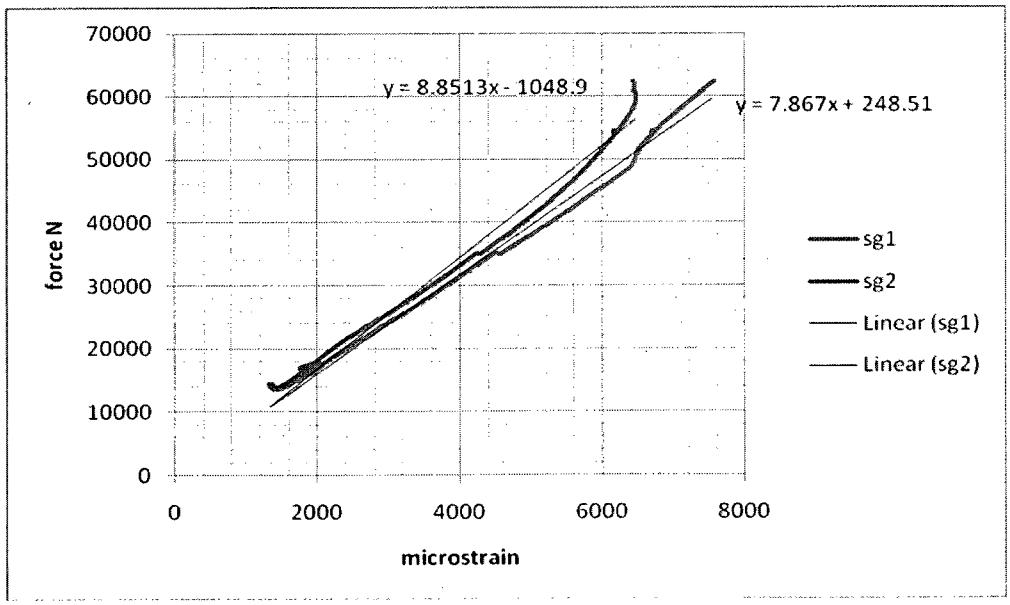

Figure A.19. Force - strain, 13 vs.6, L_d first confined specimen

Table A.20. Second confined specimen results for13 vs.6, Ld

Failure load	Avg. captured by supplementary bar	Failure mode
65.55KN	*74.32%	FRP bar ruptured
	Sg1	Sg2
Slope of best trend line	10.4	14.04
Strain at failure	7200	5360

* Concrete cover did not integrate the assembly preopely (manufacture error)

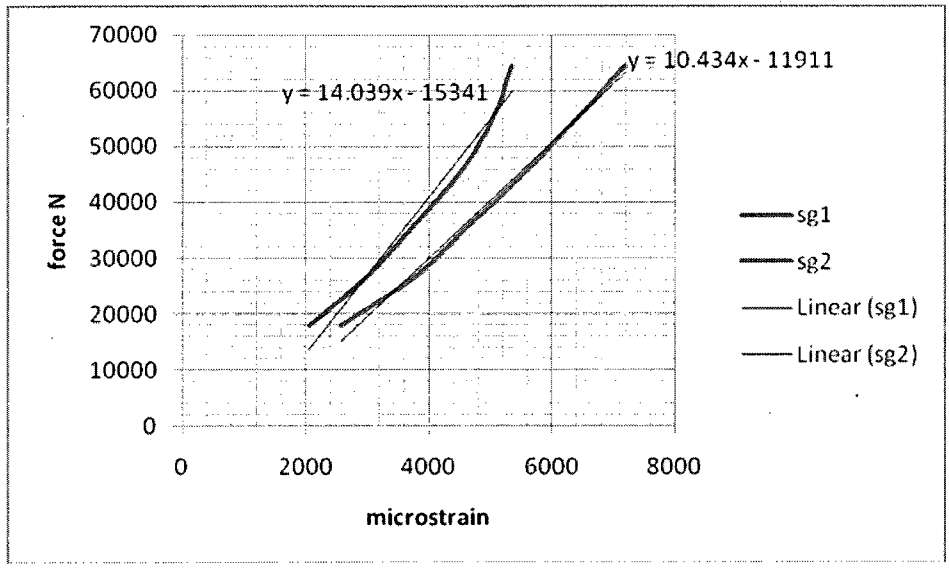

Figure A.20. Force - strain, 13 vs. 6, L_d second confined specimen

A.12. #13mm Main bar vs. #6mm supplementary bar of one and a half development length (465mm) long, confined in concrete

Table A.21. First confined specimen results for13 vs.6, 1.5Ld

Failure load	Avg. captured by supplementary bar	Failure mode
67.4KN	69.8%	FRP bar ruptured
	Sg1	Sg2
Slope of best trend line	6.5964	9.4486
Strain at failure	9872	6406

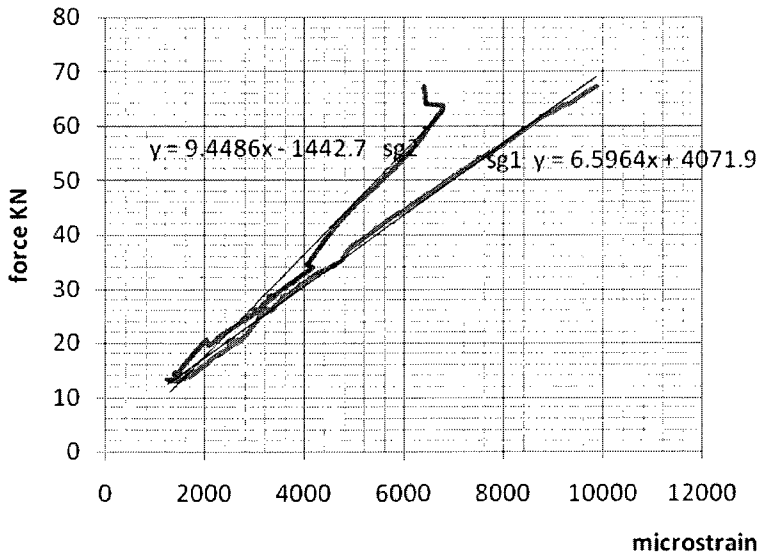

Figure A.21. Force - strain, 13 vs.6, 1.5L_d first confined specimen

Table A.22. Second confined specimen results for13 vs.6, 1.5Ld

Failure load	Avg. captured by supplementary bar	Failure mode
56.52KN	87.1%	Sensor went off scale
	Sg1	Sg2
Slope of best trend line	6.8255	7.8364
Strain at failure	8102	5943

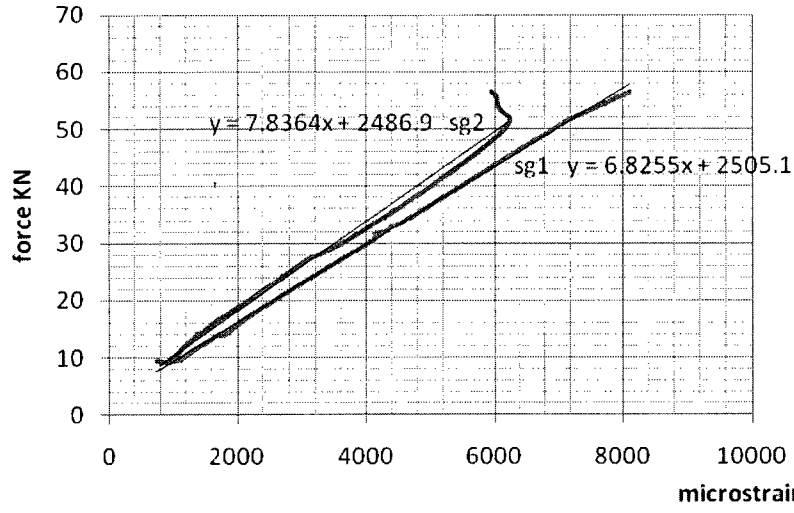

Figure A.22. Force - strain, 13 vs.6, 1.5L_d second confined specimen

A.13. #13mm main bar vs. #6mm supplementary bar of two development length (620mm), confined in concrete

Table A.23. Second confined specimen results for13 vs.6, 2Ld

Failure load	Avg. captured by supplementary bar	Failure mode
57.6KN	98.69%	Concrete disintegrated
	Sg1	Sg2
Slope of best trend line	6.91	7
Strain at failure	7866	6863

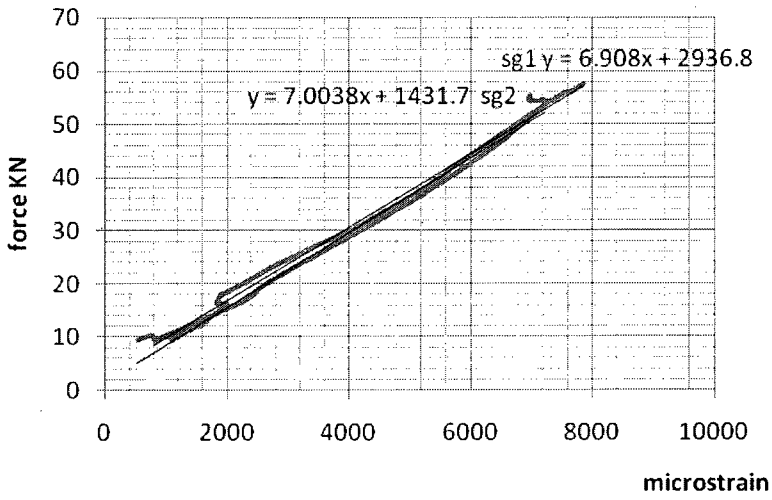

Figure A.23. Force - strain, 13 vs.6, $2L_d$ second confined specimen

A.14.#13mm main bar vs. #10mm supplementary bar of one development length (420mm), confined in concrete

Table A.24 First confined specimen results for13 vs.10, L_d

Failure load	Avg. captured by supplementary bar	Failure mode
92KN	*26%	Anchorage failure
	Sg1	Sg2
Slope of best trend line	7.4232	27.68
Strain at failure	11954	4056

* Concrete cover did not integrate the assembly preopely (manufacture error)

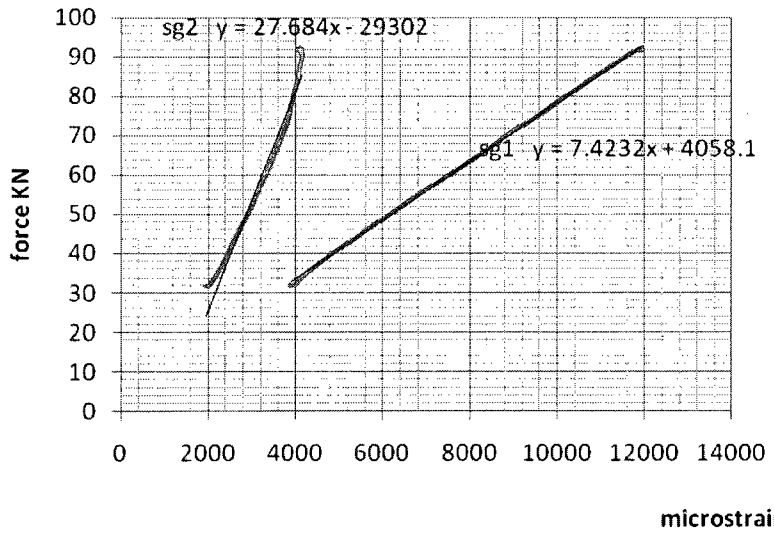

Figure A.24. Force -strain, 13 vs.10, L_d first confined specimen

Table A.25. Second confined specimen results for13 vs.10, L_d

Failure load	Avg. captured by supplementary bar	Failure mode
91.45KN	71.61%	Anchorage failure
	Sg1	Sg2
Slope of best trend line	7.21	10.068
Strain at failure	9933	6937

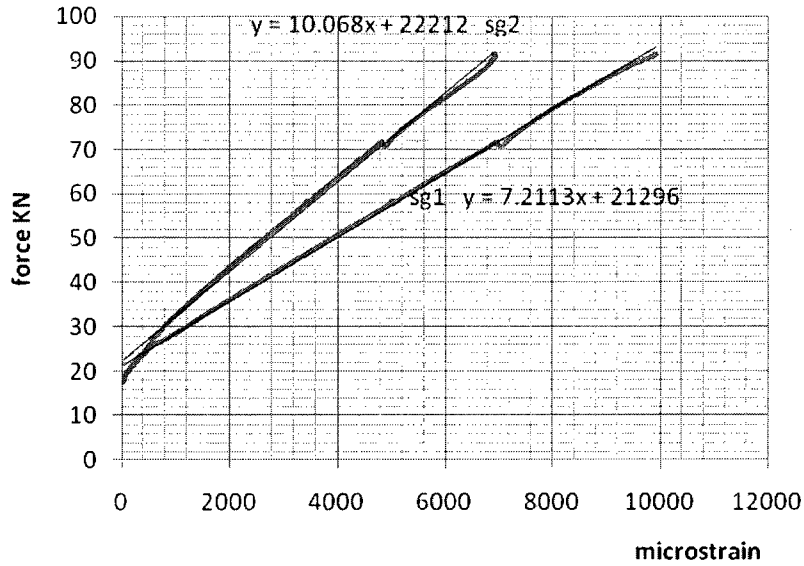

Figure A.25. Force - strain, 13 vs.10, L_d second confined specimen

A.15. #13mm main bar vs. #10mm supplementary bar of one and a half development length (630mm), confined in concrete

Table A.26. First confined specimen results for13 vs.10, $1.5L_d$

Failure load	Avg. captured by supplementary bar	Failure mode
50KN	70%	SG got off scale
	Sg1	Sg2
Slope of best trend line	7.67	10.97
Strain at failure	5749	3619

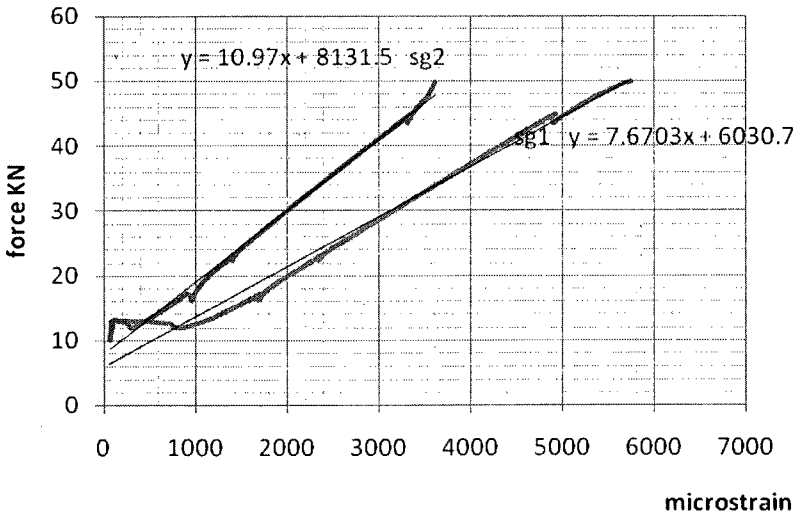

Figure A.26. Force - strain, 13 vs.10, $1.5L_d$ first confined specimen

Table A.27. Second confined specimen results for13 vs.10, 1.5Ld

Failure load	Avg. captured by supplementary bar	Failure mode
79KN	96.6%	SG got off scale
	Sg1	Sg2
Slope of best trend line	7.54	7.8
Strain at failure	7372	4644

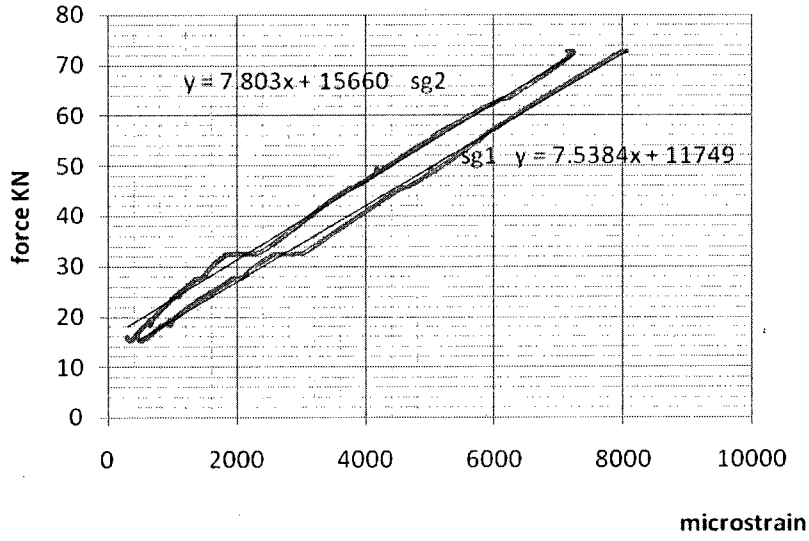

Figure A.27. Force - strain, 13 vs.10, 1.5L_d second confined specimen

A.16. #19mm main bar vs. #6mm supplementary bar of one development length (310mm), confined in concrete

Table A.28. First confined specimen results for19 vs.6, L_d

Failure load	Avg. captured by supplementary bar	Failure mode
110KN	0.82%	Concrete disintegrated
	Sg1	Sg2
Slope of best trend line	14.62	17.879
Strain at failure	7068	5307

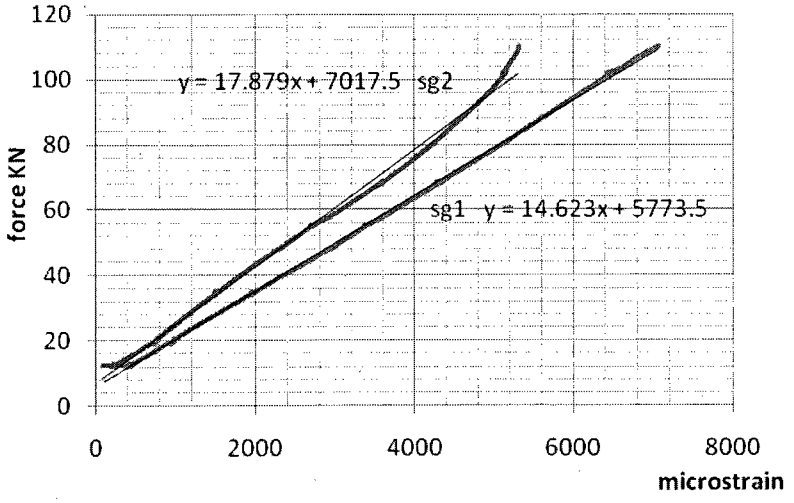

Figure A.28. Force - strain, 19 vs.6, L_d first confined specimen

Table A.29. Second confined specimen results for19 vs.6, L_d

Failure load	Avg. captured by supplementary bar	Failure mode
104.5KN	91.6%	Concrete disintegrated
	Sg1	Sg2
Slope of best trend line	14.3	15.6
Strain at failure	6701	6012

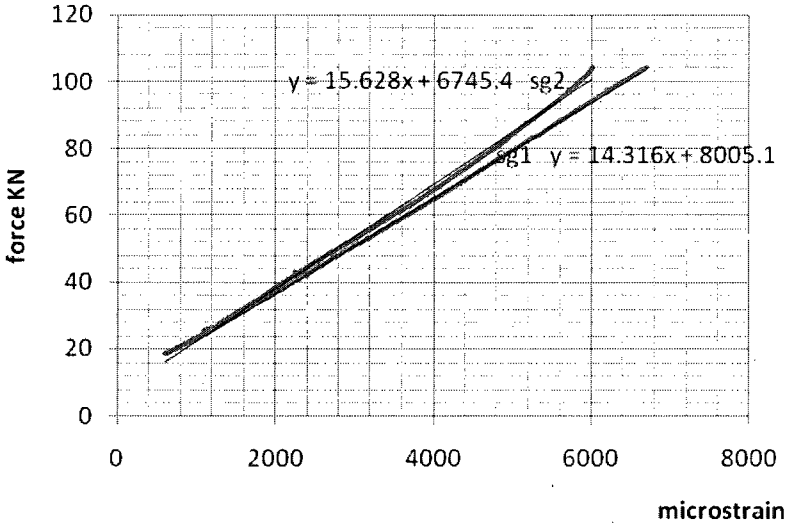

Figure A.29. Force -strain, 19 vs.6, L_d second confined specimen

A.17. #19mm main bar vs. #6mm supplementary bar of one and a half development length (465mm), confined in concrete

Table A.30. First confined specimen results for19 vs.6, $1.5L_d$

Failure load	Avg. captured by supplementary bar	Failure mode
103.5KN	85.4%	Concrete disintegrated
	Sg1	Sg2
Slope of best trend line	14.44	16.91
Strain at failure	6576	5586

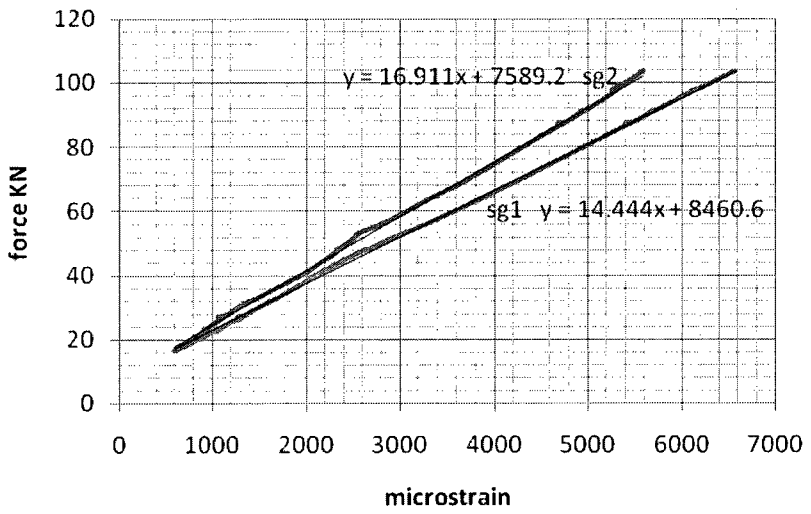

Figure A.30. Force - strain, 19 vs.6, $1.5L_d$ first confined specimen

Table A.31. Second confined specimen results for19 vs.6, $1.5L_d$

Failure load	Avg. captured by supplementary bar	Failure mode
39.6KN	45%	Concrete disintegrated
	Sg1	Sg2
Slope of best trend line	17.4	38.3
Strain at failure	2084	1073

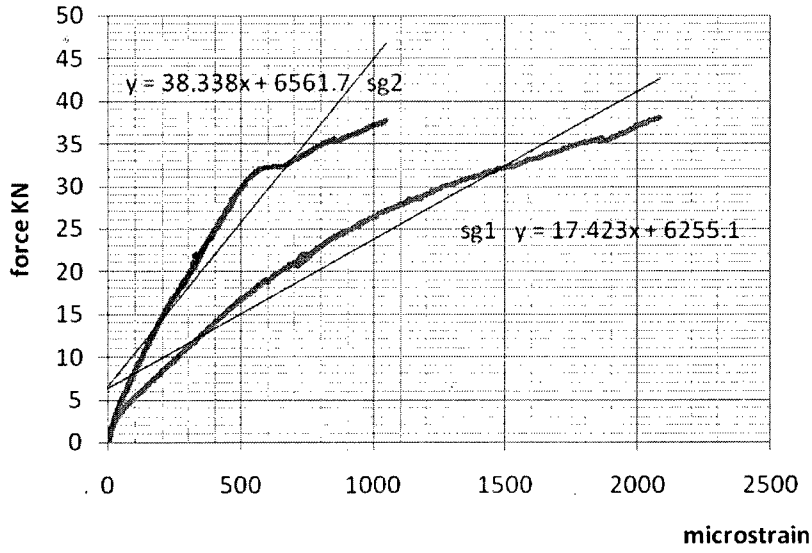

Figure A.31. Force - strain, 19 vs.6, $1.5L_d$ second confined specimen

A.18. #19mm main bar vs. #6mm supplementary bar of two development length (620mm), confined in concrete

Table A.32. Second confined specimen results for19 vs.6, $2L_d$

Failure load	Avg. captured by supplementary bar	Failure mode
53.9KN	83.2%	Anchorage failure
	Sg1	Sg2
Slope of best trend line	13.14	15.8
Strain at failure	3814	3421

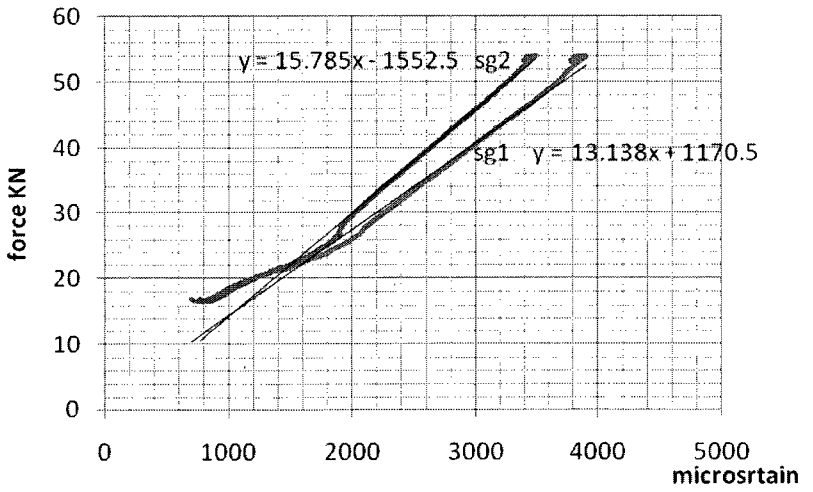

Figure A.32. Force - strain, 19 vs.6, $2L_d$ second confined specimen

A.19. 19mm diameter main bar vs. 10mm diameter supplementary bar of one development length (420mm), confined in concrete

Table A.33. First confined specimen results for19 vs.10, L_d

Failure load	Avg. captured by supplementary bar	Failure mode
70KN	74.5%	Anchorage failure
	Sg1	Sg2
Slope of best trend line	13.7	18.4
Strain at failure	5060	3705

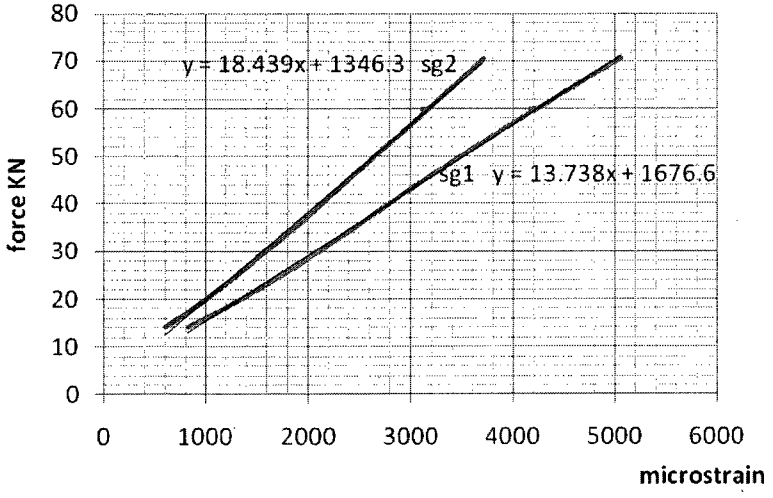

Figure A.33. Force -strain, 19 vs.10, L_d first confined specimen

Table A.34. Second confined specimen results for19 vs.10, L_d

Failure load	Avg. captured by supplementary bar	Failure mode
80KN	65%	Concrete disintegrated
	Sg1	Sg2
Slope of best trend line	13.7	20.9
Strain at failure	5505	3653

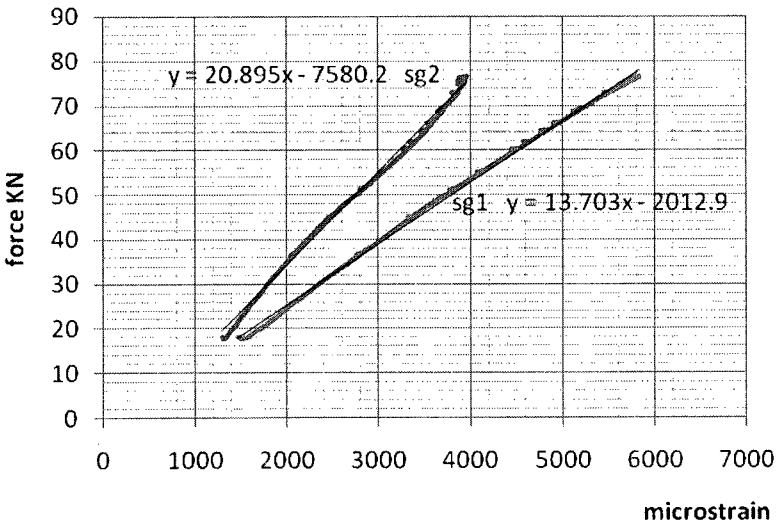

Figure A.34. Force -strain, 19 vs.10, L_d second confined specimen

A.20. #19mm main bar vs. #10mm supplementary bar of one and a half development length (630mm), confined in concrete

Table A.35. First confined specimen results for19 vs.10, $1.5L_d$

Failure load	Avg. captured by supplementary bar	Failure mode
63.7KN	86.5%	Concrete disintegrated
	Sg1	Sg2
Slope of best trend line	12	13.9
Strain at failure	3518	3401

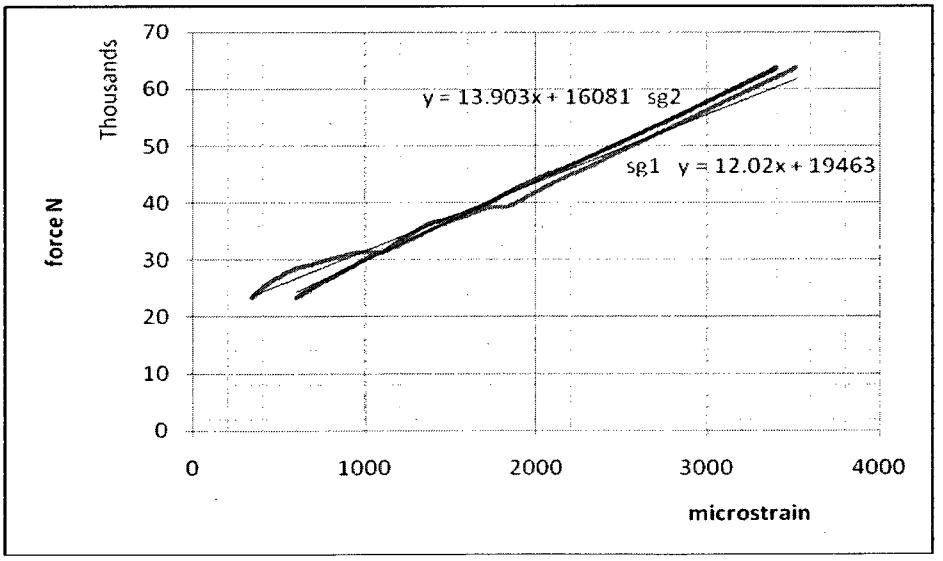

Figure A.35. Force - strain, 19 vs.10, $1.5L_d$ first confined specimen

Second Specimen results:

Table A.36. Second confined specimen results for19 vs.10, $1.5L_d$

Failure load	Avg. captured by supplementary bar	Failure mode
75.3KN	81.8%	Concrete disintegrated
	Sg1	Sg2
Slope of best trend line	14.6	17.85
Strain at failure	4525	3522

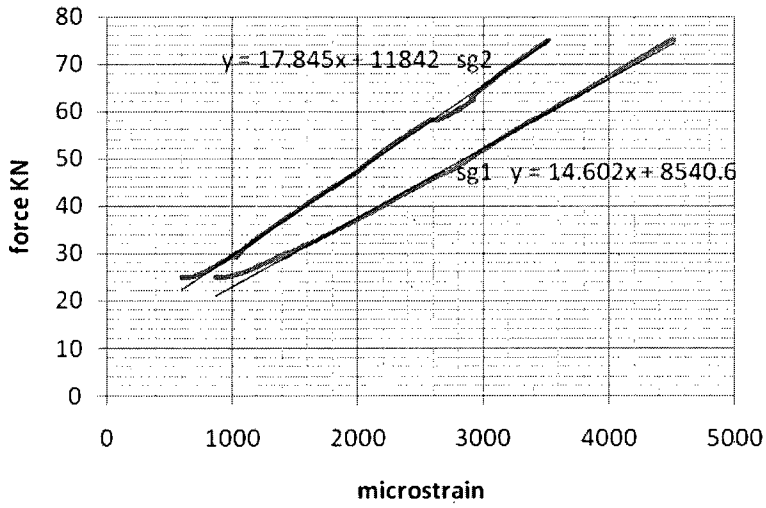

Figure A.36. Force - strain, 19 vs.10, $1.5L_d$ second confined specimen

A.21. #13mm main bar vs. #6mm supplementary bar of one development length (310mm), CFRP wrapped and confined in concrete (table and graph in chapter 4)

A.22. #13mm main bar vs. #6mm supplementary bar of one and a half development length (465mm), CFRP wrapped and confined in concrete

Table A.37. C-W specimen results for13 vs.6, $1.5L_d$

Failure load	Avg. captured by supplementary bar	Failure mode
68KN	98%	SG got off scale
	Sg1	Sg2
Slope of best trend line	6.96	7.1
Strain at failure	9766	9404

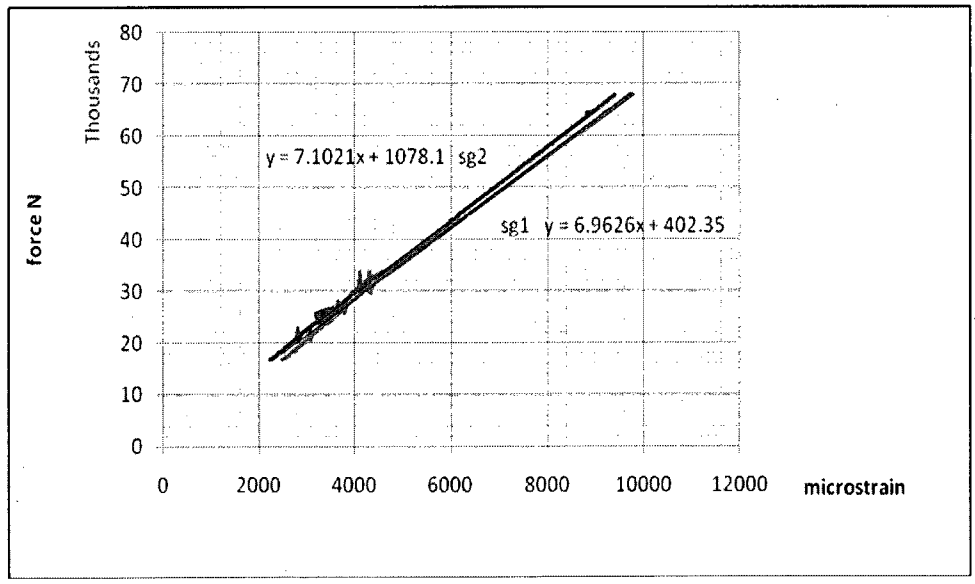

Figure A.37. Force - strain, 13 vs. 6, $1.5L_d$ C-W specimen

A.23. #13mm main bar vs. #6mm supplementary bar of two development length (610mm), CFRP wrapped and confined in concrete

Table A.38. C-W specimen results for13 vs.6, $2L_d$

Failure load	Avg. captured by supplementary bar	Failure mode
80KN	95%	SG got off scale
	Sg1	Sg2
Slope of best trend line	6.45	6.79
Strain at failure	12213	11836

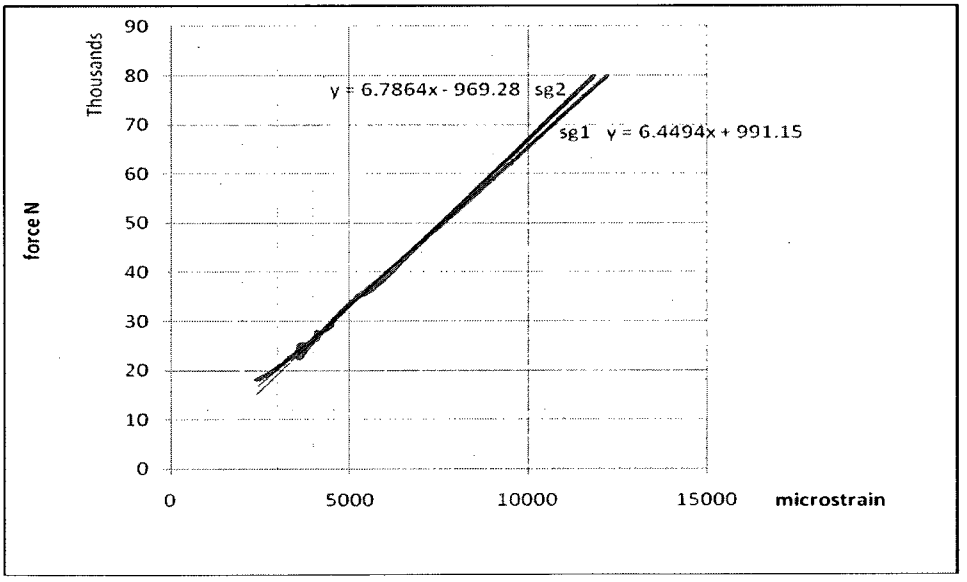

Figure A.38. Force - strain, 13 vs.6, $2L_d$ C-W specimen

A.24. #13mm main bar vs. #10mm supplementary bar of one and a half development length (630mm), CFRP wrapped and confined in concrete

Table A.39. C-W specimen results for13 vs.10, $1.5L_d$

Failure load	Avg. captured by supplementary bar	Failure mode
80.7KN	99.5%	Concrete cover cracked
	Sg1	Sg2
Slope of best trend line	9.22	9.17
Strain at failure	9025	8541

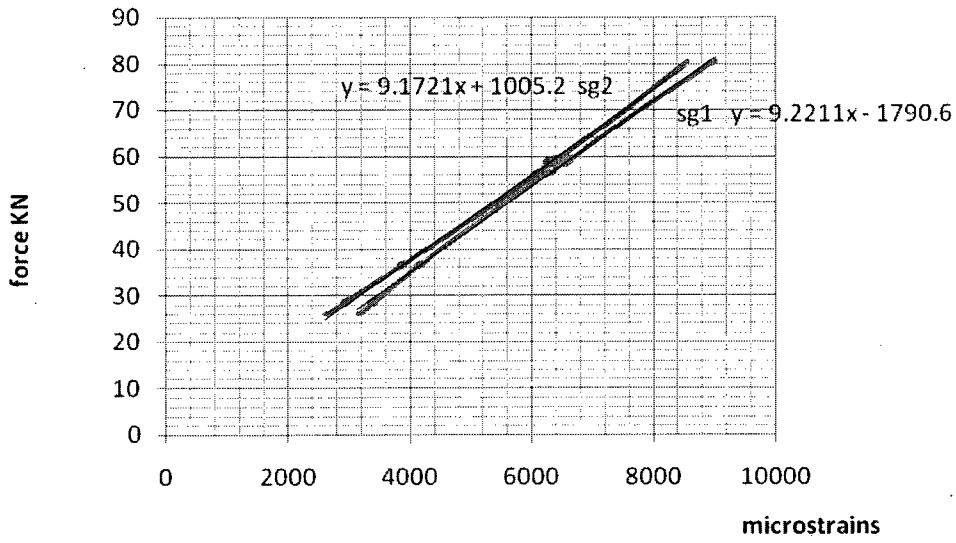

Figure A.39. Force - strain, 13 vs. 10, 1.5 L_d C-W specimen

A.25. #19mm Main bar vs. #6mm supplementary bar of one and a half development length (630mm), CFRP wrapped and confined in concrete

Table A.40. C-W specimen results for19 vs.6, $1.5L_d$

Failure load	Avg. captured by supplementary bar	Failure mode
111.1KN	96.4	Concrete cover cracked
	Sg1	Sg2
Slope of best trend line	15.65	16.24
Strain at failure	7205	6787

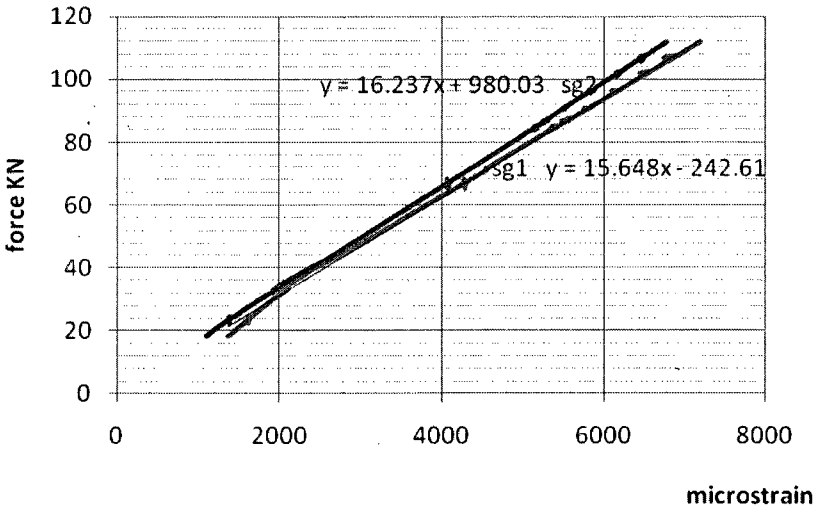

Figure A.40. Force - strain, 19 vs.6, $1.5L_d$ C-W specimen

A.26. #19mm Main bar vs. #6mm supplementary bar of two development length (620mm), CFRP wrapped and confined in concrete

Table A.41. C-W specimen results for19 vs.6, $2L_d$

Failure load	Avg. captured by supplementary bar	Failure mode
170KN	93.4%	concrete cover cracked
	Sg1	Sg2
Slope of best trend line	16.75	17.94
Strain at failure	9256	8747

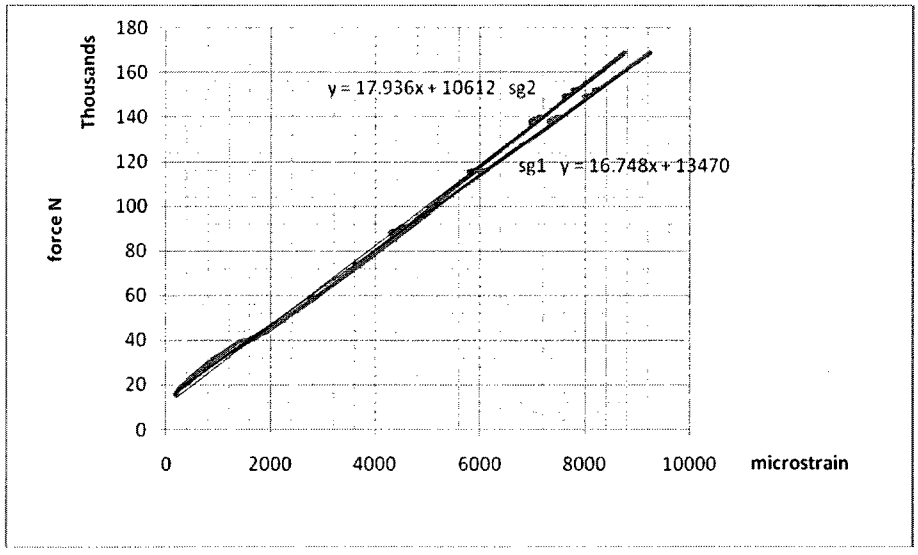

Figure A.41. Force - strain, 19 vs.6, $2L_d$ C-W specimen

A.27. #19mm Main bar vs. #10mm supplementary bar of one and a half development length (630mm), CFRP wrapped and confined in concrete (Table and graph in chapter 4)

APPENDIX B: SECTION ANALYSIS

In this appendix, section analysis for the tested beams is presented in details to explain the way the flexural capacity of the GFRP-reinforced beams is calculated in Chapter 5.

Dimensions of each beam:

Clear span: $L = 2400\ mm$

Width: $b = 240\ mm$

Height: $h = 320\ mm$

Properties of the concrete:

Compressive strength: $f'_c = 30\ MPa$

Modulus of rupture: $f_r = 3.29 MPa$

Ultimate compressive strain of concrete: $\varepsilon_u = 0.0035$

Reinforcement specifications:

Type of the rebars: GFRP

Number of the rebars: 4

Diameter of the rebars: 13 *mm*

Effective depth: $d = 280\ mm$

Modulus of elasticity: $E_{FRP} = 46.3\ GPa$

Ultimate tensile strength: $f_{u,FRP} = 786\ MPa$

Ultimate tensile strain: $\varepsilon_{FRPu} = 0.0017$

Calculation of the cracking moment:

$I_g = bh^3/12 = 655.36 \times 10^6\ mm^4$

$S_g = I_g/c = 4.096 \times 10^6\ mm^3$

$M_{cr} = R \times S_g = 13.46\ kN.M$

Calculation of the flexural strength:

$A_{FRP}=4\times\pi(13)^2/4=530.93\ mm^2$

$\alpha_1=0.805$

$\beta_1=0.895$

$\rho_{FRPb}= (\alpha_1 \beta_1 f'c/ f_{FRPu}) [\varepsilon_u/ (\varepsilon_u+ \varepsilon_{FRPu})] = 0.0047$

$\rho_{FRP} =A_{FRP}/ bd =0.0066> 0.0047$ *compression failure happens*

Performing an iterative strain –compatibility analysis will give c=58.5 mm. Then:

$M_n = A_{FRP} f_{FRPu} (d- \beta c/2) = 75kN.M$

Repeating the same process using $\Phi_{GFRP} = 0.4$ and $\Phi_c=0.65$ *would yield:*

$M_r= 40.12\ kN.M$

With a distributed loading of 50 kPa on the beam:

$M_f= 36\ kN.M$ *and* $M_s =27\ kN.M$